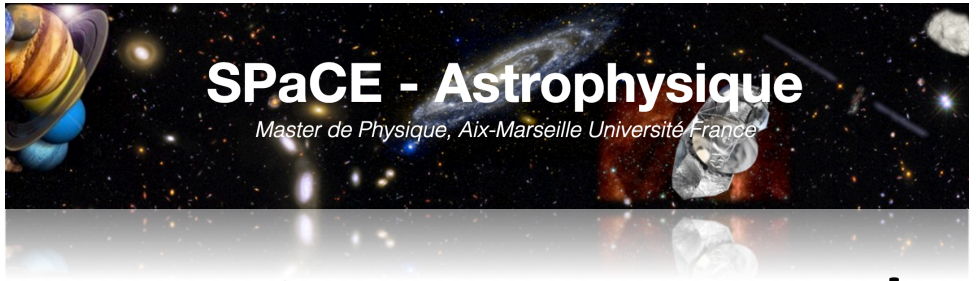

Star Formation: Now and Then

Denis Burgarella, Astronomer

Laboratoire d'Astrophysique de Marseille, France

denis.burgarella@lam.fr

SECOND COSMOLOGY SCHOOL

Ministry of Science and Higher Education
Republic of Poland

INTRODUCTION TO COSMOLOGY
Kielce, Poland 11.07 - 24.07.2016

HECOLS
Polish-French collaboration in astrophysics

CAMK PAN

Naukaonline.pl

Did we detect poplll stars (or galaxies)?

EVIDENCE FOR POPIII-LIKE STELLAR POPULATIONS IN THE MOST LUMINOUS LYMAN-α EMITTERS AT THE EPOCH OF RE-IONISATION: SPECTROSCOPIC CONFIRMATION

DAVID SOBRAL[1,2,3], JORRYT MATTHEE[3], BEHNAM DARVISH[4], DANIEL SCHAERER[5,6], BAHRAM MOBASHER[4], HUUB J. A. RÖTTGERING[3], SÉRGIO SANTOS[1,2], SHOUBANEH HEMMATI[4]

Accepted for publication in The Astrophysical Journal, June 4, 2015

Located in the COSMOS field, an intensely studied patch of sky in the constellation of Sextans, this galaxy is three times brighter than the brightest distant galaxy known up to now. Its nickname was inspired by the Portuguese soccer player Cristiano Ronaldo (also known as CR7).

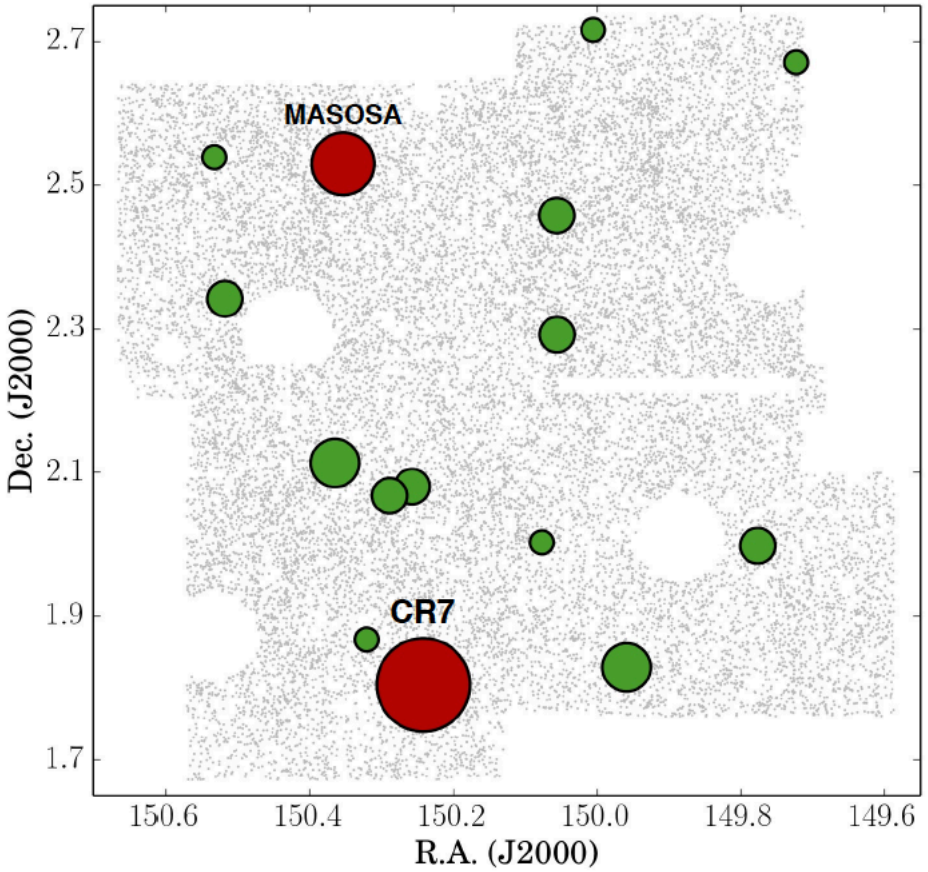

FIG. 1.— Projected positions on sky of all Lyα candidates (green circles) found in the COSMOS/UltraVISTA field. The grey background points represent all detected sources with the NB921 filter, highlighting the masking applied (due to the presence of artefacts caused by bright stars and noisy regions, see Matthee et al. 2015). Lyα candidates are plotted with a symbol size proportional to their Lyα luminosity. CR7 and MASOSA are highlighted in red: these are the most luminous sources found in the field. Their coordinates are given in Table 1.

EVIDENCE FOR POPIII-LIKE STELLAR POPULATIONS IN THE MOST LUMINOUS LYMAN-α EMITTERS AT THE EPOCH OF RE-IONISATION: SPECTROSCOPIC CONFIRMATION

DAVID SOBRAL[1,2,3], JORRYT MATTHEE[3], BEHNAM DARVISH[4], DANIEL SCHAERER[5,6], BAHRAM MOBASHER[4], HUUB J. A. RÖTTGERING[3], SÉRGIO SANTOS[1,2], SHOUBANEH HEMMATI[4]

Accepted for publication in The Astrophysical Journal, June 4, 2015

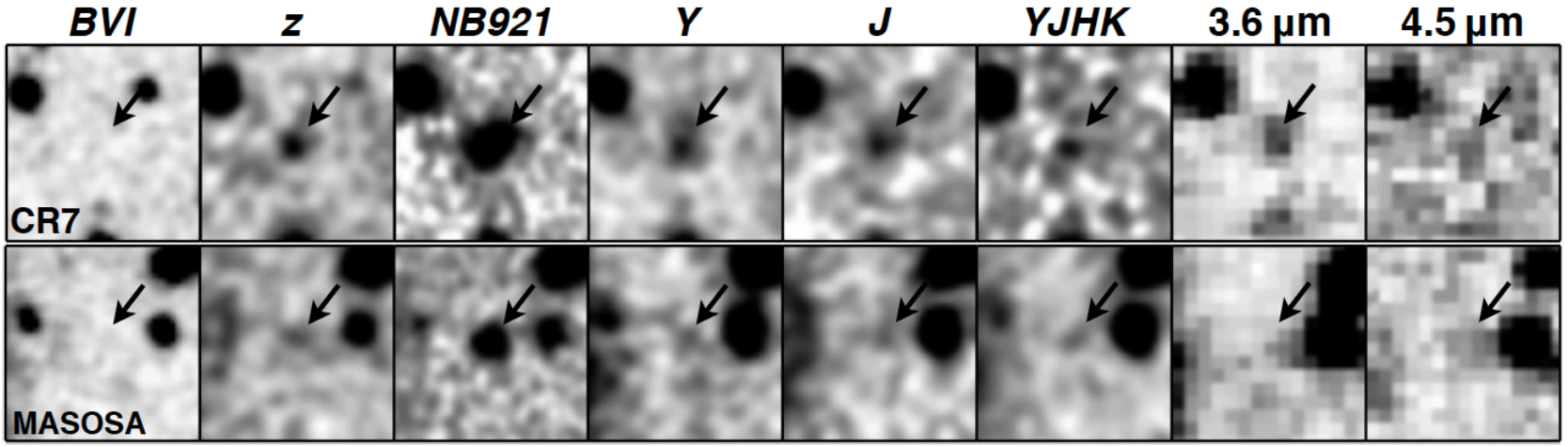

FIG. 2.— Thumbnails of both luminous Lyα emitters in the optical to MIR from left to right. Each thumbnail is $8 \times 8''$, corresponding to $\sim 44 \times 44$ kpc at $z \sim 6.6$. Note that while for MASOSA the Lyα emission line is detected by the NB921 filter at full transmission, for CR7 the Lyα is only detected at $\sim 50\%$ transmission. Therefore, the NB921 only captures $\sim 50\%$ of the Lyα flux: the observed flux coming from the source is $\sim 2\times$ larger.

EVIDENCE FOR POPIII-LIKE STELLAR POPULATIONS IN THE MOST LUMINOUS LYMAN-α EMITTERS AT THE EPOCH OF RE-IONISATION: SPECTROSCOPIC CONFIRMATION

David Sobral[1,2,3], Jorryt Matthee[3], Behnam Darvish[4], Daniel Schaerer[5,6], Bahram Mobasher[4], Huub J. A. Röttgering[3], Sérgio Santos[1,2], Shoubaneh Hemmati[4]

Accepted for publication in The Astrophysical Journal, June 4, 2015

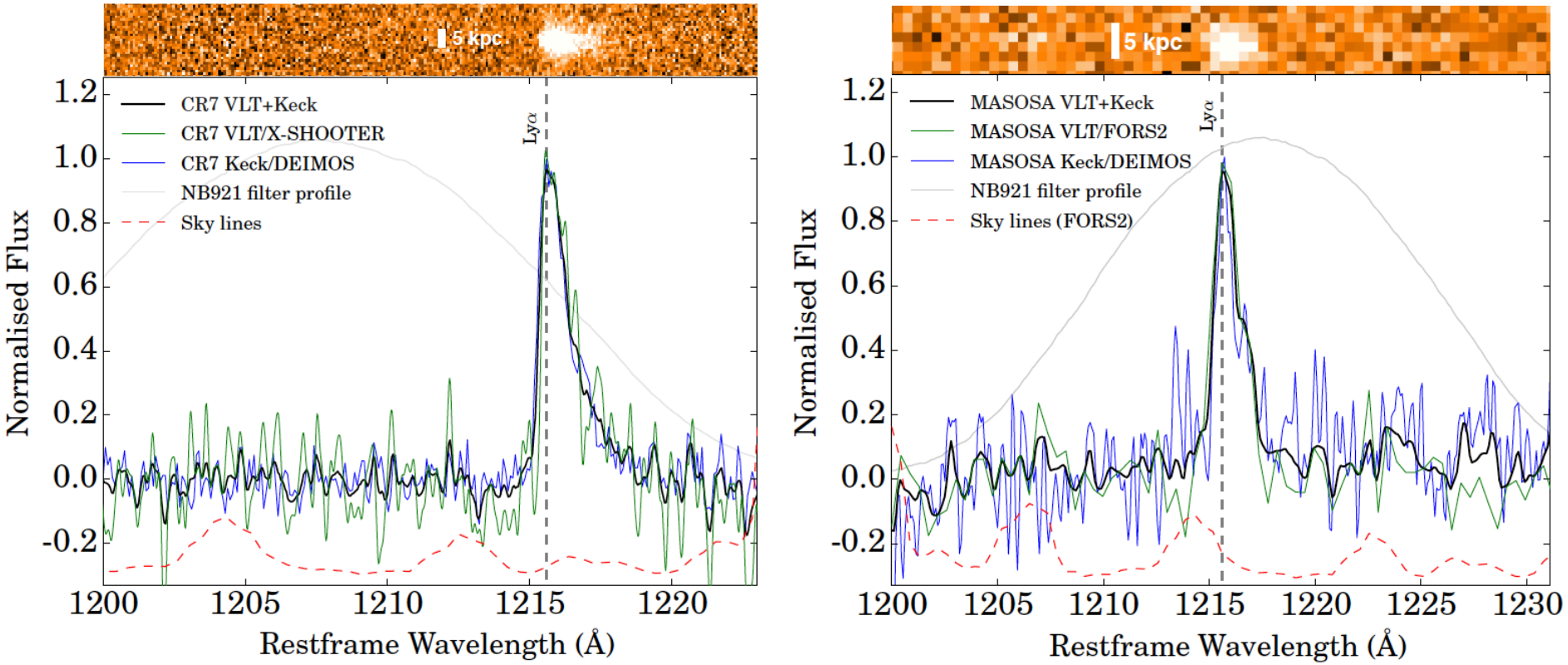

FIG. 3.— *Left*: 'CR7' 1-D and 2-D optical spectra, showing the strong and clear Lyα emission line. We also show the NB921 filter profile which was used to select the source. Note that Lyα is detected at the wing of the NB921 filter. Thus, while the NB921 photometry already implied the source was very luminous, its true luminosity was still underestimated by a factor of two. We show both our Keck/DEIMOS and VLT/X-SHOOTER spectra, which show perfect agreement, but with X-SHOOTER providing an even higher spectral resolution, while the DEIMOS spectrum gives an even higher S/N. *Right*: 'MASOSA' 1-D and 2-D optical spectra (FORS2), showing the strong and clear Lyα emission line. We also show the NB921 filter profile which was used to select the source. We show both the VLT/FORS2 and Keck/DEIMOS spectra, showing they agree very well. The DEIMOS spectrum provides higher resolution, but both clearly reveal the asymmetry of the line, confirming it as Lyα without any doubt.

EVIDENCE FOR POPIII-LIKE STELLAR POPULATIONS IN THE MOST LUMINOUS LYMAN-α EMITTERS AT THE EPOCH OF RE-IONISATION: SPECTROSCOPIC CONFIRMATION

DAVID SOBRAL[1,2,3], JORRYT MATTHEE[3], BEHNAM DARVISH[4], DANIEL SCHAERER[5,6], BAHRAM MOBASHER[4], HUUB J. A. RÖTTGERING[3], SÉRGIO SANTOS[1,2], SHOUBANEH HEMMATI[4]

Accepted for publication in The Astrophysical Journal, June 4, 2015

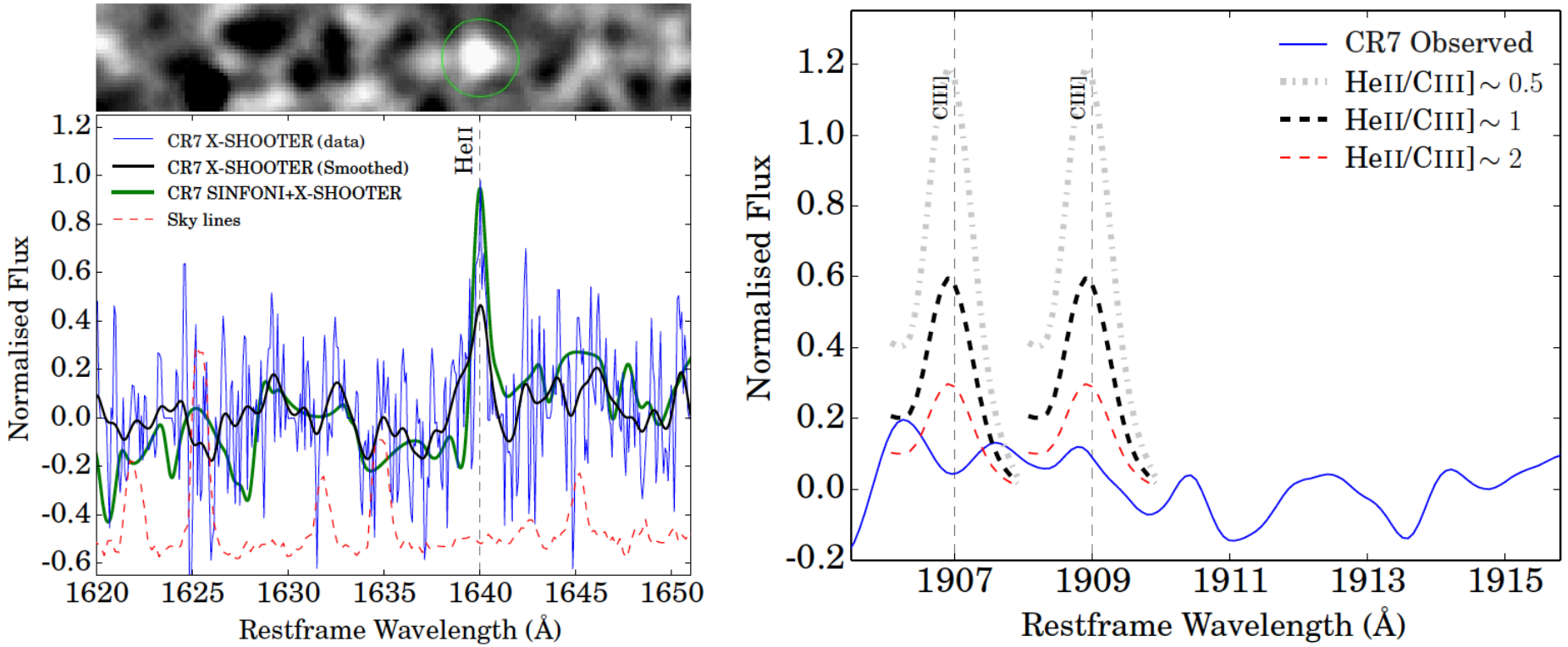

FIG. 4.— *Left:* Our X-SHOOTER NIR spectrum of CR7, revealing a significant detection of the HeII1640 Å emission line. We show both the data at full resolution and binning in wavelength (with a resolution of 0.4 Å). We also show the combined X-SHOOTER and SINFONI data and also show the sky spectrum. We note that sky lines were explicitly masked, but some residuals are still visible, including those of two OH lines just redder of the HeII emission line, which show up as a slight flux increase and another one bluer of HeII, which has been slightly over-subtracted. We note that no continuum is found in the NIR spectra, and that we would require significantly deeper observations in order to detect it simply based on the NIR photometry. *Right:* We investigate the NIR X-SHOOTER spectrum for other emission lines (e.g. Stark et al. 2014). We do not find any other emission line apart from HeII, but we show one of the lines that should be stronger in our spectrum (typically $\sim 2\times$ stronger than HeII, thus HeII/CIII]~ 0.5). We use our HeII line detection and show it at the position of the CIII] doublet for a typical line ratio of HeII/CIII] of 0.5, but also a line ratio of ~ 1 and ~ 2. Our data allow us to place a limit of HeII/CIII]> 2.5. We also investigate the presence of NV1240, NIV1487, CIV1549, OIII]1661, OIII]1666, NIII]1750: all these are undetected.

EVIDENCE FOR POPIII-LIKE STELLAR POPULATIONS IN THE MOST LUMINOUS LYMAN-α EMITTERS AT THE EPOCH OF RE-IONISATION: SPECTROSCOPIC CONFIRMATION

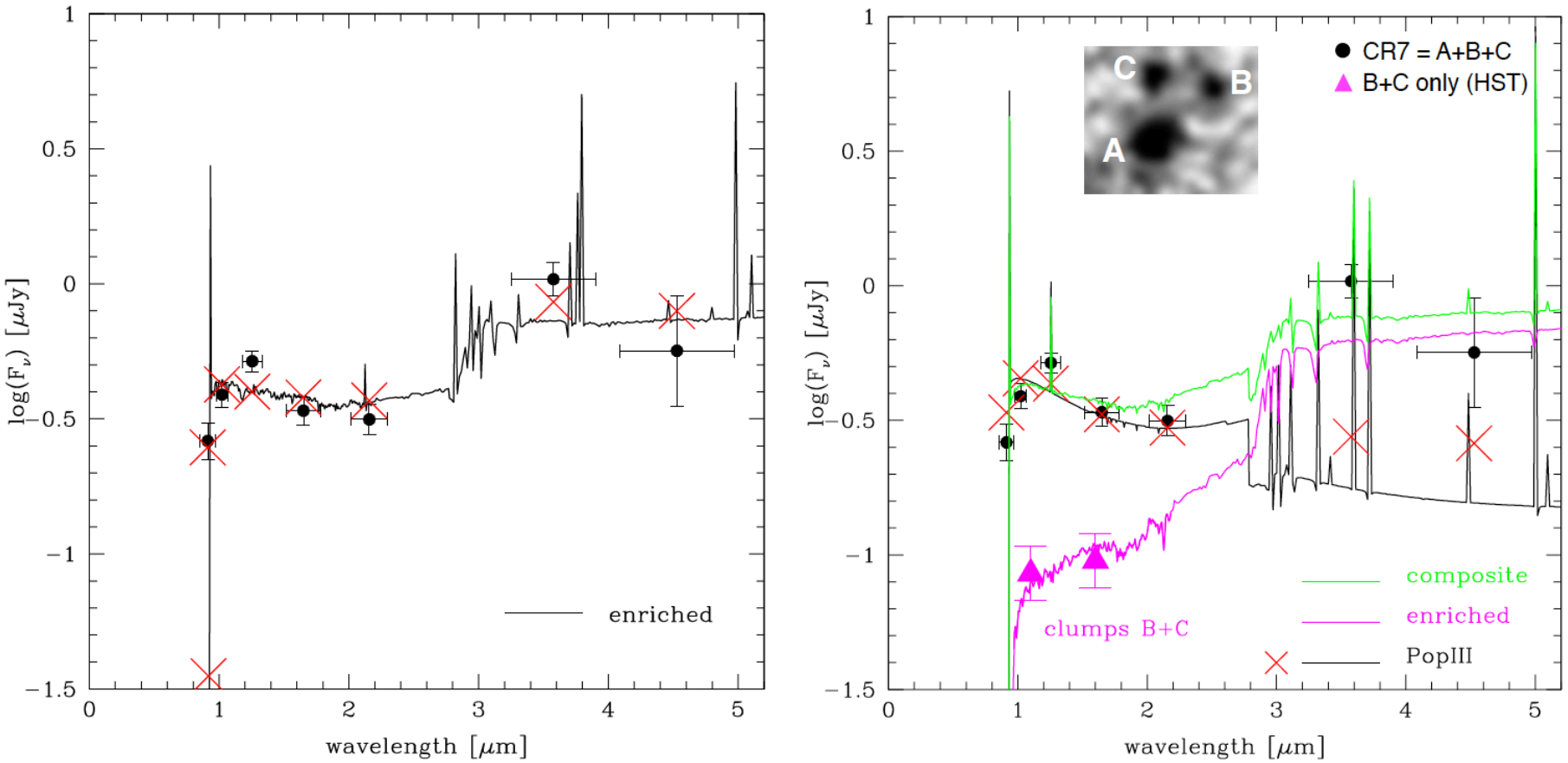

FIG. 5.— *Left*: The SED of 'CR7', from observed optical (rest-frame FUV) to observed MIR (rest-frame optical) and the best fit with a with a normal stellar population (not including PopIII stars). Red crosses indicate the flux predicted for each broad-band filter for the best fit. The fit fails to reproduce the strong Lyα emission line and also the excess in J band, due to HeII emission. Moreover, and even though the fit is unable to reproduce all the information available for the source, it requires an age of 700 Myr (the age of the Universe is 800 Myr at $z = 6.6$). In this case, the galaxy would have a SFR of $\sim 25\,M_\odot\,yr^{-1}$ and a stellar mass of $\sim 10^{10.3}\,M_\odot$. This, of course, is not able to explain the strong Lyα and the strong HeII emission line. *Right*: Same observed SED of CR7 as in the left panel plus HST photometry for clumps B+C (magenta triangles). The black line shows a fit with a pure PopIII SED to the rest-frame UV part; the magenta line the SED of an old simple stellar population with 1/5 solar metallicity which matches the flux from clumps B+C; the green line shows the predicted SED summing the two populations after rescaling the PopIII SED by a factor 0.8. The composite SED reproduces well the observed photometry. Although there is a tension between the strength of the HeII line and nebular continuum emission (cf. text), a PopIII contribution is required to explain the HeII λ1640 line and the corresponding excess in the J-band. Although HeII is very strong, we find no evidence for any other emission lines that would be characteristic of an AGN. Furthermore, the clear IRAC detections and colors, and particularly when taken as a whole, can be fully explained by a PopIII population, while normal stellar population or AGN is simply not able to.

EVIDENCE FOR POPIII-LIKE STELLAR POPULATIONS IN THE MOST LUMINOUS LYMAN-α EMITTERS AT THE EPOCH OF RE-IONISATION: SPECTROSCOPIC CONFIRMATION

DAVID SOBRAL[1,2,3], JORRYT MATTHEE[3], BEHNAM DARVISH[4], DANIEL SCHAERER[5,6], BAHRAM MOBASHER[4], HUUB J. A. RÖTTGERING[3], SÉRGIO SANTOS[1,2], SHOUBANEH HEMMATI[4]

Accepted for publication in The Astrophysical Journal, June 4, 2015

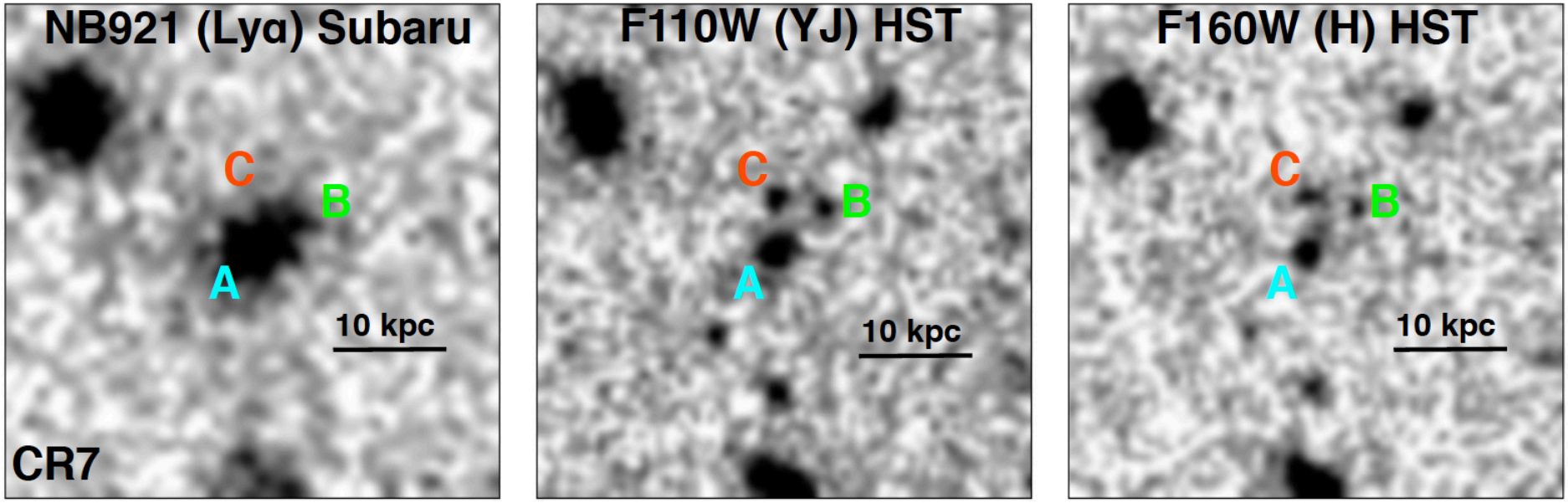

FIG. 6.— *Left:* CR7 with the NB921 filter/Suprime-cam imaging on Subaru, showing the extent of the Lyα but note that NB921 detects Lyα at only 50% transmission. *Middle:* HST imaging in YJ, revealing that CR7 clearly splits into 3 different components which we name A, B and C. *Right:* HST imaging in H, again revealing the 3 different components in CR7. We find that component A fully dominates the rest-frame UV and is coincident with the peak of Lyα emission and the location at which we detect strong HeII1640Å emission. Clumps B and C are much redder, and fully consistent with significantly contributing to the IRAC photometry. Note that because of the colours of the B and C clumps, they completely dominate the mass of the system, and thus the actual mass centre of the system would be located between C and B, and significantly away from A. This is fully consistent with a scenario in with PopIII star formation is propagated in a wave from the central position towards the outskirts.

EVIDENCE FOR POPIII-LIKE STELLAR POPULATIONS IN THE MOST LUMINOUS LYMAN-α EMITTERS AT THE EPOCH OF RE-IONISATION: SPECTROSCOPIC CONFIRMATION

DAVID SOBRAL[1,2,3], JORRYT MATTHEE[3], BEHNAM DARVISH[4], DANIEL SCHAERER[5,6], BAHRAM MOBASHER[4], HUUB J. A. RÖTTGERING[3], SÉRGIO SANTOS[1,2], SHOUBANEH HEMMATI[4]

Accepted for publication in The Astrophysical Journal, June 4, 2015

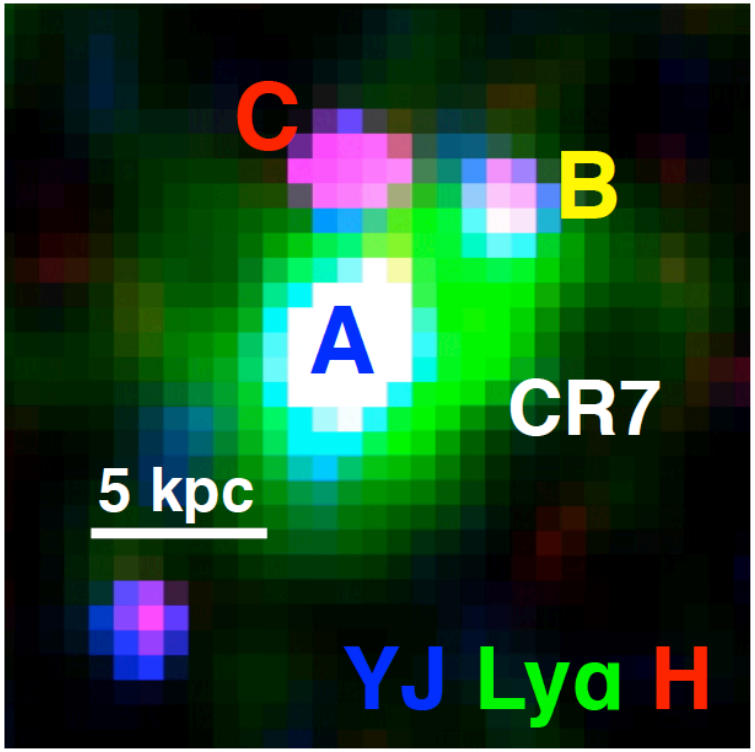

FIG. 7.— A false colour composite of CR7 by using NB921/Suprime-cam imaging (Lyα) and two *HST*/WFC3 filters: F110W (YJ) and F160W (H). This shows that while component A is the one that dominates the Lyα emission and the rest-frame UV light, the (likely) scattered Lyα emission seems to extend all the way to B and part of C, likely indicating a significant amount of gas in the system. Note that the reddest (in rest-frame UV) clump is C, with B having a more intermediate colour and with A being very blue in the rest-frame UV.

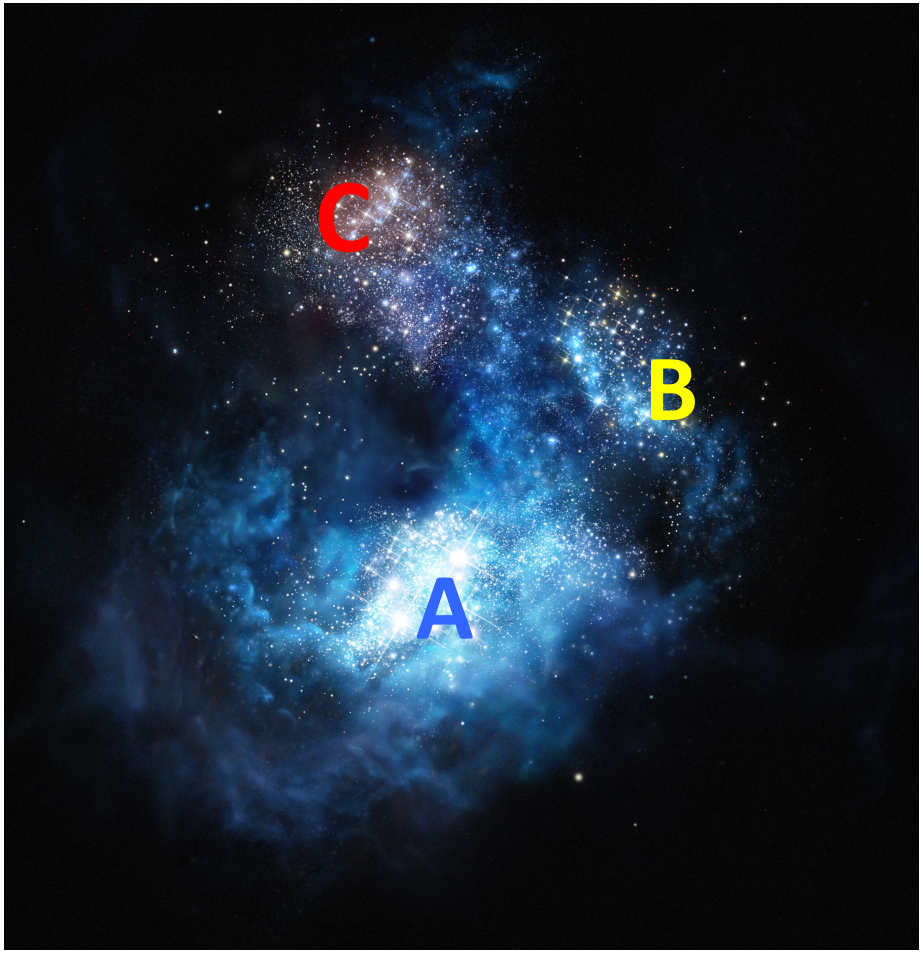

EVIDENCE FOR POPIII-LIKE STELLAR POPULATIONS IN THE MOST LUMINOUS LYMAN-α EMITTERS AT THE EPOCH OF RE-IONISATION: SPECTROSCOPIC CONFIRMATION

DAVID SOBRAL[1,2,3], JORRYT MATTHEE[3], BEHNAM DARVISH[4], DANIEL SCHAERER[5,6], BAHRAM MOBASHER[4], HUUB J. A. RÖTTGERING[3], SÉRGIO SANTOS[1,2], SHOUBANEH HEMMATI[4]

Accepted for publication in The Astrophysical Journal, June 4, 2015

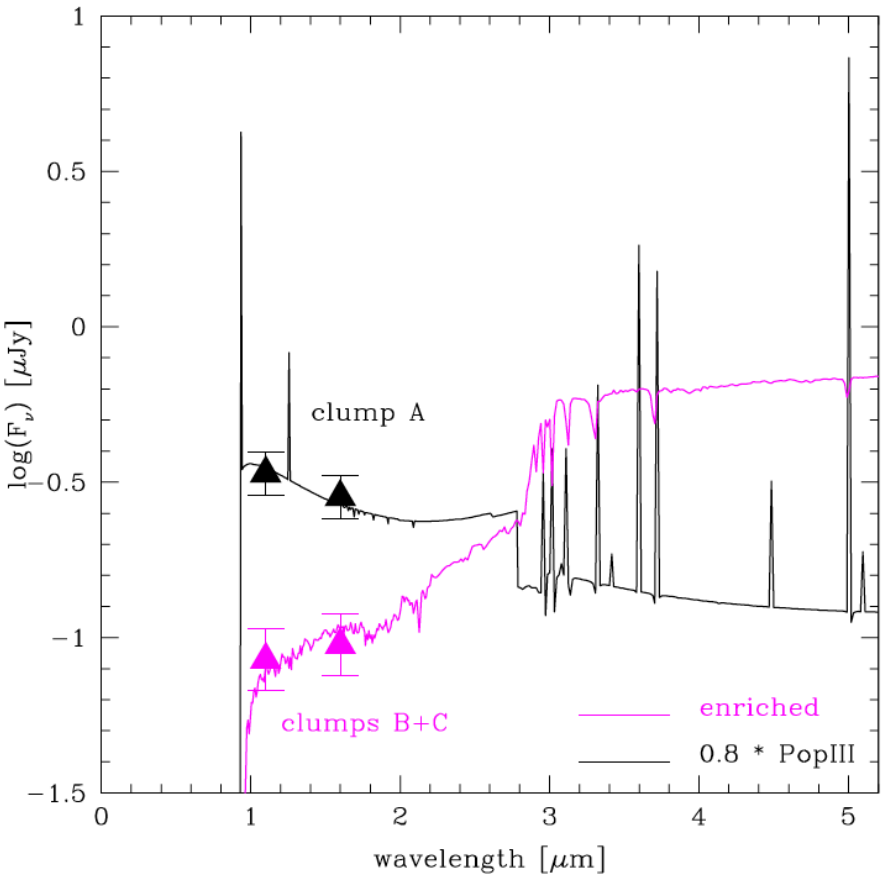

FIG. 8.— *HST* imaging in $Y\,J$ and H allows us the physically separate CR7 in two very different stellar populations and show remarkable agreement with our best-fit composite SED derived in §5.3. While clump A (see e.g. Figure 7) is very blue and dominates the rest-frame UV flux, B+C are red and likely dominate the rest-frame optical and the mass. Note that the we simply show the *HST* data together with our best fit composite model derived in §5.3 which was solely based on the full photometry and did not make use of any resolved *HST* data.

EVIDENCE FOR POPIII-LIKE STELLAR POPULATIONS IN THE MOST LUMINOUS LYMAN-α EMITTERS AT THE EPOCH OF RE-IONISATION: SPECTROSCOPIC CONFIRMATION

DAVID SOBRAL[1,2,3], JORRYT MATTHEE[3], BEHNAM DARVISH[4], DANIEL SCHAERER[5,6], BAHRAM MOBASHER[4], HUUB J. A. RÖTTGERING[3], SÉRGIO SANTOS[1,2], SHOUBANEH HEMMATI[4]

Accepted for publication in The Astrophysical Journal, June 4, 2015

ABSTRACT

Faint Lyman-α (Lyα) emitters become increasingly rarer towards the re-ionisation epoch ($z \sim 6-7$). However, observations from a very large (~ 5 deg^2) Lyα narrow-band survey at $z = 6.6$ (Matthee et al. 2015) show that this is not the case for the most luminous emitters, capable of ionising their own local bubbles. Here we present follow-up observations of the two most luminous Lyα candidates in the COSMOS field: 'MASOSA' and 'CR7'. We used X-SHOOTER, SINFONI and FORS2 on the VLT, and DEIMOS on Keck, to confirm both candidates beyond any doubt. We find redshifts of $z = 6.541$ and $z = 6.604$ for 'MASOSA' and 'CR7', respectively. MASOSA has a strong detection in Lyα with a line width of $386 \pm 30\,\mathrm{km\,s^{-1}}$ (FWHM) and with very high EW$_0$ (> 200Å), but undetected in the continuum, implying very low stellar mass and a likely young, metal-poor stellar population. 'CR7', with an observed Lyα luminosity of $10^{43.92\pm0.05}\,\mathrm{erg\,s^{-1}}$ is the most luminous Lyα emitter ever found at $z > 6$ and is spatially extended ($\sim 16\,\mathrm{kpc}$). 'CR7' reveals a narrow Lyα line with $266 \pm 15\,\mathrm{km\,s^{-1}}$ FWHM, being detected in the NIR (rest-frame UV; $\beta = -2.3 \pm 0.1$) and in IRAC/Spitzer. We detect a narrow HeII1640Å emission line (6σ, FWHM $= 130\pm30\,\mathrm{km\,s^{-1}}$) in CR7 which can explain the clear excess seen in the J band photometry (EW$_0 \sim 80$ Å). We find no other emission lines from the UV to the NIR in our X-SHOOTER spectra (HeII/OIII]1663Å > 3 and HeII/CIII]1908Å > 2.5). We conclude that CR7 is best explained by a combination of a PopIII-like population which dominates the rest-frame UV and the nebular emission and a more normal stellar population which presumably dominates the mass. *HST*/WFC3 observations show that the light is indeed spatially separated between a very blue component, coincident with Lyα and HeII emission, and two red components ($\sim 5\,\mathrm{kpc}$ away), which dominate the mass. Our findings are consistent with theoretical predictions of a PopIII wave, with PopIII star formation migrating away from the original sites of star formation.

Neglected Processes

- **Magnetic fields (MHD effects, MRI, dynamos, jets...)**
  - **e.g., Tan & Blackman 2004; Machida et al. 2006; Silk & Langer 2006**
- **Cosmic Rays (ionization, heating, chemistry...)**
  - **e.g. Shchekinov & Vasiliev 2004; Rollinde et al. 2005, 2006; Jasche et al. 2007; Stacy & Bromm 2007**
  - **➔ might lead to lower Pop III masses**
- **Possible modifications to CDM (WDM, annihilation heating...)**
  - **e.g. Yoshida et al. 2003; Gao & Theuns 2007; Spolyar et al. 2008**

Dark-Matter powered Stars: "Dark Stars" (Spolyar, Freese & Gondolo 2008; Freese et al. 2008; Iocco et al.)

- Dark Stars are the very first phase of stellar evolution in the history of the universe: the first stars to form (typically at redshifts z 10 – 50) might be powered by heating from dark matter (DM) annihilation instead of fusion (if the DM is made of particles which are their own antiparticles).
- Any DM particle which is capable of annihilating with itself in such a way as to give the correct relic abundance today will also annihilate wherever the DM density is high.
- The first protostars and stars are particularly good sites for annihilation because they form at high redshifts and in the high density centers of DM haloes.
- DM annihilation provides a powerful heat source in the first stars.

Self-annihilating WIMP DM heats stellar interior

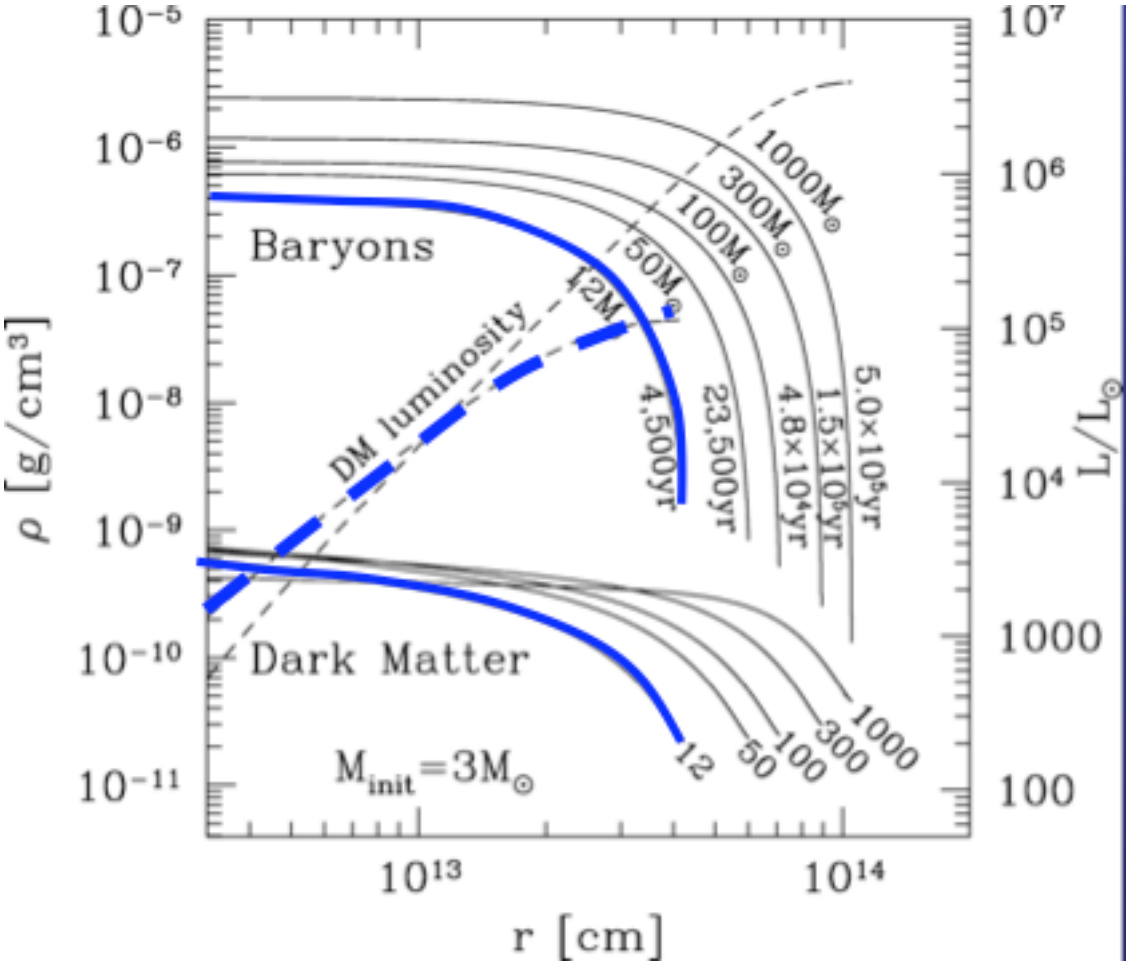

=> A red supergiant (~ 1 000 $R_\odot$) Pop III?

Universe's Timeline

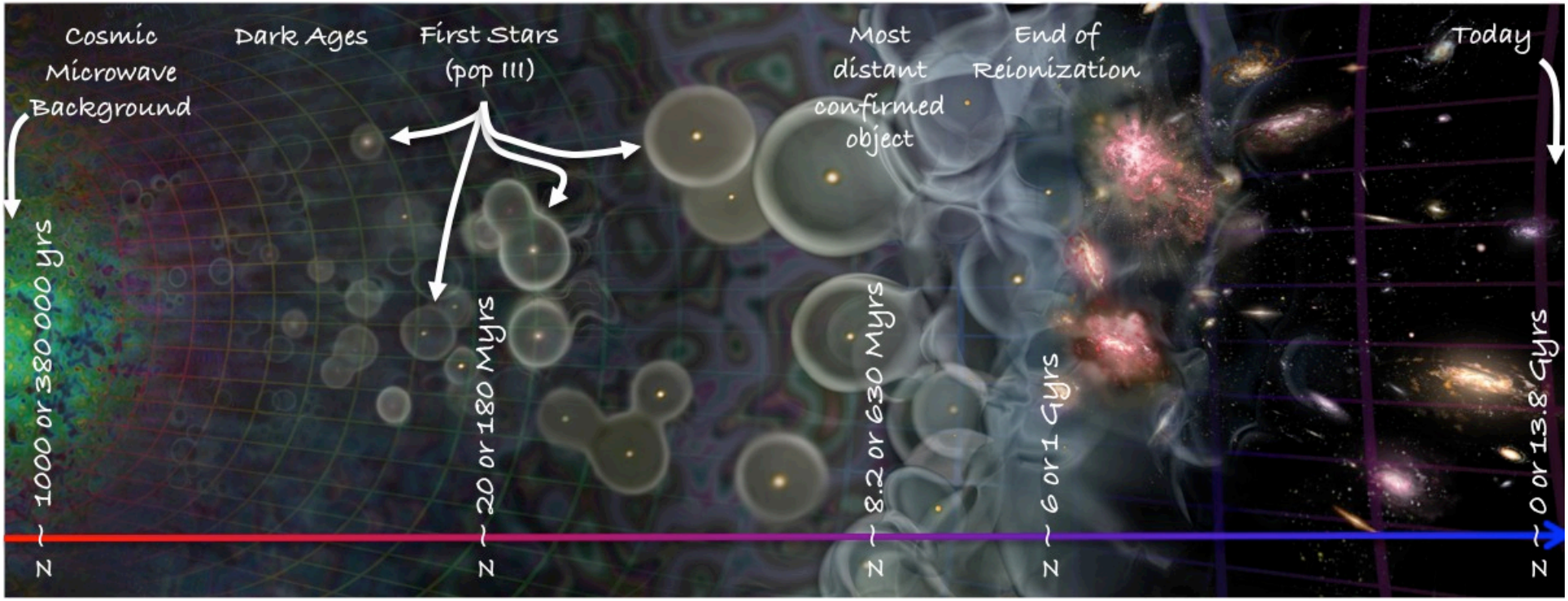

Where (in λ) should we look for the first stars?

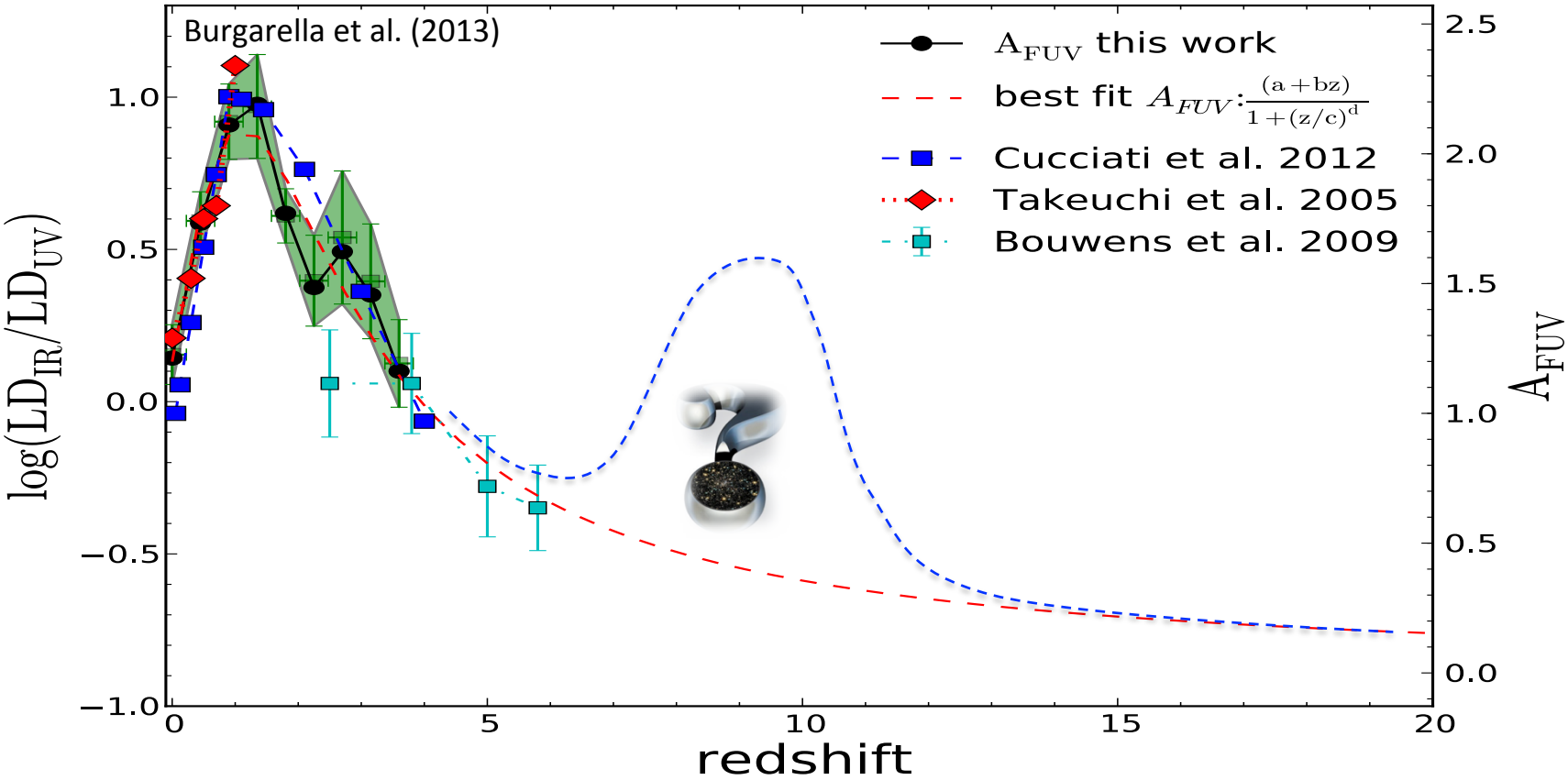

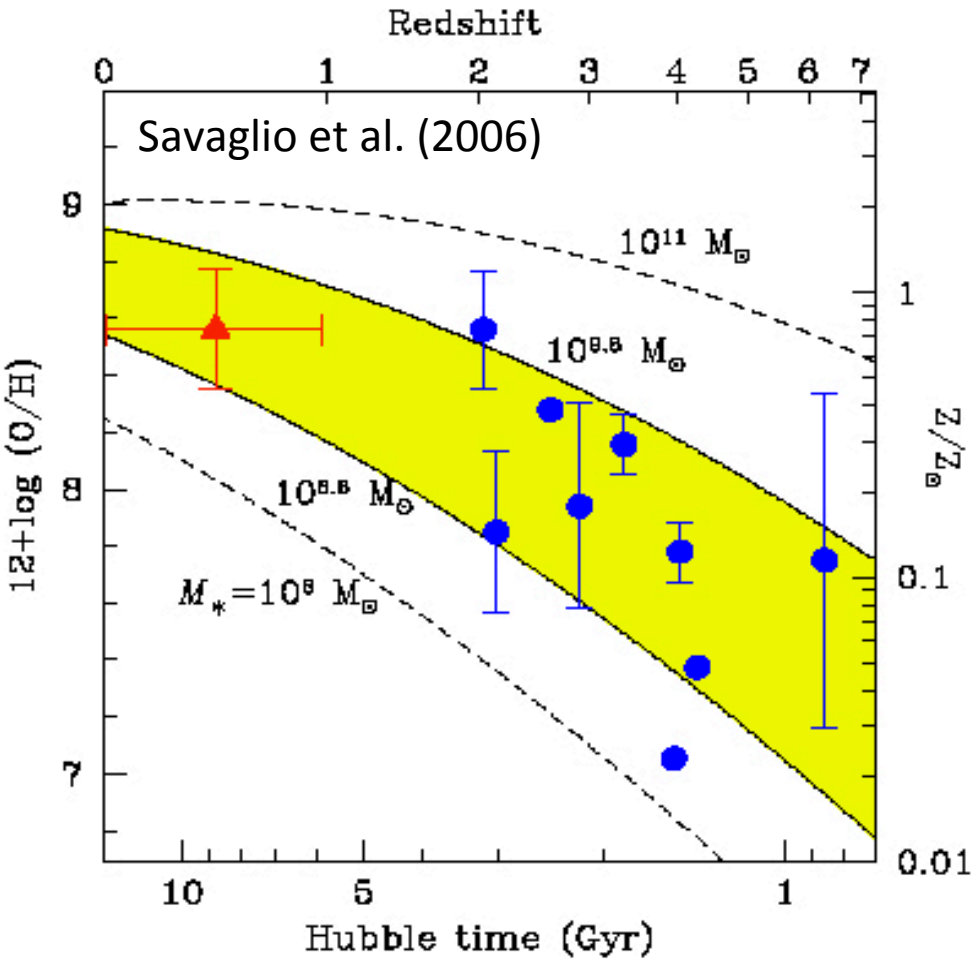

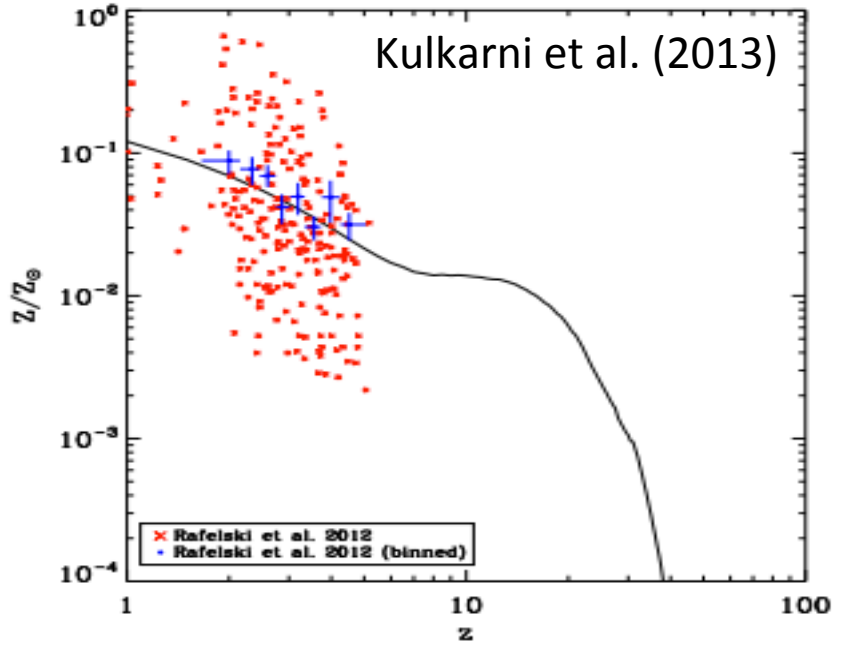

Figure 9. The "age-metallicity" relation in our model, which is given by an absorption cross section weighted average of gas phase metallicity of all mass bins. Red crosses are measurements of a sample of 241 DLAs by Rafelski et al. (2012). The blue points are mean values in different redshift bins, as presented by Rafelski et al. (2012). Vertical error bars on the blue points represent 1σ error bars.

Figure 7. Metallicity as a function of Hubble time (lower *x*-axis) or redshift (upper *x*-axis) derived for GRB-DLAs (•—as in figure 5), and the mean value derived for a sample of $z < 1$ GRB hosts (▲, vertical and horizontal bars are the 1σ dispersion and the redshift interval of the sample, respectively). The curves are predictions from the empirical model of [19], for different total stellar masses. The shaded area indicates the range of stellar masses more favourable for the observed metallicities.

- Small amounts of dust are expected in the very early universe.
- So, detecting the first galaxies should be better in the **Near/Mid-IR**.
- This is confirmed by David Sobral's detection of the pop III candidate.

How to detect large sample of first galaxies?

How to detect large sample of first galaxies?

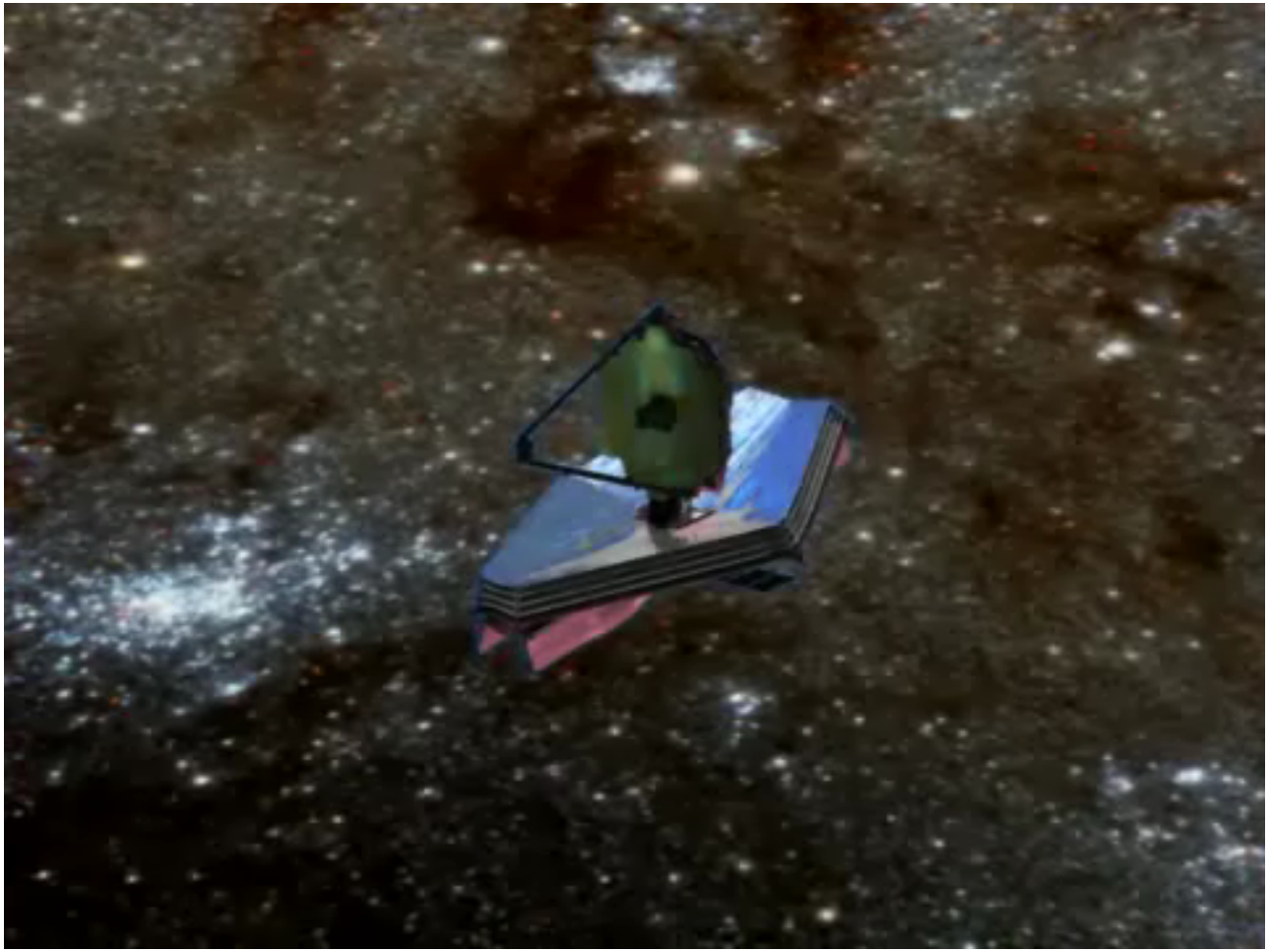

The ESA M5 FLARE Proposal: Deep and Wide-field 1-5um Imaging and Spectroscopy for the Early Universe

Denis Burgarella, Patrick Levacher & the FLARE Team
Laboratoire d'Astrophysique de Marseille
Aix-Marseille Université

First Light And Reionization Explorer

FLARE

Main Science Objectives

I. First Light And Reionization (~70-80%)

- The main objective of FLARE will be to understand the end of the dark ages and study the formation of the first objects in the universe.
- This is related to ESA's 4th theme in the Cosmic Vision 2015 – 2025 programme: « *How did the universe originate and what is it made of?* » and more specifically, « **4.2 *The universe taking shape*** **»**:
- *« Tracing cosmic history back to the time when the first luminous sources ignited, thus ending the dark ages of the Universe, has just begun. At that epoch the intergalactic medium was reionised, while large-scale structures increased in complexity, leading to galaxies and their supermassive black holes. ».*
- One of the most important goals will be to: « *Find the very first gravitationally-bound structures that were assembled in the Universe – precursors to today's galaxies, groups and clusters of galaxies – and trace the subsequent co-evolution of galaxies and super-massive black holes*. »

First Light And Reionization Explorer

FLARE

Main Science Objectives

II. Formation of Stars (and Planets) in the Milky Way (~10-20%)

- A second objective will be to understand the formation of stars.
- This is related to ESA's 1st theme in Cosmic Vision: « What are the conditions for planet formation and the emergence of life? » and more specifically, **« 1.1 From gas and dust to stars and planets »**:
- *« We still lack a comprehensive theory explaining why and how stars form from interstellar matter. The formation of planets has to be considered in the wider context of star formation and circumstellar disc evolution. »*
- The goal will be to: « *Map the birth of stars and planets by peering into the highly obscured cocoons where they form* » by *« Investigating star-formation areas, proto-stars and proto-planetary discs. »*

First Light And Reionization Explorer

FLARE

FLARE will create **an unbiased census of 'first-light' objects that dwell in the early universe, before the end of reionisation** in the same 1–5μm range than JWST, but over much larger fields of view (x100 JWST)

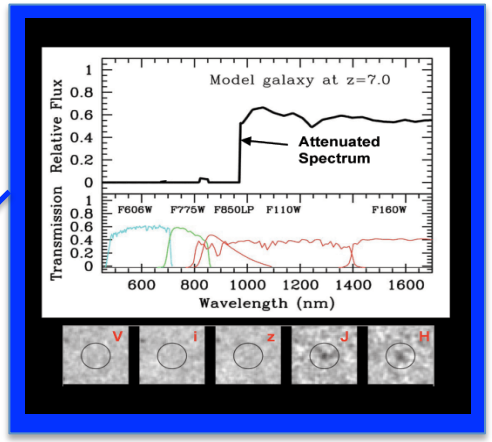

- **Photometric selection:** 100 "first-light" z ~ 15 objects (m_{AB}=28) over 100deg^2.

First Light And Reionization Explorer

FLARE

FLARE will create **an unbiased census of 'first-light' objects that dwell in the early universe, before the end of reionisation** in the same 1–5μm range than JWST, but over much larger fields of view (x100 JWST)

- **Photometric selection:** 100 "first-light" z ~ 15 objects (m_{AB}=28) over 100deg^2.
- **Emission line selection:** blind integral-field spectroscopic survey over 1–2deg^2.

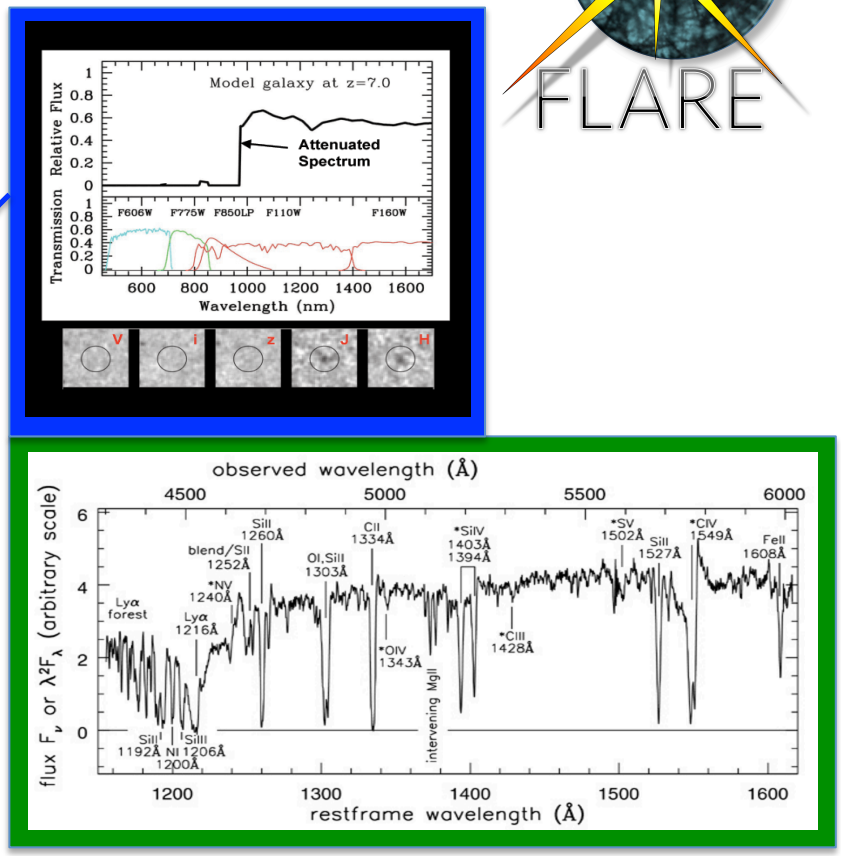

First Light And Reionization Explorer

FLARE

FLARE will create **an unbiased census of 'first-light' objects that dwell in the early universe, before the end of reionisation** in the same 1–5μm range than JWST, but over much larger fields of view (x100 JWST)

- **Photometric selection:** 100 "first-light" z ~ 15 objects (m_{AB}=28) over 100deg^2.
- **Emission line selection: b**lind integral-field spectroscopic survey over 1–2deg^2.
- **Pointed observations of quasars and their early black holes at z > 6**

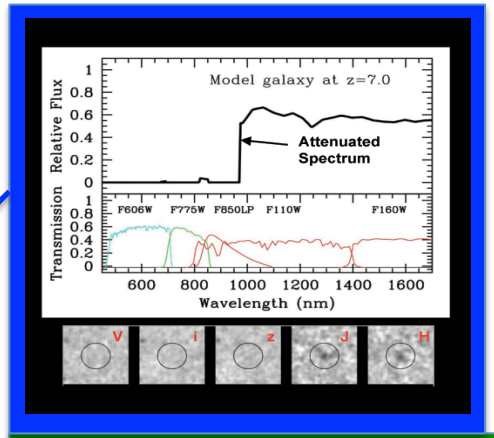

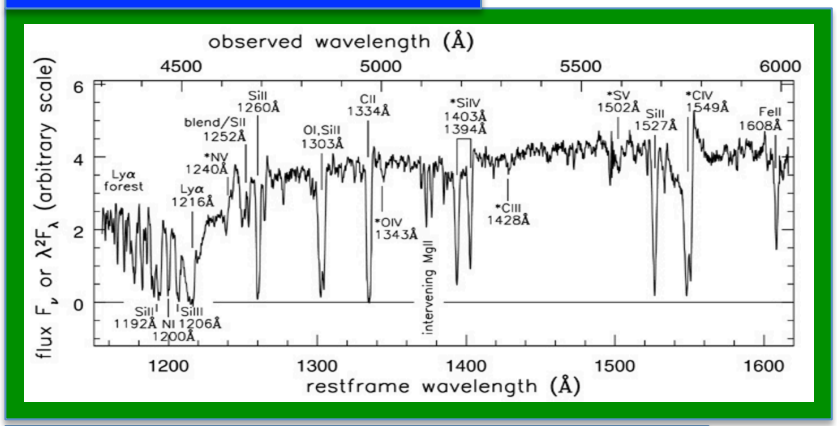

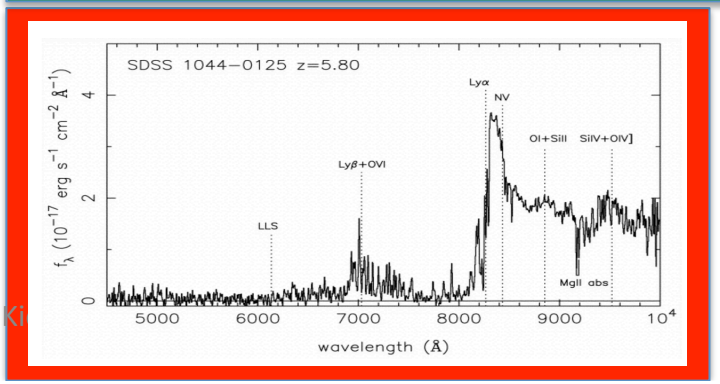

First Light And Reionization Explorer

FLARE

FLARE will create **an unbiased census of 'first-light' objects that dwell in the early universe, before the end of reionisation** in the same 1–5µm range than JWST, but over much larger fields of view (x100 JWST)

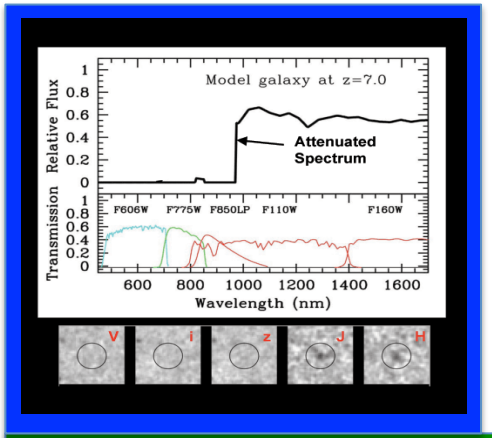

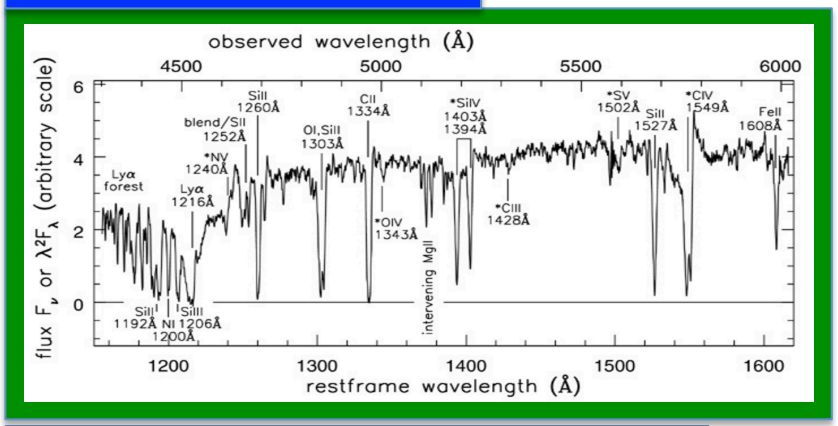

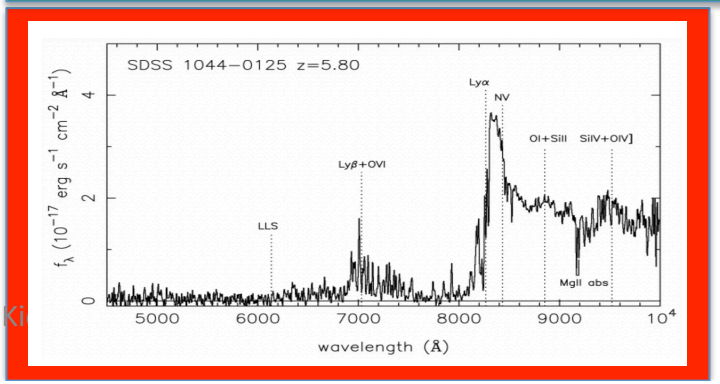

1 mission with parallel imaging & integral-field spectroscopy → 3 populations of objects in the early universe before the End of Reionisation

First Light And Reionization Explorer

FLARE

Top-level science requirements

- Wavelength range: 1 - 5µm
  - 6 filters: identical to JWST NIRCam widebands
  - R=750 in spectroscopy

Purely reflective design
No moving parts: leading to a non-conventional observing strategy

- Sky coverage:
  - Imaging mode: 100 - 200deg2
  - Spectroscopic mode: 1 - 2deg2
  - Wide fields ~ 100 x JWST

Mission Lifetime: > 5 years
Orbit: L2 (Ariane Launcher)
Number of detectors: 12 (10) + 12 (8)
Parallel imaging / spectroscopy (R = 750)

- Imaging Sensitivity: better than 27-28AB (5σ) with 5h per pixel in total

Primary Mirror Diameter: 1.7 – 1.8m
Cooling: Mirrors < 100K, Detectors < 40K

- Deep blind spectroscopic survey ~10^{-18} erg/cm^3/s

Integral-field spectrograph

- Pixel Scale (imaging): ~ 0.22”

Pointing Stability: <0.07” for 300 seconds

First Light And Reionization Explorer

FLARE

Top-level science requirements

- Wavelength range: 1 - 5µm
  - 6 filters: identical to JWST NIRCam widebands
  - R=750 in spectroscopy

Purely reflective design
No moving parts: leading to a non-conventional observing strategy

- Sky coverage:
  - Imaging mode: 100 - 200deg2
  - Spectroscopic mode: 1 - 2deg2
  - Wide fields ~ 100 x JWST

Mission Lifetime: > 5 years
Orbit: L2 (Ariane Launcher)
Number of detectors: 12 (10) + 12 (8)
Parallel imaging / spectroscopy (R = 750)

- Imaging Sensitivity: better than 27-28AB (5σ) with 5h per pixel in total

Primary Mirror Diameter: 1.7 – 1.8m
Cooling: Mirrors < 100K, Detectors < 40K

- Deep blind spectroscopic survey ~10^{-18} erg/cm^3/s

Integral-field spectrograph

- Pixel Scale (imaging): ~ 0.22”

Pointing Stability: <0.07” for 300 seconds

a) 1–5µm
b) fields of view (x100 JWST)
c) blind integral-field spectroscopic survey

3 + 1 questions to define FLARE

a) Why $\lambda > 2$ µm?
b) Why a wide-field survey?
c) Why a blind spectroscopic survey?
d) When?
   - ESA M5 Projects ~ 2029
   - After JWST , Euclid, WFIRST
   - In operation with E-ELT, ATHENA, SKA, ALMA => high synergy

First Light And Reionization Explorer

FLARE

Why λ > 2 μm?

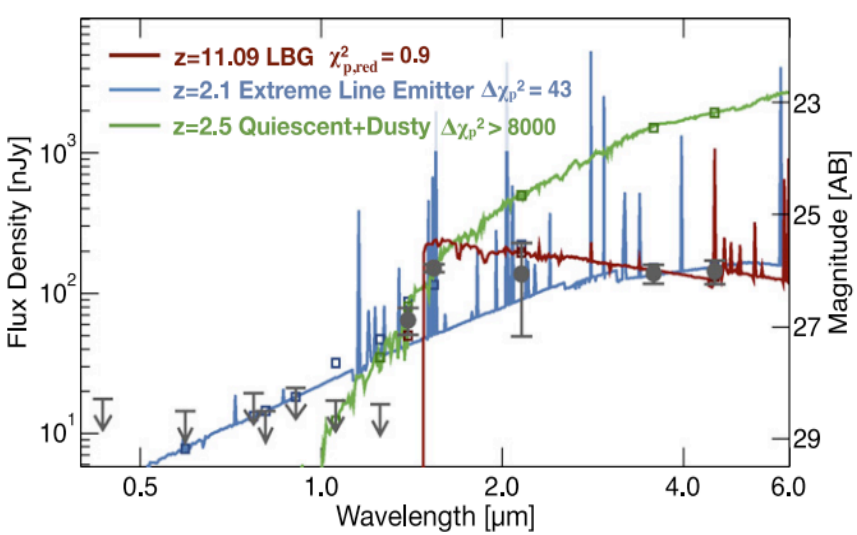

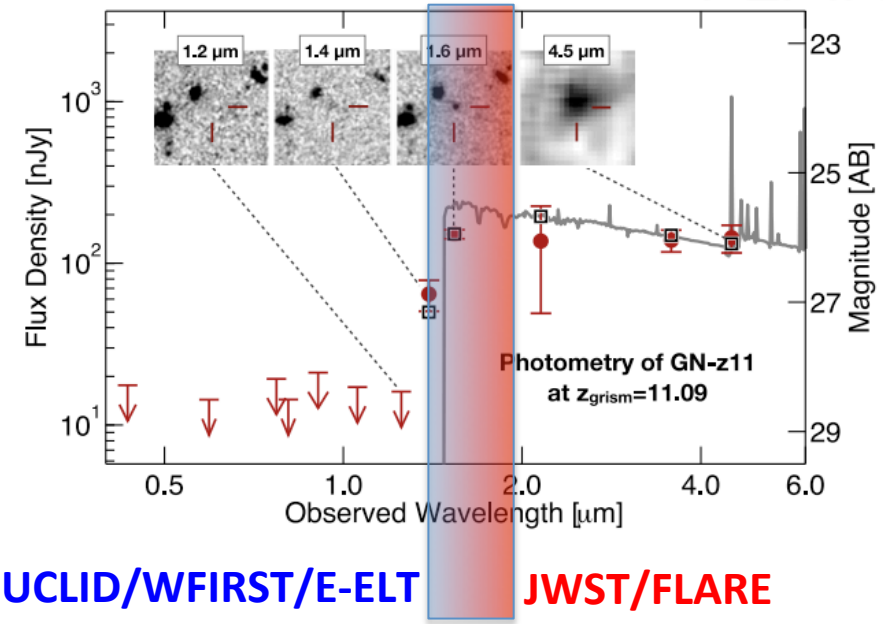

EUCLID/WFIRST/E-ELT JWST/FLARE

The Spectral Energy Distribution of the galaxy discovered at z = 11.09 (Oesch et al. 2016) presents a break around λ = 1.6μm. To get a good estimate of the redshifts in the 10 < z < 15, it is mandatory to collect data before and after the break. The 1 – 5μm wavelength range is therefore needed. This is JWST's choice and, also FLARE's.

Why a Wide-Field Survey?

How many objects at z > 8 – 15?

From I. Iwata		Number Density [objects per 1 deg^2] for AB < 28.0		
	redshift	No Evolution	Empirical	SAM
1.0μm-drop	8-9	4,000	1,700	630
1.4μm-drop	11-12	2,400	100	50
1.8μm-drop	14-17	1,200	0.72	1.1

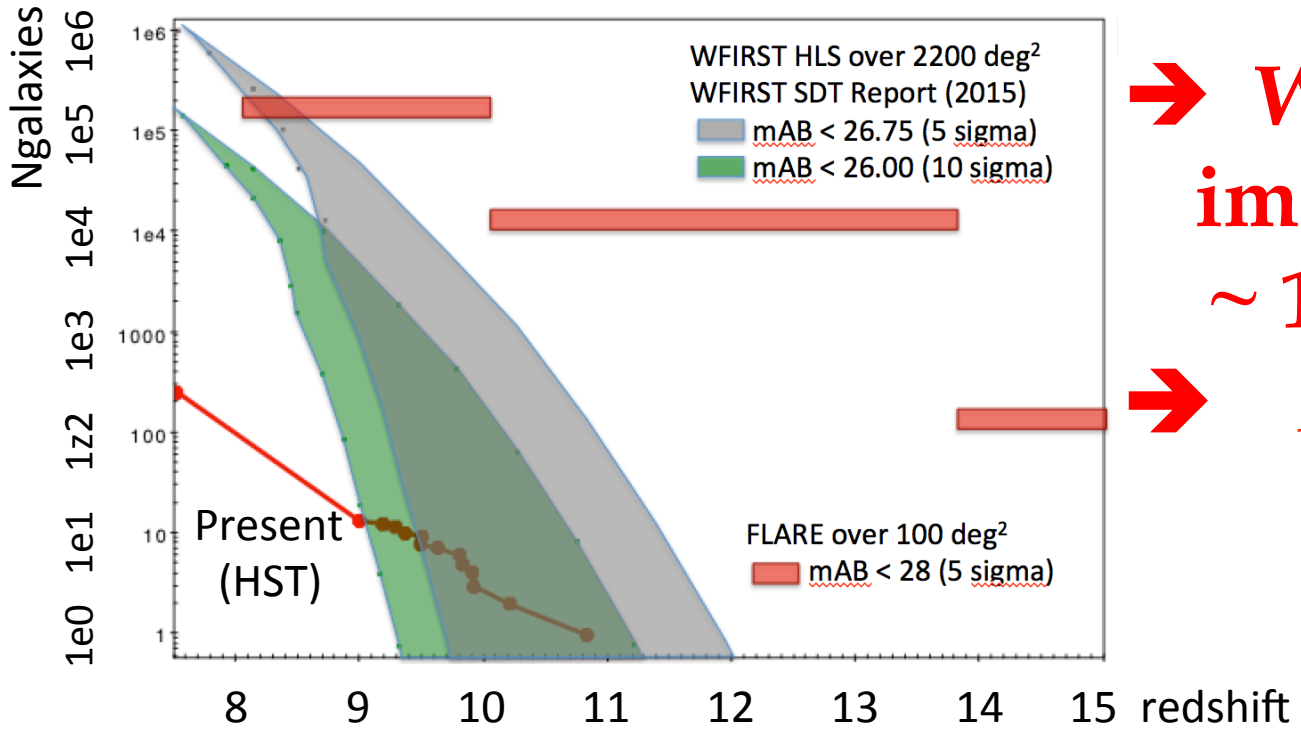

➔ **Wide field imaging survey ~ 100 – 200 deg^2**

➔ ***FLARE***

Why a Wide-Field Survey?

How many objects at z > 8 – 15?

From I. Iwata		Number Density [objects per 1 deg^2] for AB < 28.0		
	redshift	No Evolution	Empirical	SAM
1.0μm-drop	8-9	4,000	1,700	630
1.4μm-drop	11-12	2,400	100	50
1.8μm-drop	14-17	1,200	0.72	1.1

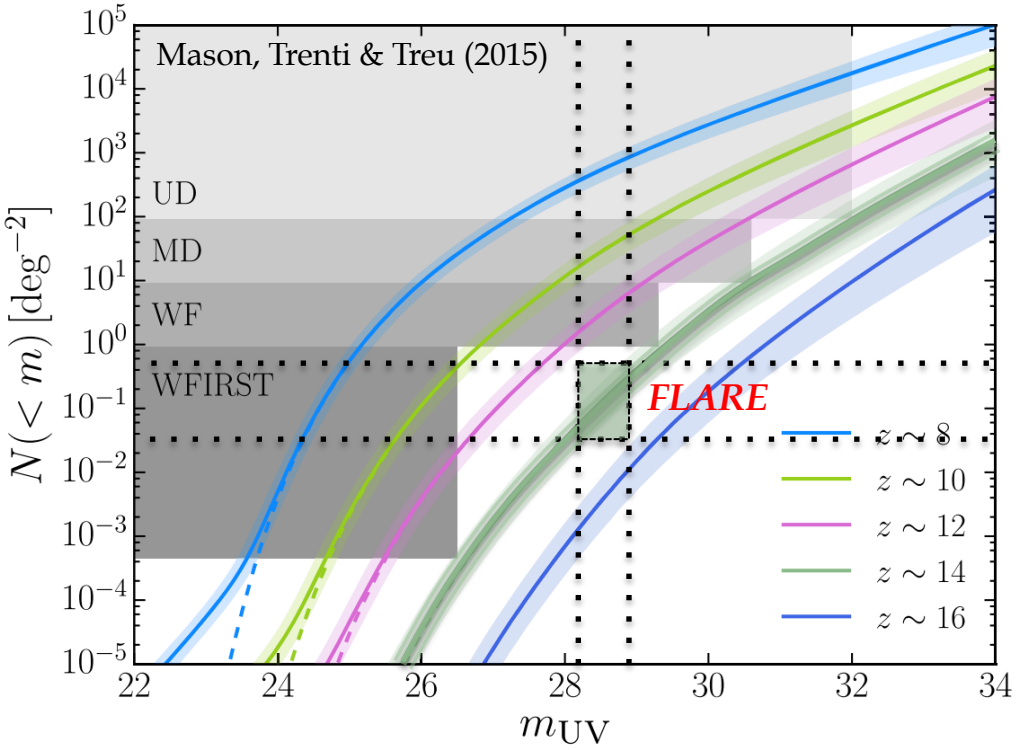

➔ **Wide field imaging survey ~ 100 – 200 deg^2**

➔ ***FLARE***

First Light And Reionization Explorer

FLARE

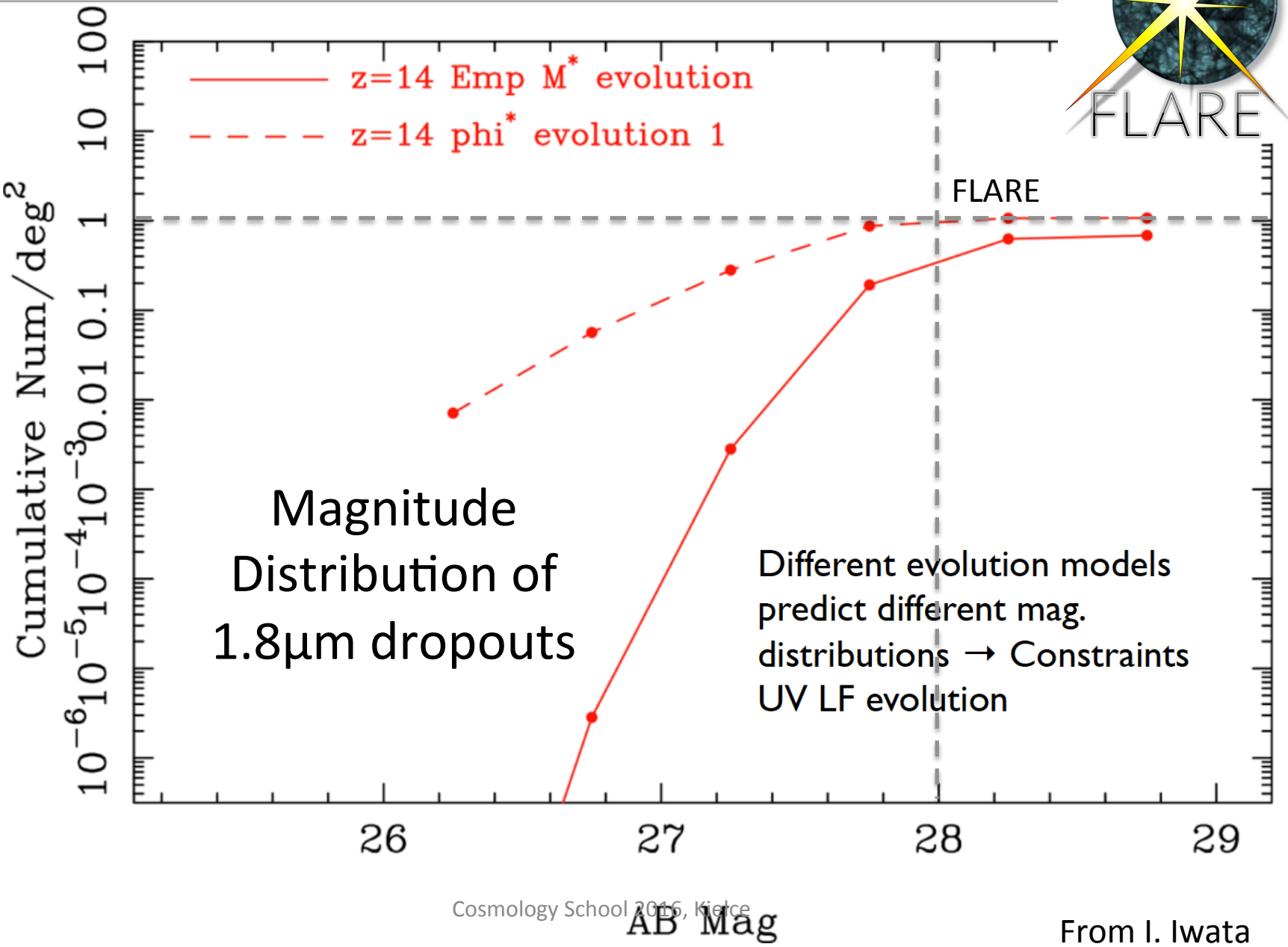

From I. Iwata

Why a blind spectroscopic survey?

Integral-field spectroscopic obs. with MUSE on the VLT (Bacon et al. 2015, A&A 575, A75) in the Hubble Deep Field South allowed to detect as many as

30% of entire Lyα emitter sample, have no HST counterparts with I814 > 29.5.

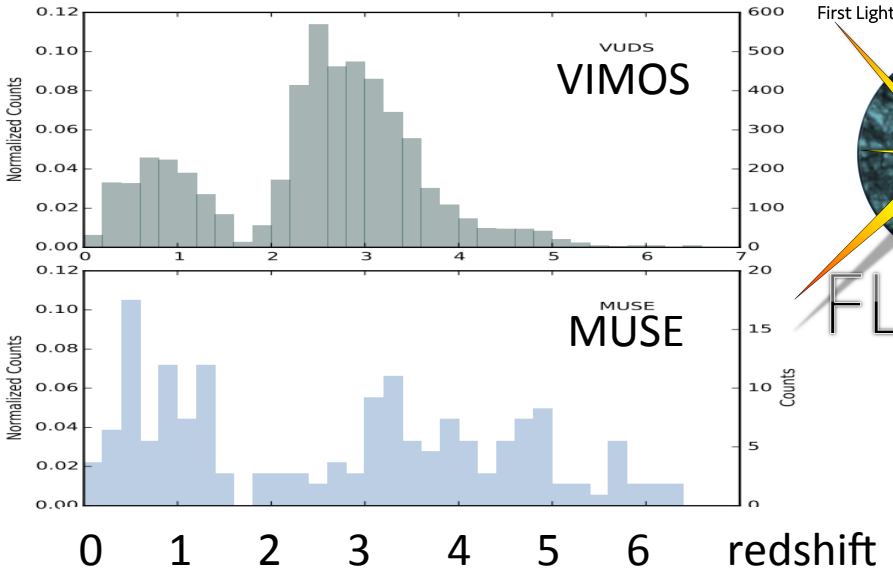

First Light And Reionization Explorer

FLARE

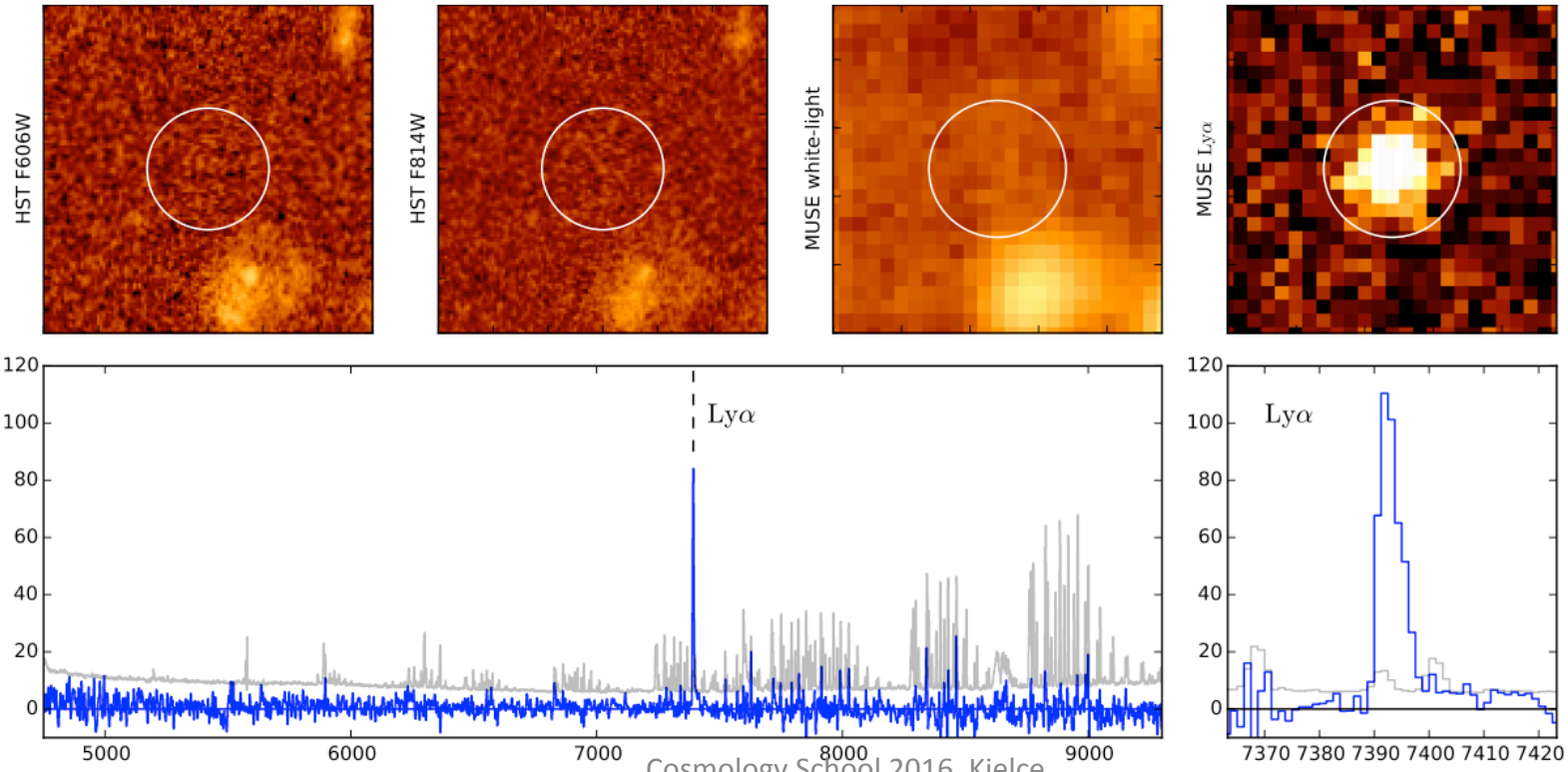

Simulations of an integral-field observation (1 arcmin^2) using our code *CIGALE*. About 5000 galaxy (N(z) from from eGalics SAM, Cousin et al. 2015) spectra included in these FLARE simulations.

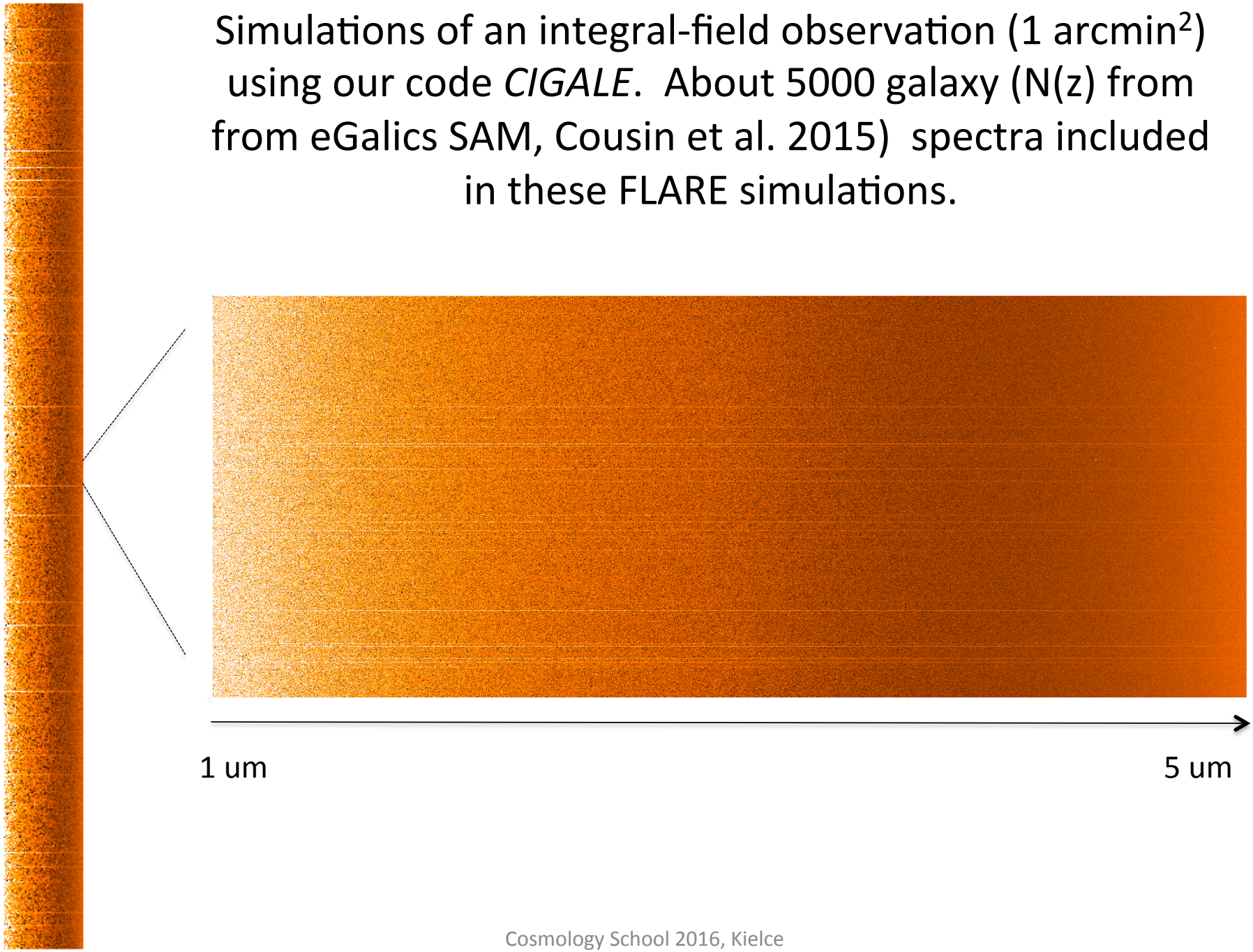

CIGALE Galaxy Emission Modelling

1 um 5 um

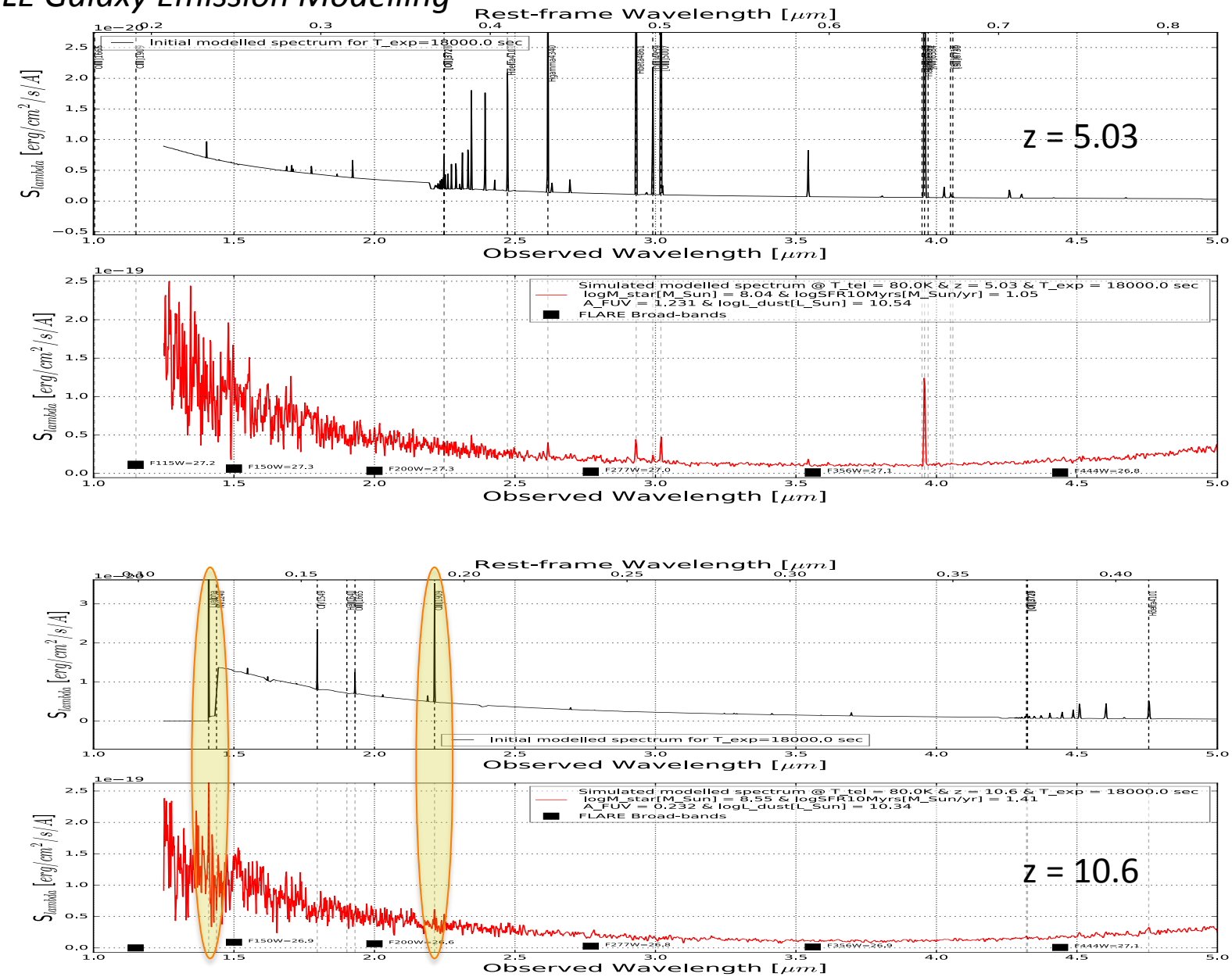

A spectroscopic mode for WISH (assuming 1.5m-telescope)

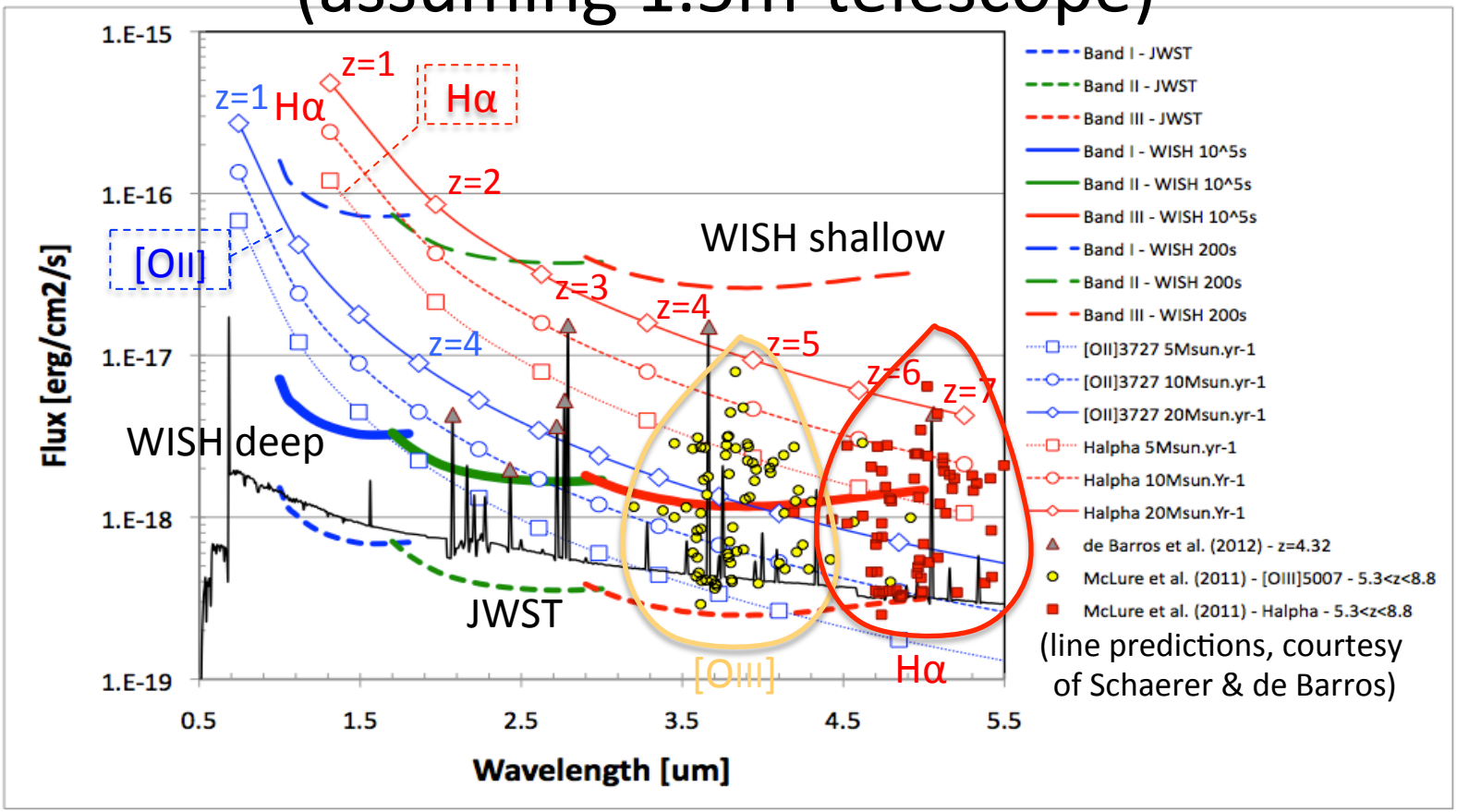

Expected lines fluxes and sensitivity of WISH and JWST. We overplot a spectrum of a sub-L LBG (M_{UV} = -20.) at z = 4.32 from de Barros et al. (2012, black). The* ***main lines in the rest-frame optical range can be detected at S/N=10****. Yellow dots and red boxes correspond to [OIII]5007 and Hα lines from McLure et al. (2011) at 5.3 < z < 8.8. Almost half of them can be detected showing that we are able to confirm the redshift of these objects and to measure in detail the strength of these lines. Thin blue lines (continuous, dashed, dotted for 20 M_{Sun}/yr, 10 M_{Sun}/yr & 5 M_{Sun}/yr) correspond to [OII]3727 from z = 1 to z = 11 while the thin red lines (same as blue but from z = 1 to z = 7) correspond to Hα. Both are computed assuming Kennicutt (1998).*

FLARE's observational strategy

First Light And Reionization Explorer

FLARE

see movie at http://mission.lam.fr/flare/SurveysMar2016.html

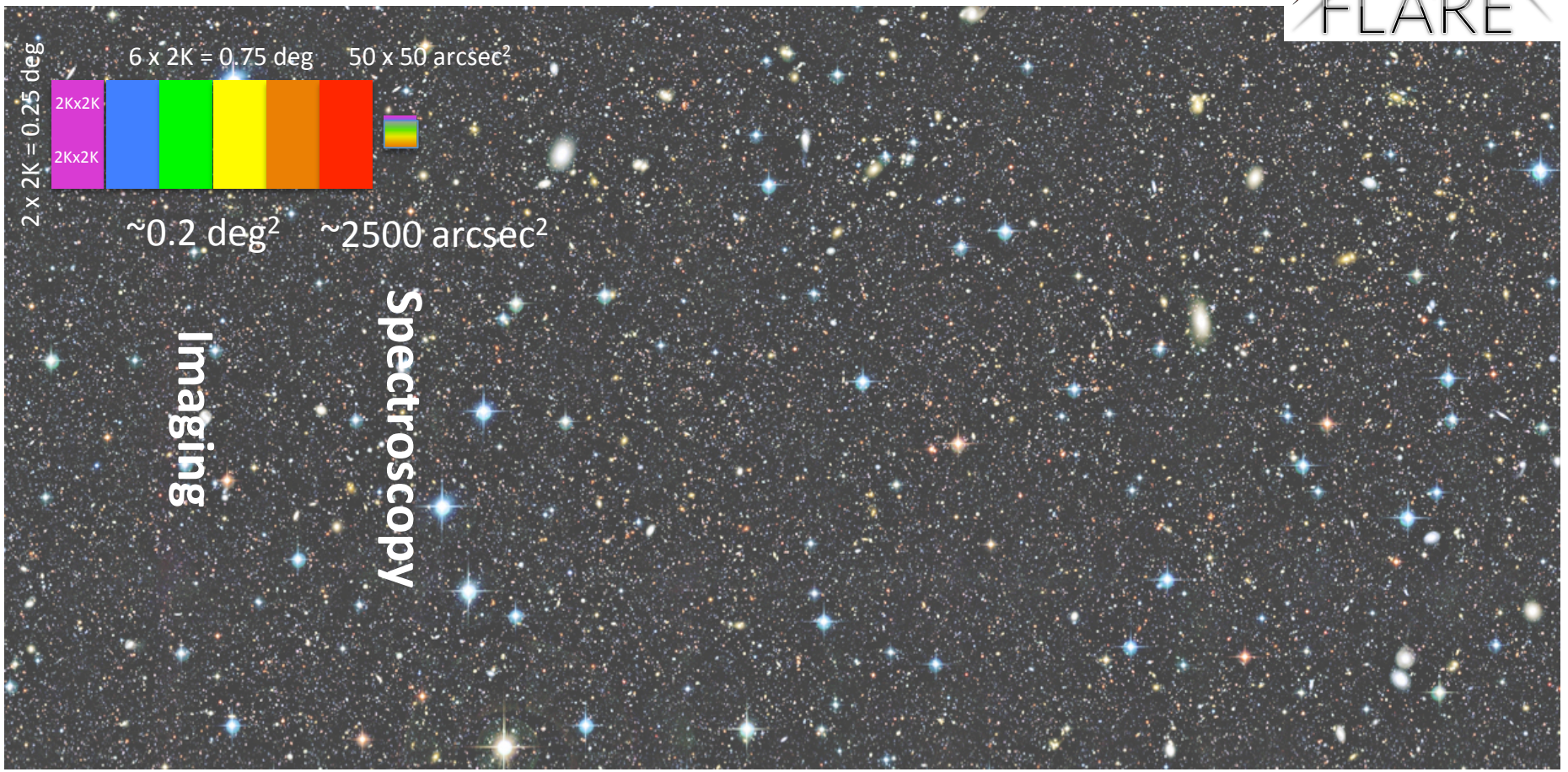

Imaging and spectroscopic fields of view not at the same scale.

First Light And Reionization Explorer

FLARE

see movie at http://mission.lam.fr/flare/SurveysMar2016.html

Imaging and spectroscopic fields of view not at the same scale.

First Light And Reionization Explorer

FLARE

see movie at http://mission.lam.fr/flare/SurveysMar2016.html

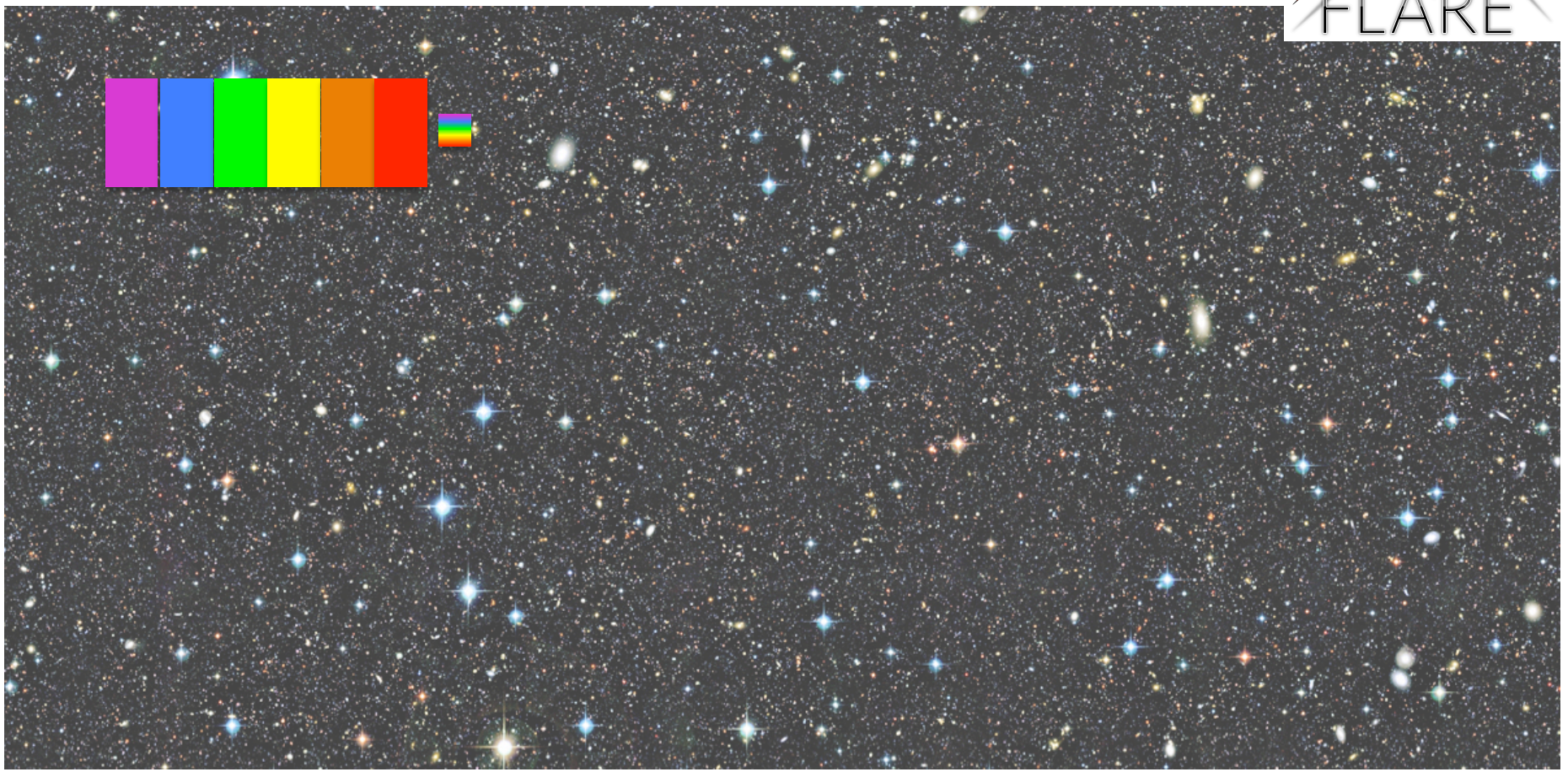

Imaging and spectroscopic fields of view not at the same scale.

First Light And Reionization Explorer

FLARE

see movie at http://mission.lam.fr/flare/SurveysMar2016.html

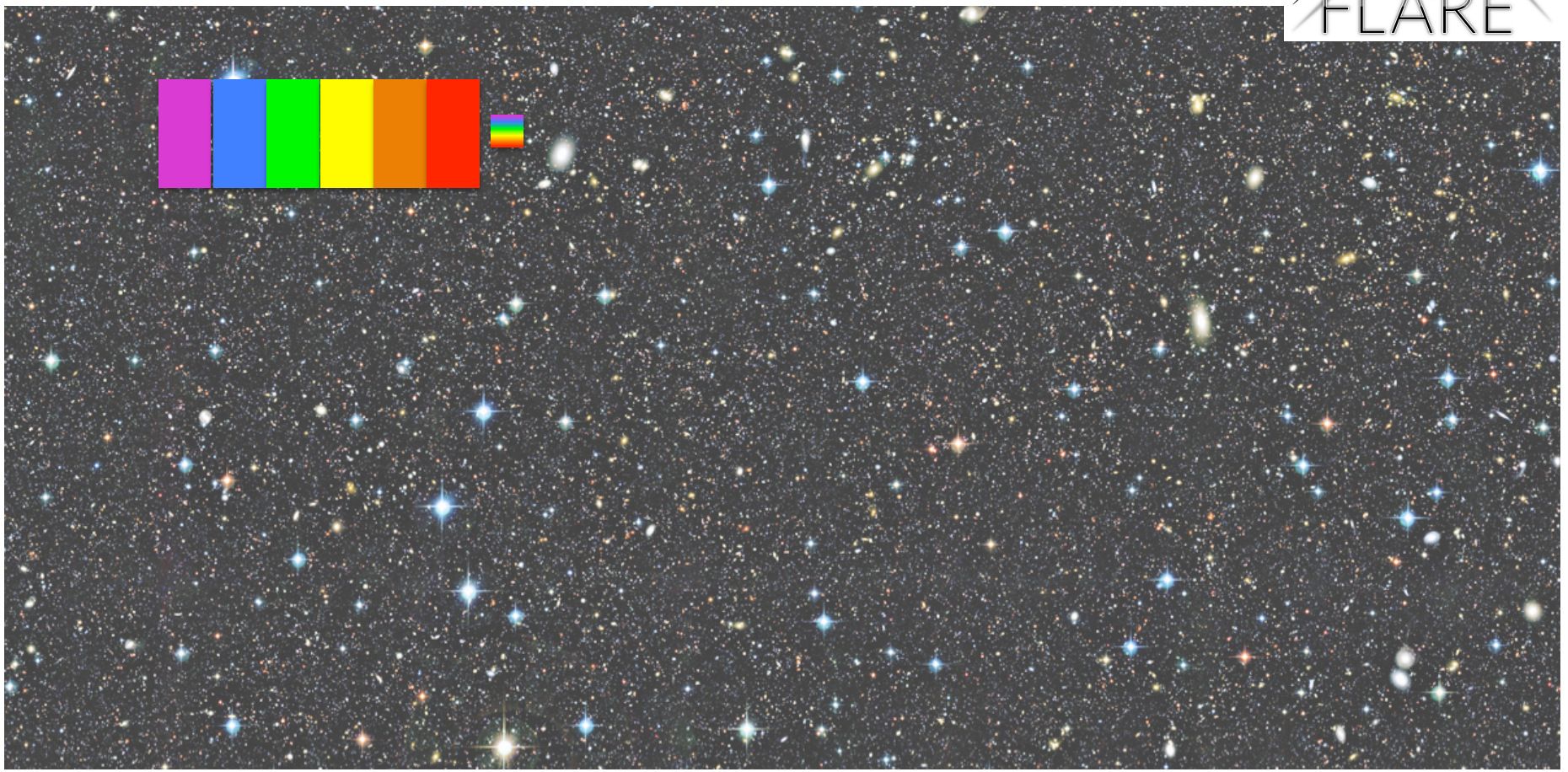

Imaging and spectroscopic fields of view not at the same scale.

First Light And Reionization Explorer

FLARE

see movie at http://mission.lam.fr/flare/SurveysMar2016.html

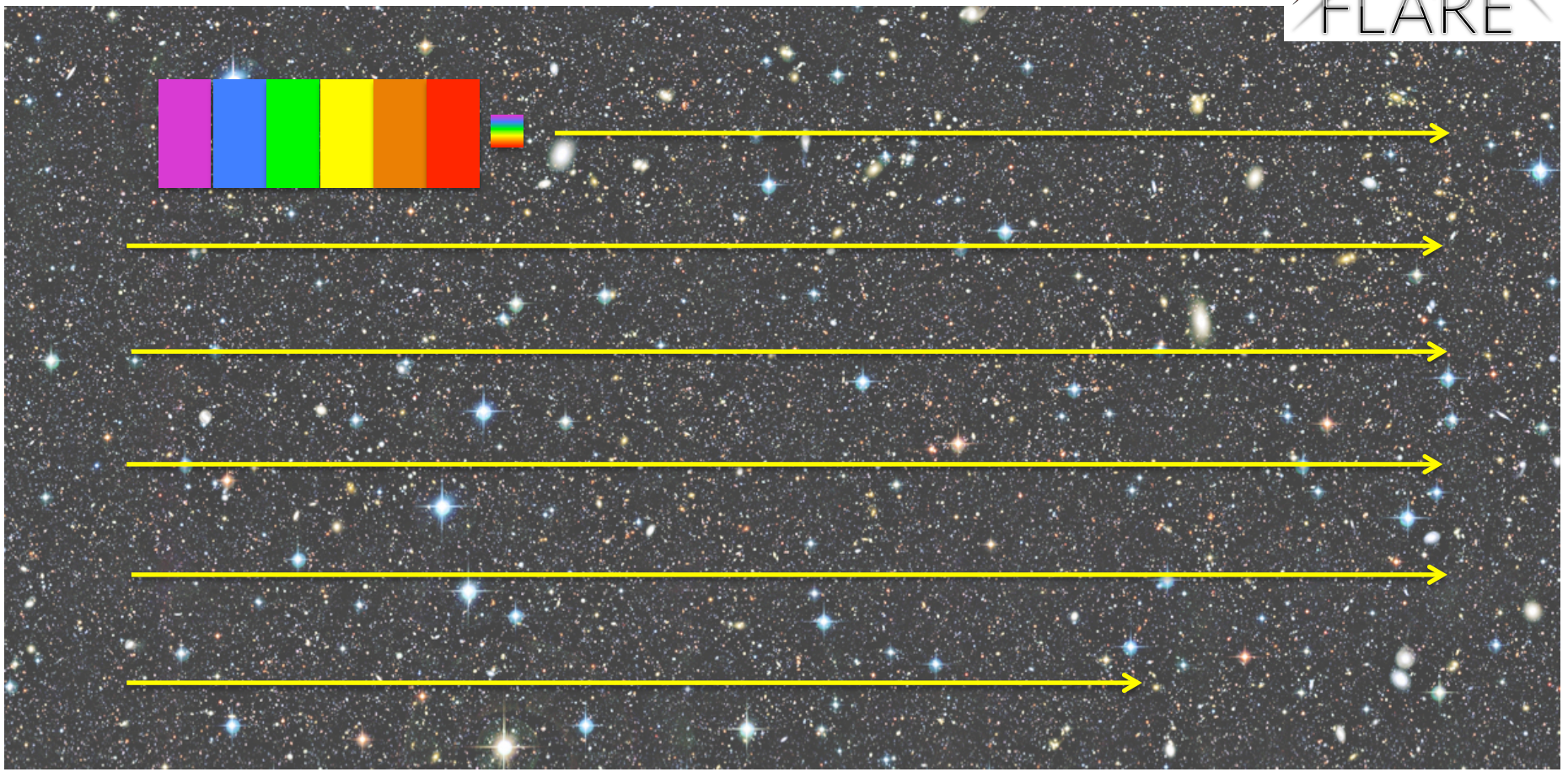

Imaging and spectroscopic fields of view not at the same scale.

FLARE Observational Strategy

see movie at http://mission.lam.fr/flare/SurveysMar2016.html

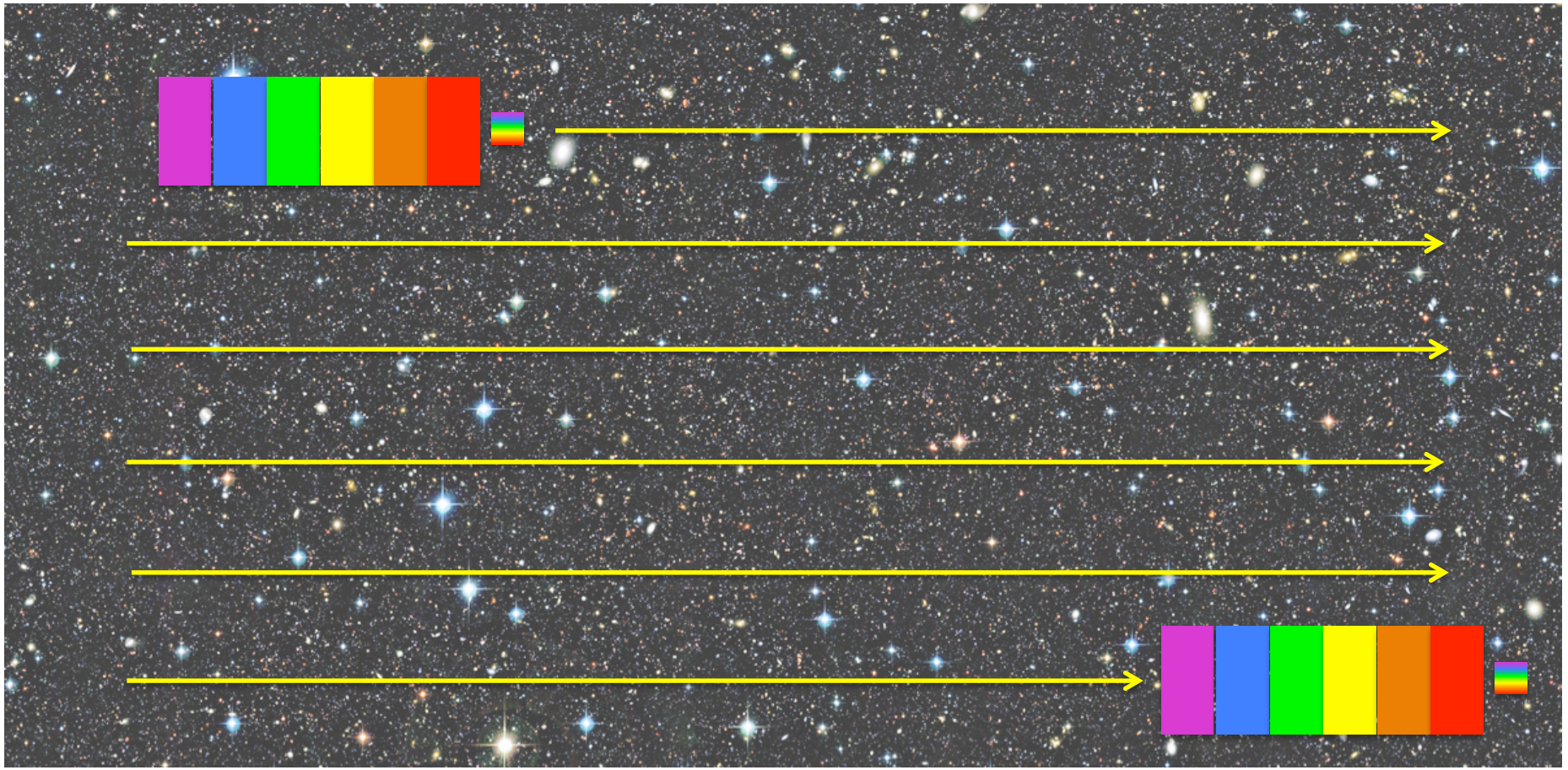

Imaging and spectroscopic fields of view not at the same scale.

FLARE Observational Strategy

see movie at http://mission.lam.fr/flare/SurveysMar2016.html

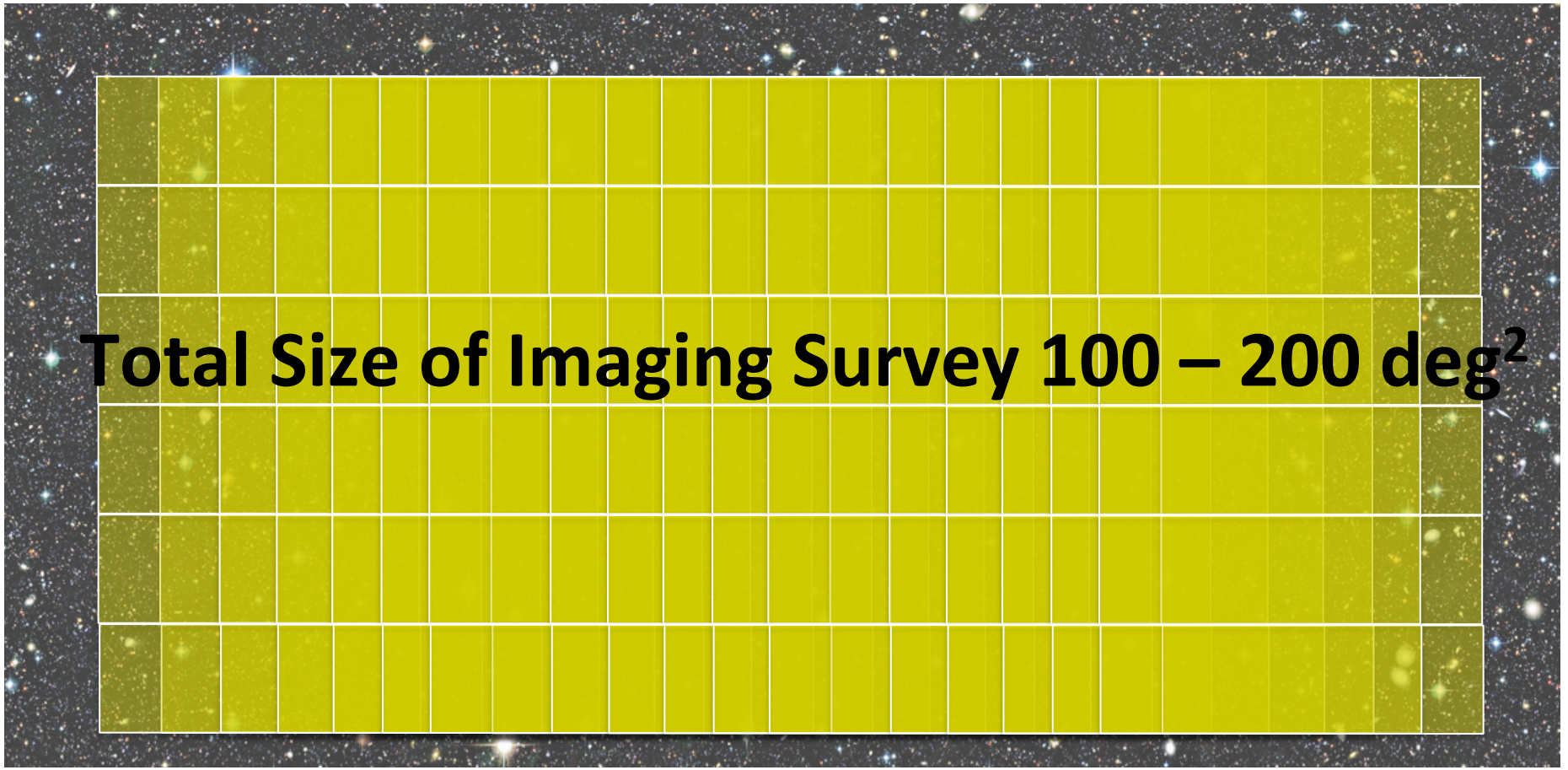

Imaging and spectroscopic fields of view not at the same scale.

FLARE Observational Strategy

see movie at http://mission.lam.fr/flare/SurveysMar2016.html

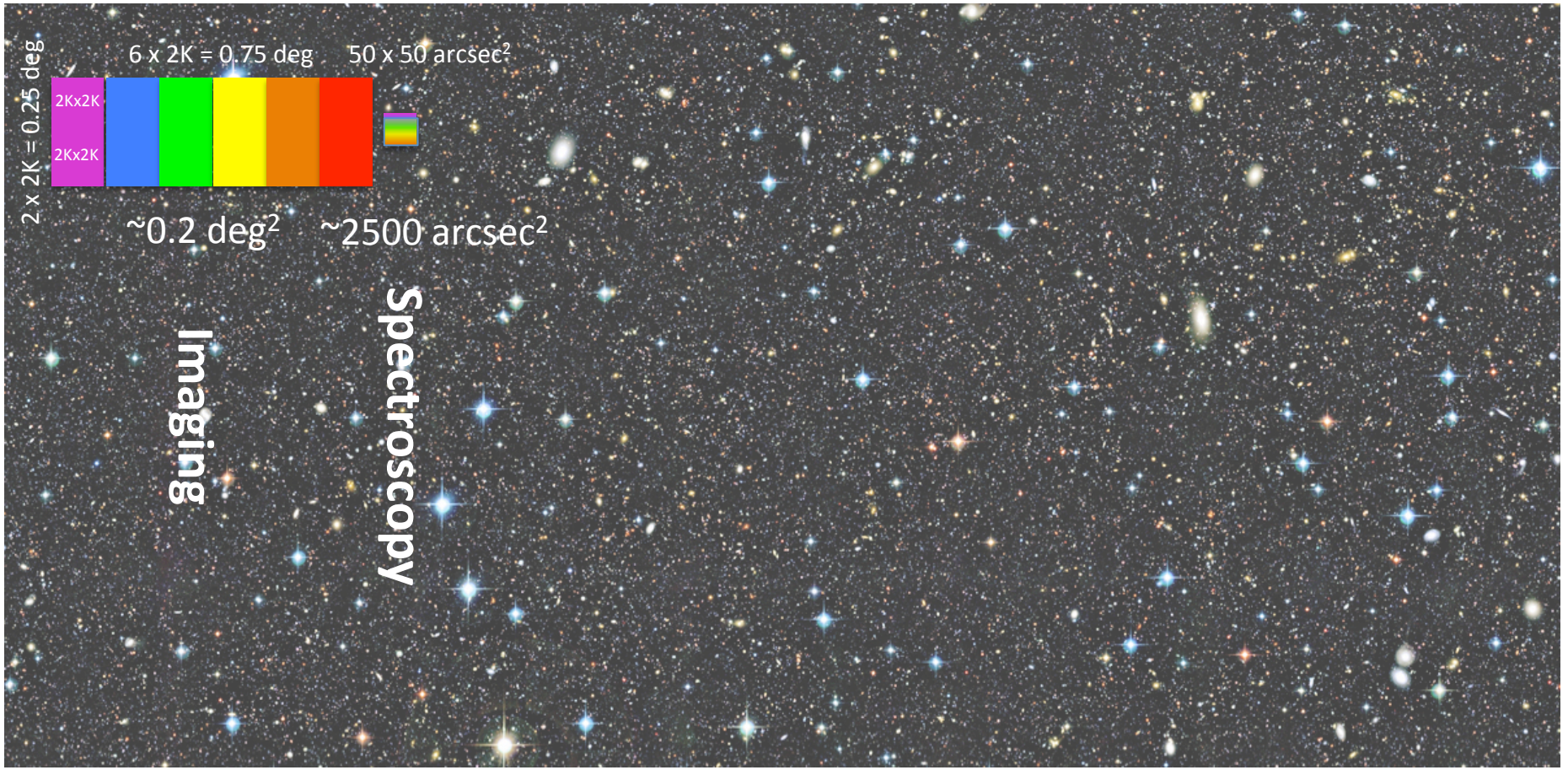

Imaging and spectroscopic fields of view not at the same scale.

First Light And Reionization Explorer

FLARE

Non contiguous Spectroscopic Survey

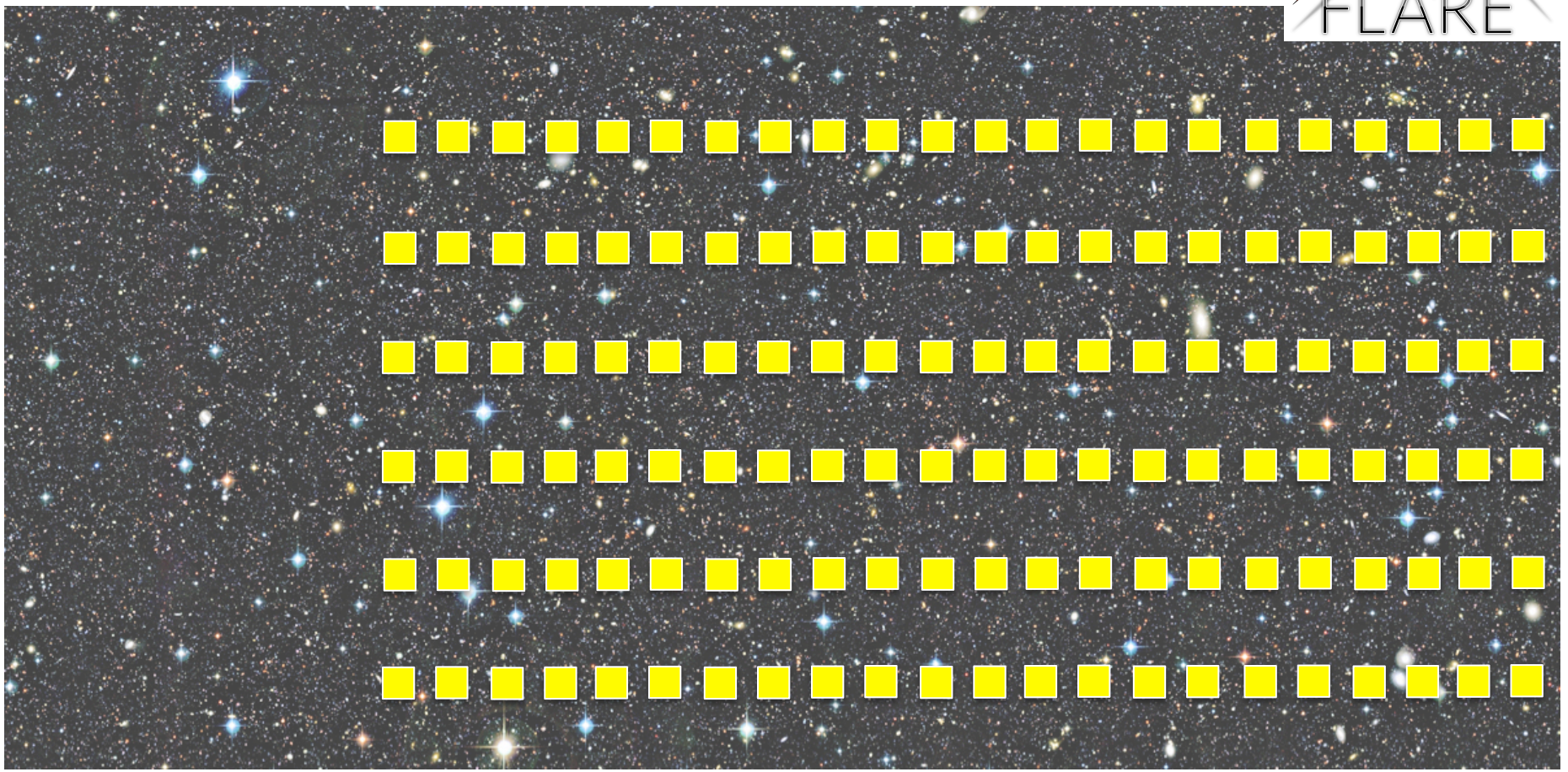

Imaging and spectroscopic fields of view not at the same scale.

First Light And Reionization Explorer

FLARE

Total Size of Spectroscopic Survey 1 – 2 deg²

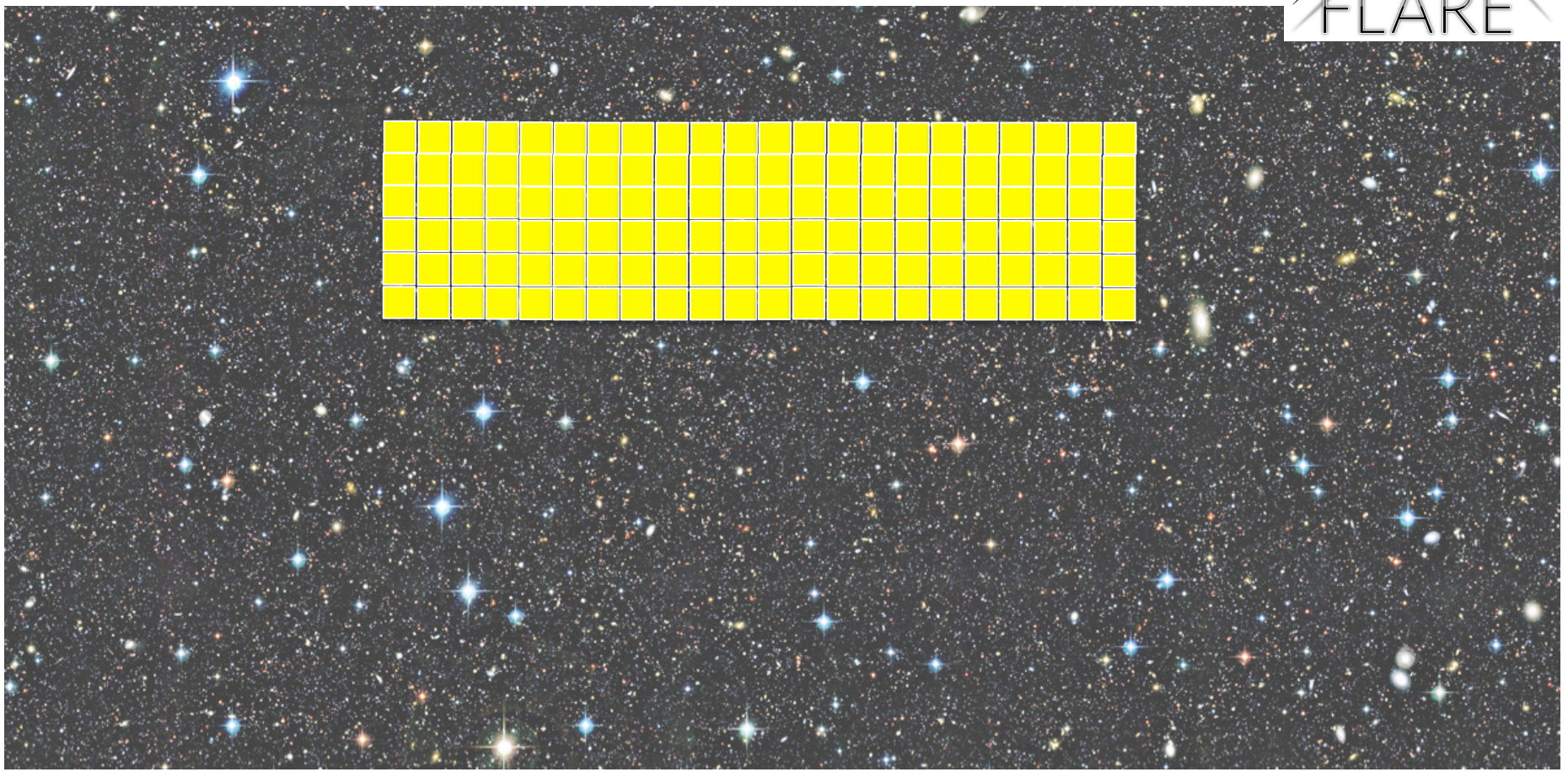

Imaging and spectroscopic fields of view not at the same scale.


First Light And Reionization Explorer
FLARE
First Light And Reionization Explorer (FLARE)
A mission proposal for ESA M5
The Starry Night - Vincent van Gogh - Arles 1889
dénis.burgarella@lam.fr

WFIRST HLS - WFIRST SDT Report (2015)

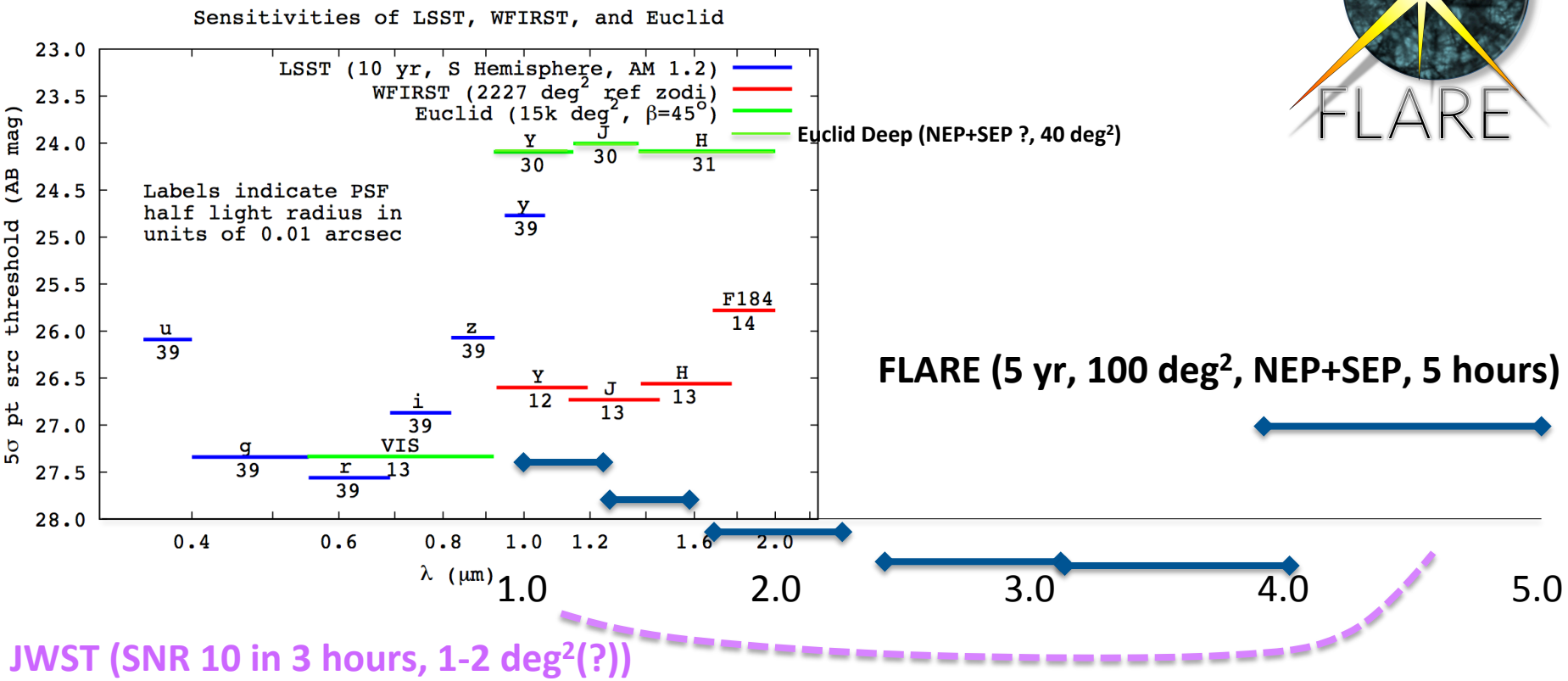

Depth in ABmag of WFIRST (**red**) Euclid (**green**) and LSST (**blue**) imaging surveys. Labels indicate the size of the PSF in units of 0.01 arcsec. JWST (**lavander**) and FLARE (**ocean**).

Line sensitivity of FLARE predicted by CIGALE SIM

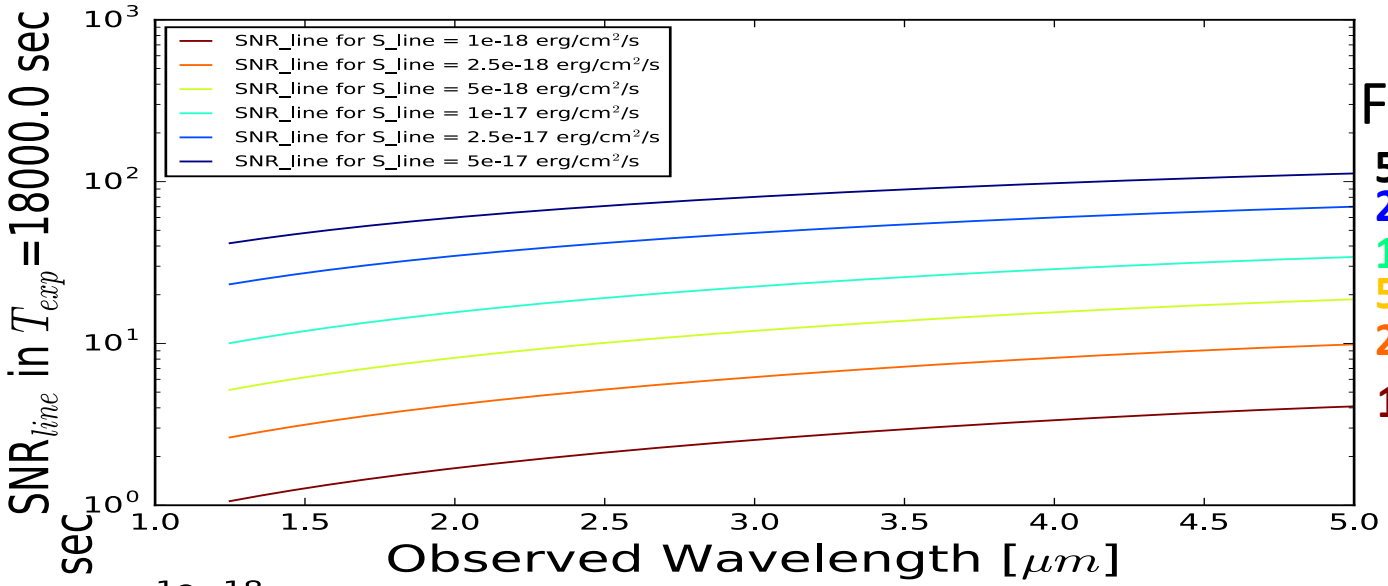

F_λ [erg/cm²/s]

5.0x10^{-17}
2.5x10^{-17}
1.0x10^{-17}
5.0x10^{-18}
2.5x10^{-18}
1.0x10^{-18}

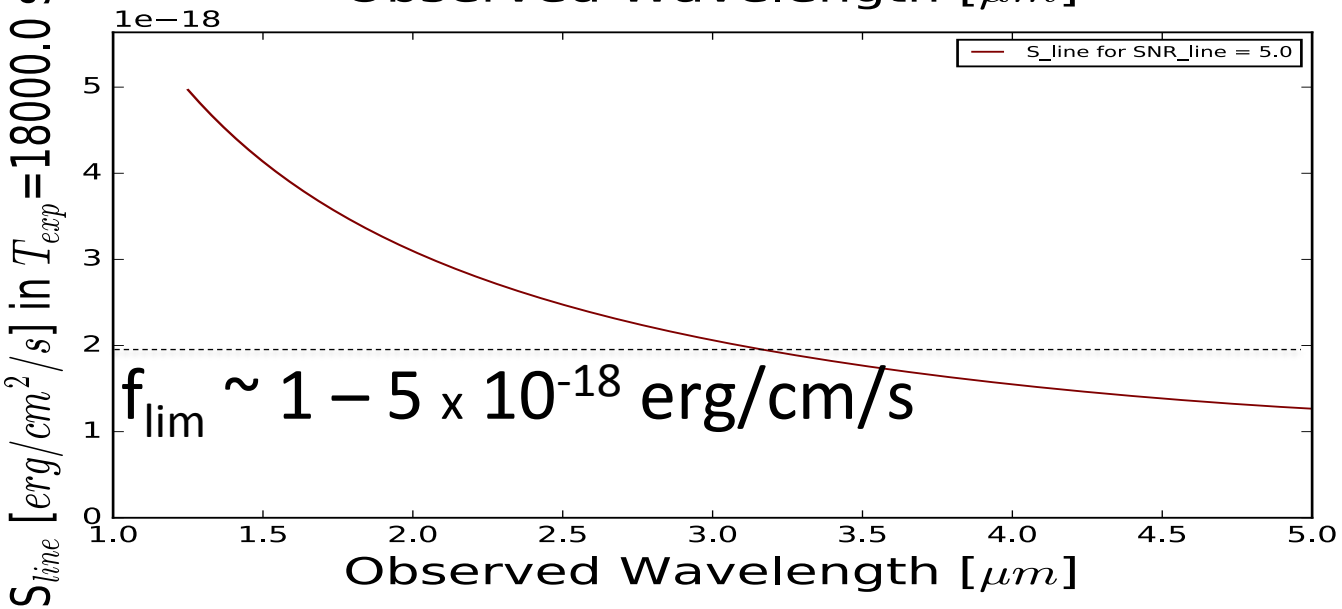

$f_{lim} \sim 1 - 5 \times 10^{-18}$ erg/cm/s

Number of galaxies detected at 5.5<z<6.5 in Halpha by FLARE @R=750 and JWST NIRSpec

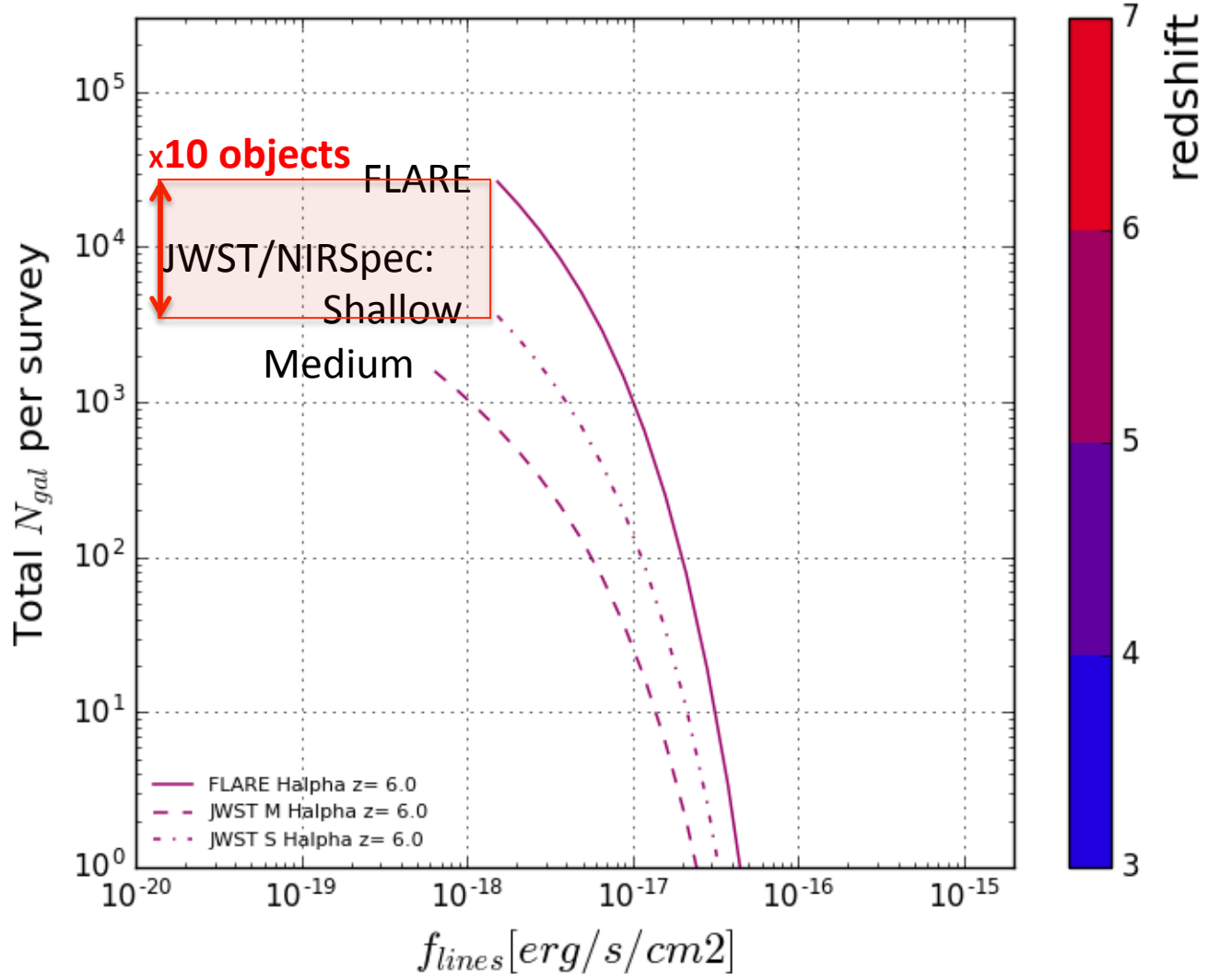

First Light And Reionization Explorer

FLARE

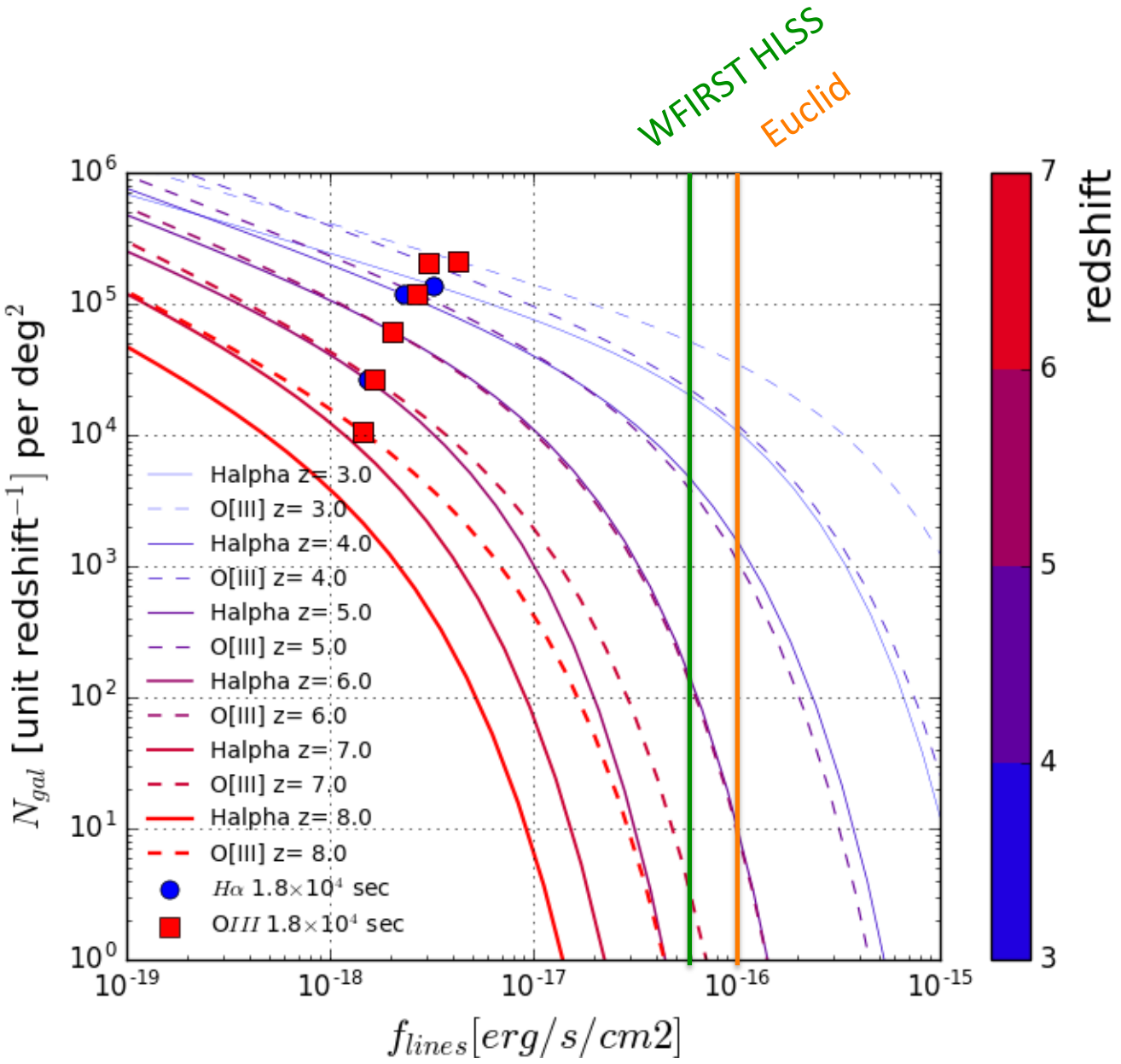

Number of galaxies detected at 2.5<z<8.5 in Halpha and [OIII]5007 by FLARE


ATTENTION SPAN REMAINING:
3
27
Minutes
Seconds
CARTOONSTOCK .com
Search ID: bven577
©NELEY

Calanque En Vau

Cosmology School 2016, Kielce

Calanque En Vau

Cosmology School 2016, Kielce

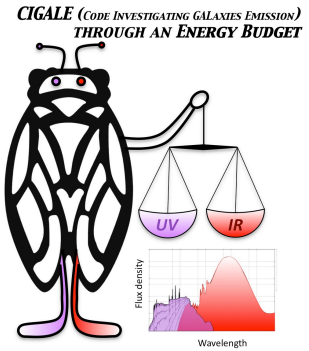

The Emission of Galaxies over the Whole Electromagnetic Spectrum

Denis Burgarella, Astronomer

Laboratoire d'Astrophysique de Marseille, France

denis.burgarella@lam.fr

SECOND COSMOLOGY SCHOOL

INTRODUCTION TO COSMOLOGY
Kielce, Poland 11.07 - 24.07.2016

What are Spectral Energy Distributions?

The spectral energy distributions (SEDs) of galaxies are shaped by nearly every physical property of the galaxy and among others:

- the star formation history,
- the metal content,
- the chemical compositions and their evolution,
- the dust characteristics (amount, attenuation law, etc.),
- the grain size distribution,
- the star-dust geometry,
- the interstellar radiation field,
- the initial mass function,
- etc.

http://ned.ipac.caltech.edu/level5/March13/Lagache/Lagache2.html

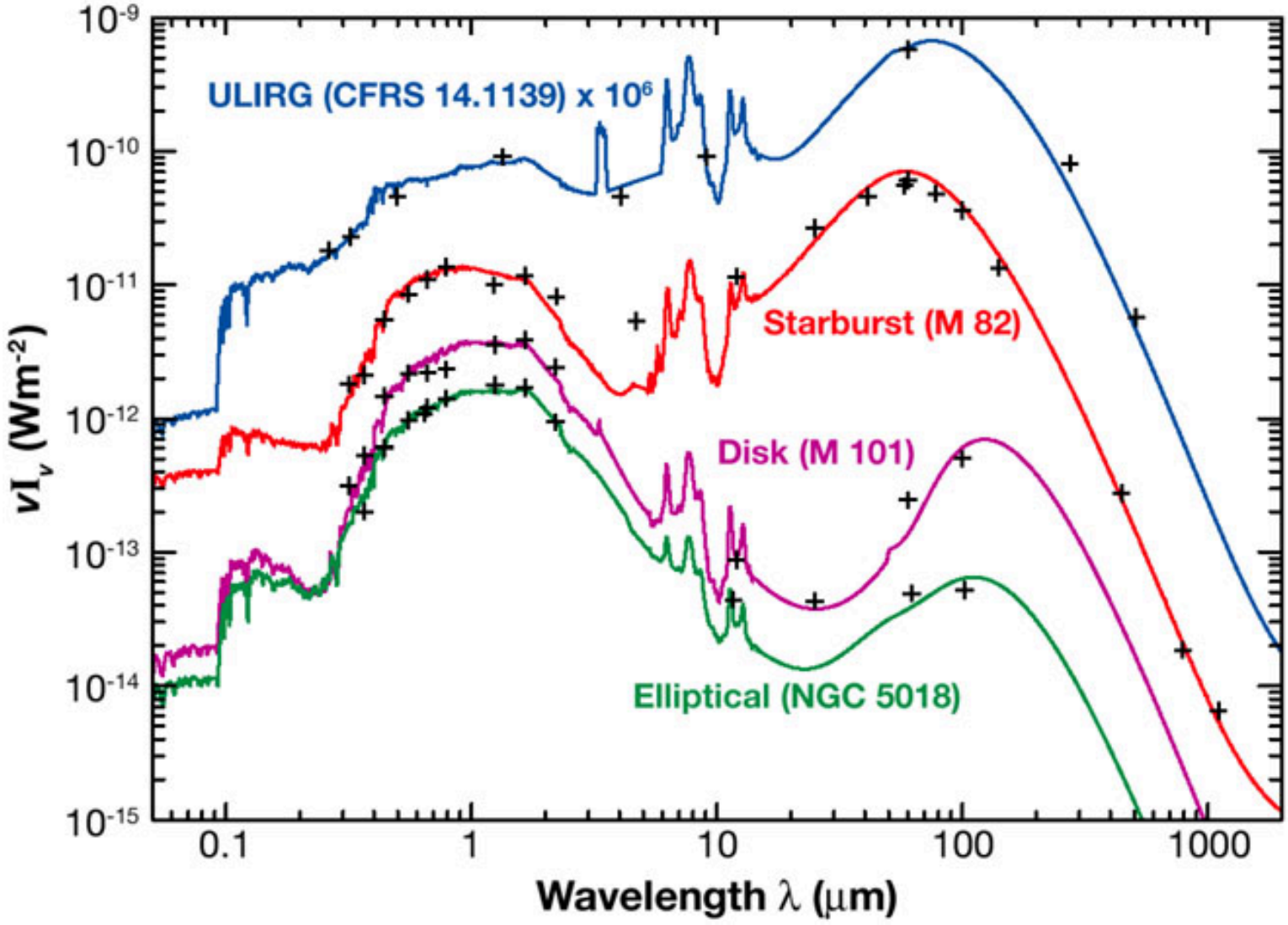

Spectral energy distributions of galaxies from UV to the millimeter. The ULIRG is observed at redshift z = 0.66 and is represented here in the rest-frame (from Galliano 2004).

Many of the fundamental properties of unresolved stellar populations are encoded in their SEDs.

These properties include the star formation history (SFH), stellar metallicity and abundance pattern, stellar initial mass function (IMF), total mass in stars, and the physical state and quantity of dust and gas.

Some of these properties are easier to measure than others, and each provides important clues regarding the formation and evolution of galaxies.

It is precisely these quantities, measured from the SEDs of galaxies, that have provided the foundation for our modern understanding of galaxy formation and evolution.

What information can we extract from the Spectral Energy Distributions?

The principal goal of SED fitting is to extract the previous parameters from observed SEDs.

In this review, I will present an overview of the Population Synthesis technique and discuss what can be reliably measured from galaxy SEDs.

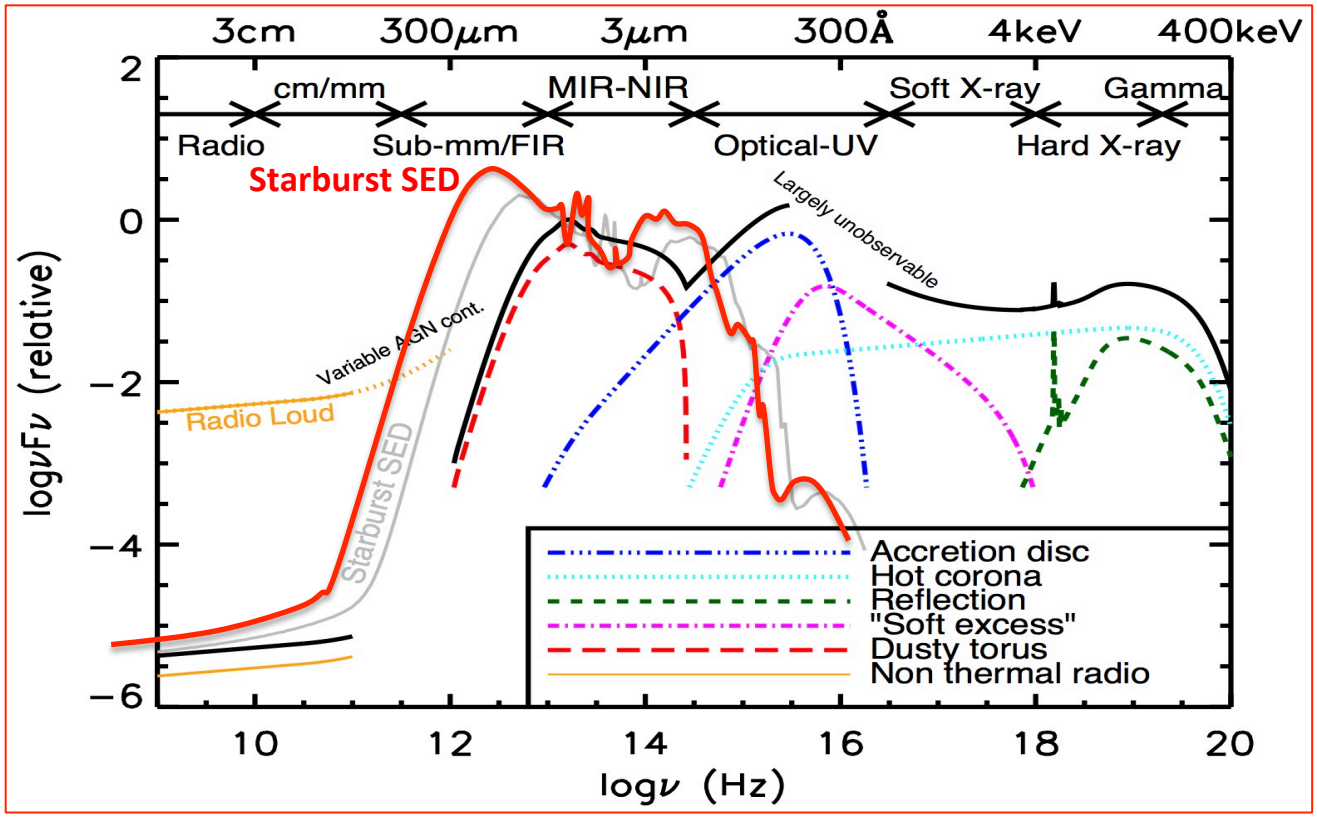

The starting point of any SED model is the simple stellar population (SSP), which describes the evolution in time of the SED of a single, coeval stellar population at a single metallicity and abundance pattern.

An SSP therefore requires three basic inputs: stellar evolution theory in the form of isochrones, stellar spectral libraries, and an IMF, each of which may in principle be a function of metallicity and/or elemental abundance pattern. These components are typically combined in the following way:

$$f_{\rm SSP}(t,Z) = \int_{m_{\rm lo}}^{m_{\rm up}(t)} f_{\rm star}\left[T_{\rm eff}(M), \log g(M) | t, Z\right] \Phi(M)\, {\rm d}M,$$

where M is the initial (zero-age main sequence) stellar mass, Φ(M) is the initial mass function, f_{star} is a stellar spectrum, and f_{SSP} is the resulting time and metallicity-dependent SSP spectrum. The lower limit of integration, m_{lo}, is typically taken to by the hydrogen burning limit (either 0.08 or 0.1$M_\odot$ depending on the model), and the upper limit is dictated by stellar evolution. The isochrones determine the relation between T_{eff}, log g, and M for a given t and Z.

Constructing stellar models might be difficult

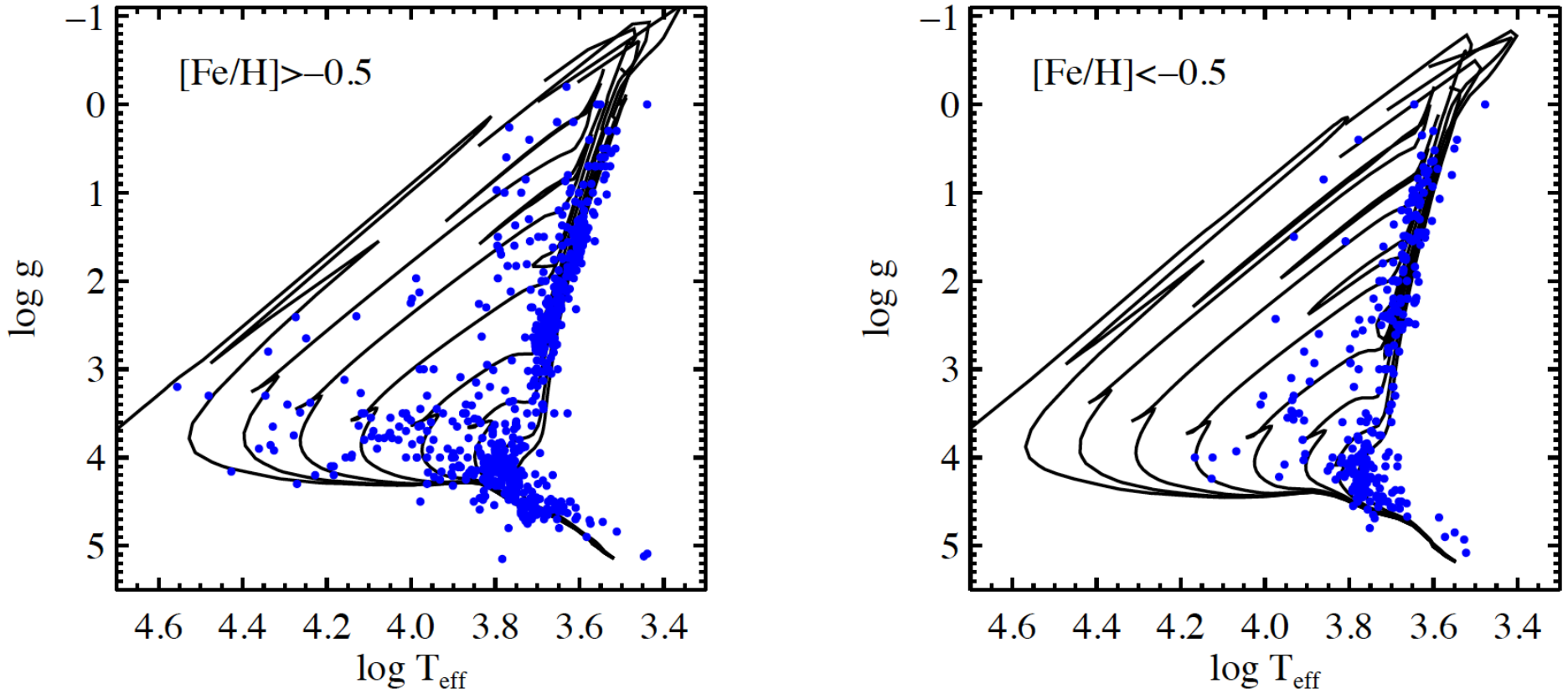

From Conroy (2013)

Figure 2:

Physical properties of the MILES empirical spectral library, separated by [Fe/H] (solid symbols). Isochrones from the Padova group are overplotted for $t = 3 \times 10^6 - 10^{10}$ yr. Typical errors on $T_{\rm eff}$ and $\log g$ are $60 - 100$ K and 0.2 dex, respectively (Cenarro et al. 2007). Notice that the MILES library covers the lower main sequence and RGB both at high and low metallicity, but it only sparsely covers the upper main sequence and supergiants. This figure highlights the difficulty in constructing SPS models based on empirical stellar libraries, especially at low metallicity.

Changing the IMF can strongly impact the modelled SED

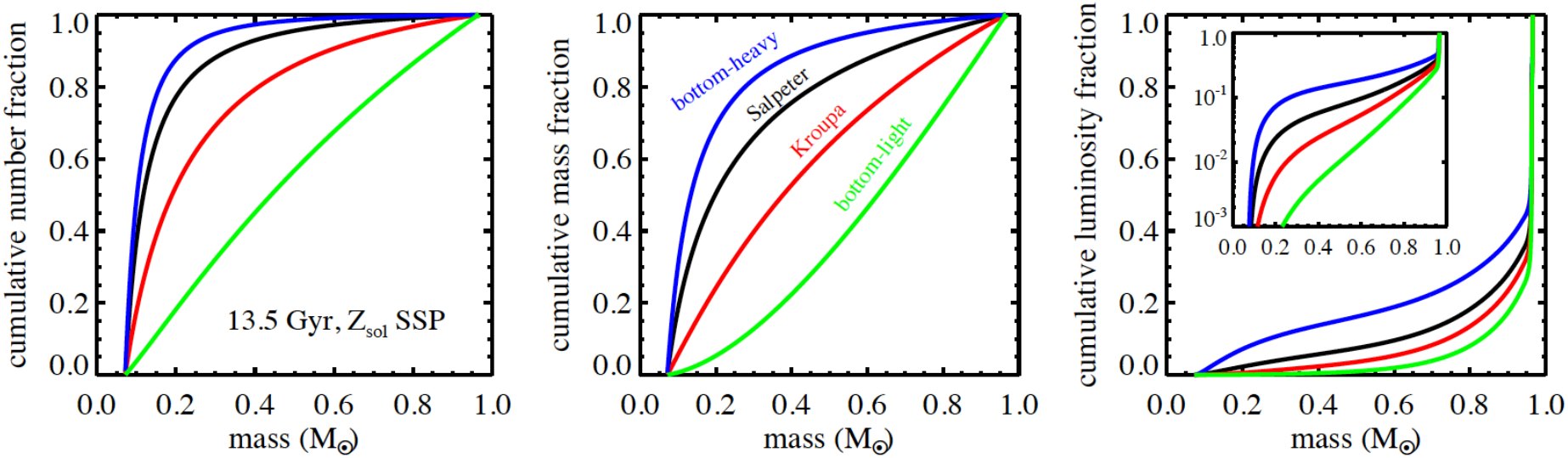

From Conroy (2013)

Figure 4:

Fractional contribution to the total number, mass, and bolometric luminosity as a function of stellar mass for a 13.5 Gyr solar metallicity model. Lines correspond to different IMFs: a bottom-heavy with logarithmic slope $x = 3.0$ (blue line); Salpeter ($x = 2.35$; black line); MW IMF (specifically a Kroupa IMF; red line); a bottom-light IMF (specifically of the form advocated by van Dokkum (2008); green line). The inset in the right panel shows the cumulative luminosity fraction in logarithmic units. Low mass stars dominate the total number and mass in stars, but contribute a tiny fraction of the luminosity of old stellar populations.

From SSPs to CSPs

Composite Stellar Populations: The simple stellar populations are the building blocks for more complex stellar systems. Composite stellar populations (CSPs) differ from simple ones in three respects:

(1) they contain stars with a range of ages given by their SFH;
(2) they contain stars with a range in metallicities as given by their time-dependent metallicity distribution function, P(Z, t);
(3) they contain dust. These components are combined in the following way:

$$f_{\rm CSP}(t) = \int_{t'=0}^{t'=t} \int_{Z=0}^{Z_{\rm max}} \left({\rm SFR}(t-t')\, P(Z, t-t')\, f_{\rm SSP}(t', Z)\, e^{-\tau_d(t')} + A\, f_{\rm dust}(t', Z) \right) {\rm d}t'\, {\rm d}Z$$

where the integration variables are the stellar population age, *t'*, and metallicity, *Z*. Time-dependent dust attenuation is modeled via the dust optical depth, *τd(t')* and dust emission is incorporated in the parameter fdust. The normalization constant *A* is set by balancing the luminosity absorbed by dust with the total luminosity re-radiated by dust.

Impact of the Star Formation History

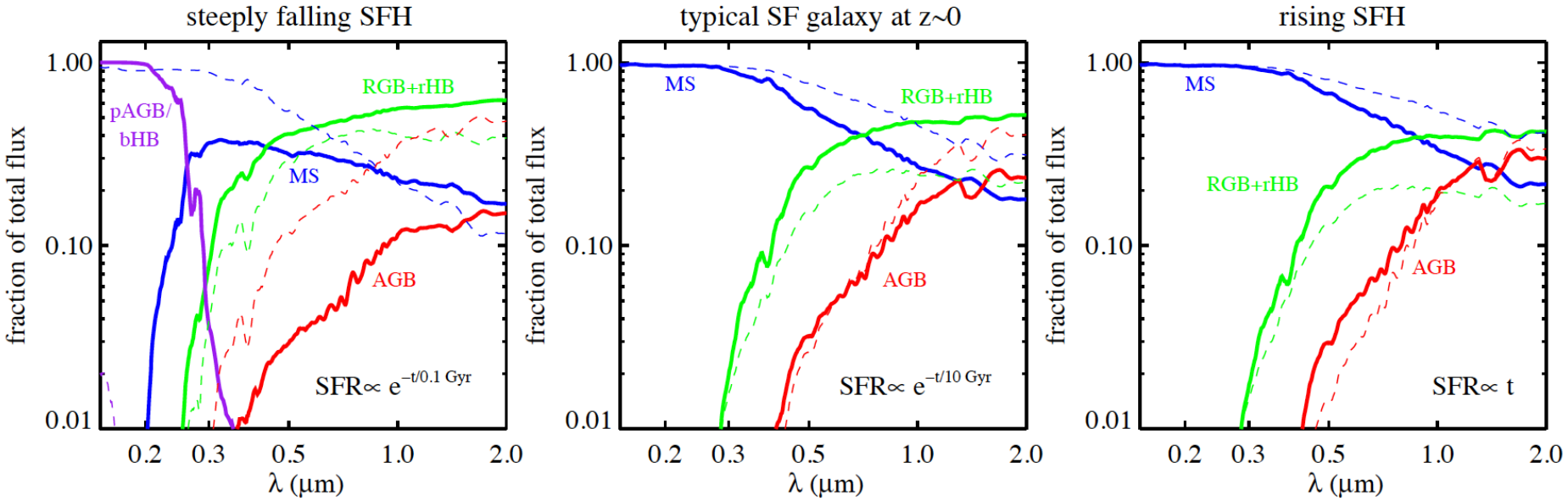

From Conroy (2013)

Top Panels: Fractional contribution to the total flux from stars in various evolutionary phases, for three different SFHs. The left panel is representative of a galaxy that formed nearly all of its stars very rapidly at early times, the middle panel is representative of a typical star-forming galaxy at $z \sim 0$, and the right panel may be representative of the typical galaxy at high redshift. Flux contributions are at 13 Gyr (solid lines) and 1 Gyr (dashed lines) after the commencement of star formation; all models are solar metallicity, dust-free, and are from FSPS (v2.3; Conroy, Gunn & White 2009). Labeled phases include the main sequence (MS), red giant branch (RGB), asymptotic giant branch (AGB, including the TP-AGB), post-AGB (pAGB), and the blue and red horizontal branch (bHB and rHB).

STARBURST 99

Continuous star formation history

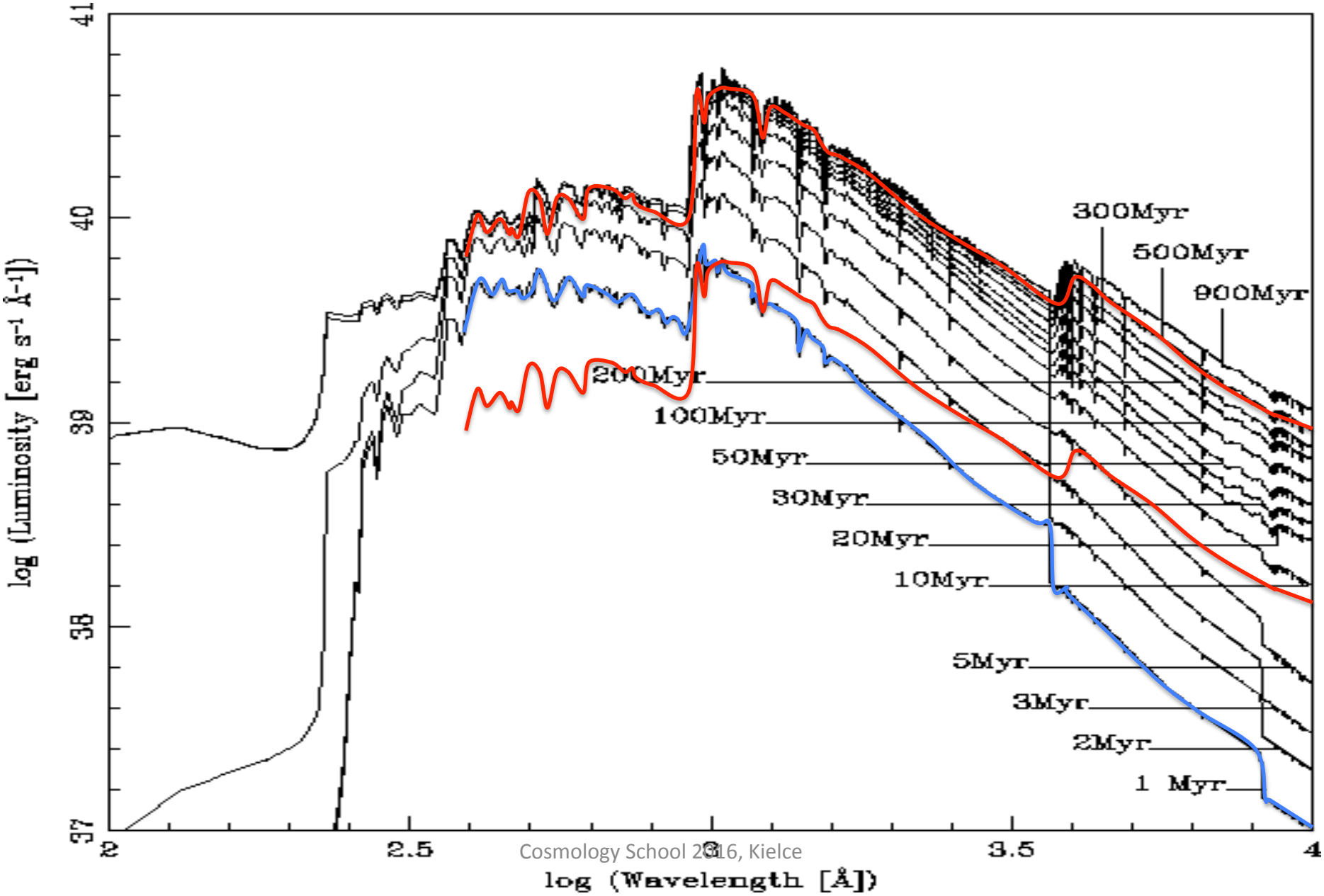

STARBURST 99

Instantaneous star formation history

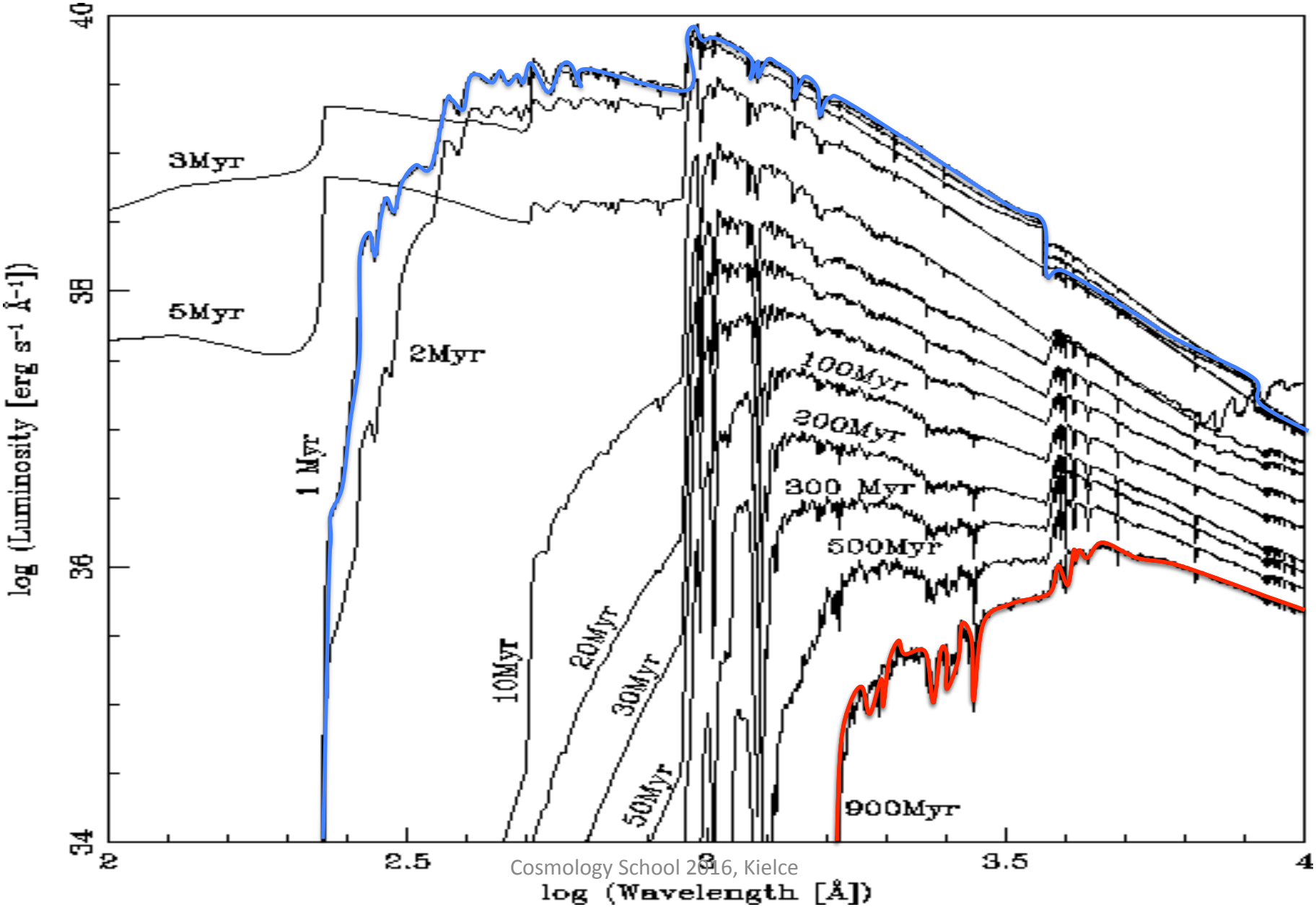

Fitting models to observed SEDs

The comparison of model and noise-affected object photometry, i.e. of fmod,i (per M) and fobs,i for k filters, is carried out for each model by the minimisation of

$$\chi^2(M_{\rm gal}) = \sum_{i=1}^{k} \frac{(M_{\rm gal} f_{{\rm mod},i} - f_{{\rm obs},i})^2}{\sigma^2_{{\rm obs},i}}$$

with the galaxy mass M_{gal} (in M_{Sun}) as a free parameter. The statistical photometric errors are considered by $\sigma_{obs,i}$. The resulting minimum *χ2* of each model can be compared to the observed data to determine the model showing the best *χ2* of the entire model grid for the object SED investigated. Moreover, the model-related χ2 allow us to perform a more sophisticated analysis to obtain galaxy properties based on probability distribution functions (PDFs).

In a nutshell, the method uses the fact that - assuming Gaussian uncertainties - the probability of the data (*D*) given the model (*M*) is given by *P(D|M)*:

$$P\left(D/M\right) \propto \exp^{-\frac{\chi^2}{2}}$$

Taking the $P_i(x)$ as weights for each bin for each analyzed parameter, the expectation values of each parameter are given as:

$$\langle x \rangle = \frac{\sum_{i=1}^{b} P_i x_i}{\sum_{i=1}^{b} P_i} .$$

For x_i we directly use the parameter value of the best-fit model of each bin. Finally, the standard deviation is derived by:

$$\sigma_x = \sqrt{\frac{\sum_{i=1}^{b} P_i (x_i - \langle x \rangle)^2}{\sum_{i=1}^{b} P_i}} .$$

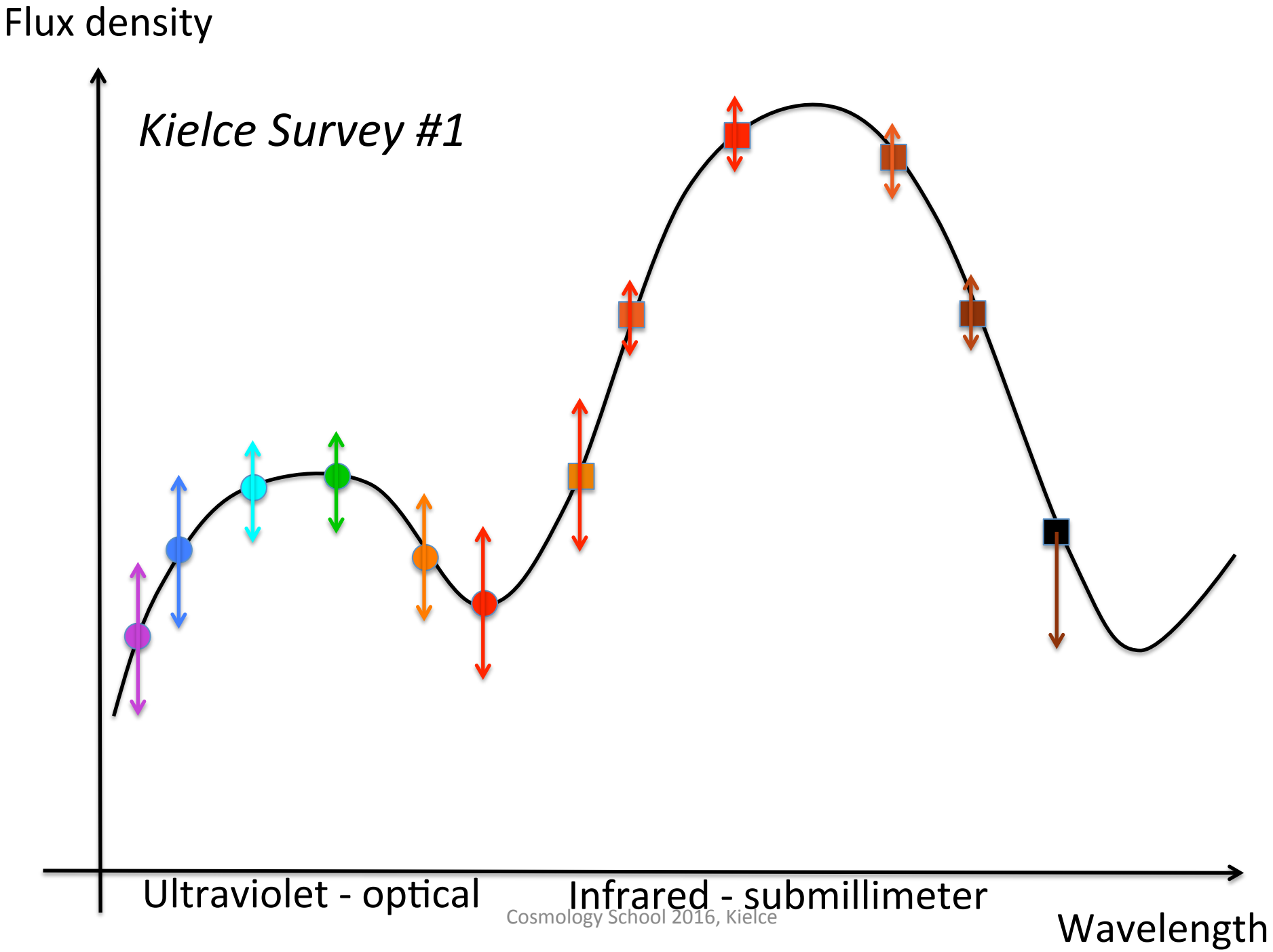
Flux density
Kielce Survey #1
Ultraviolet - optical
Infrared - submillimeter
Wavelength

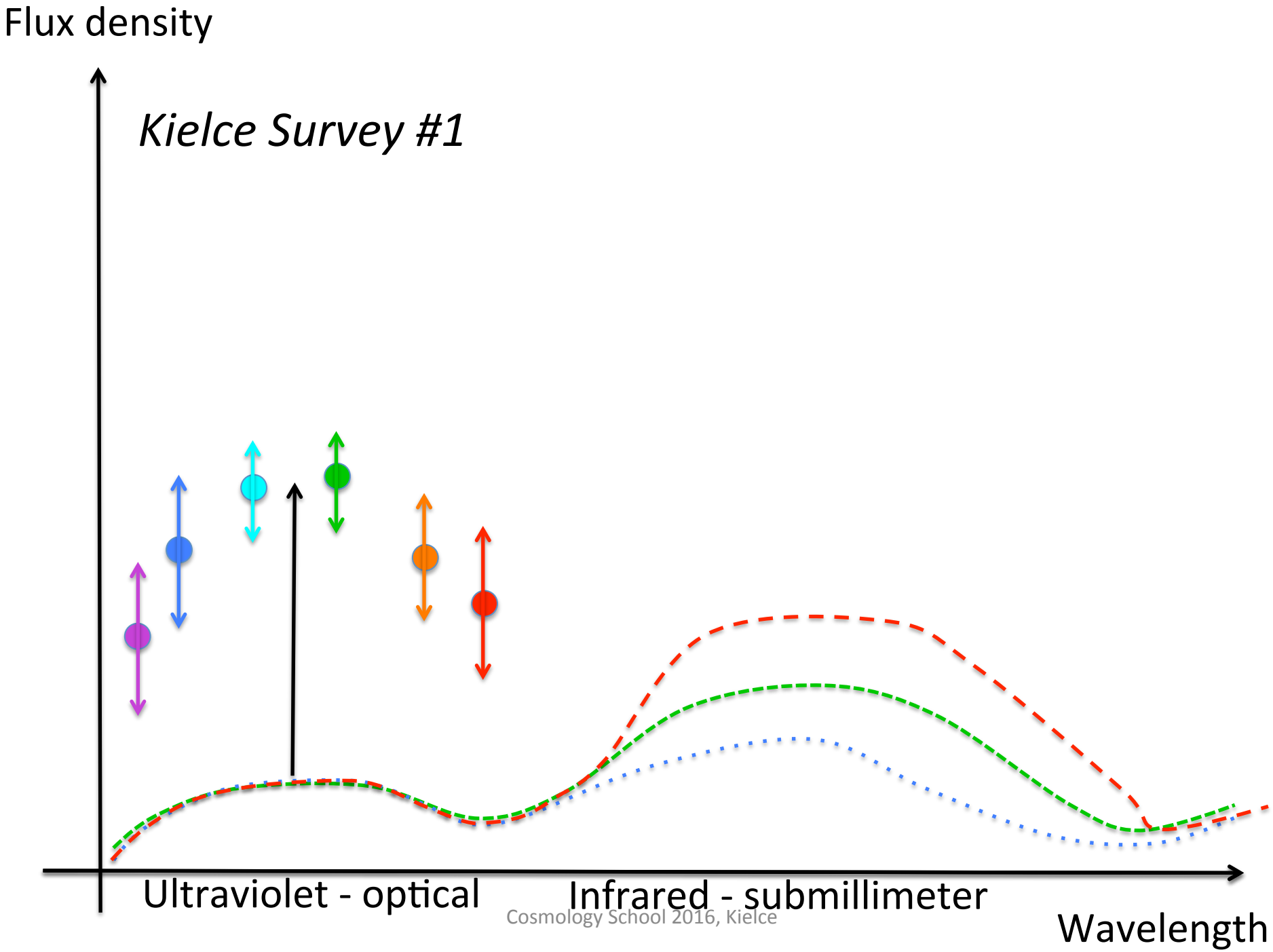
Flux density
Kielce Survey #1
Ultraviolet - optical
Infrared - submillimeter
Wavelength

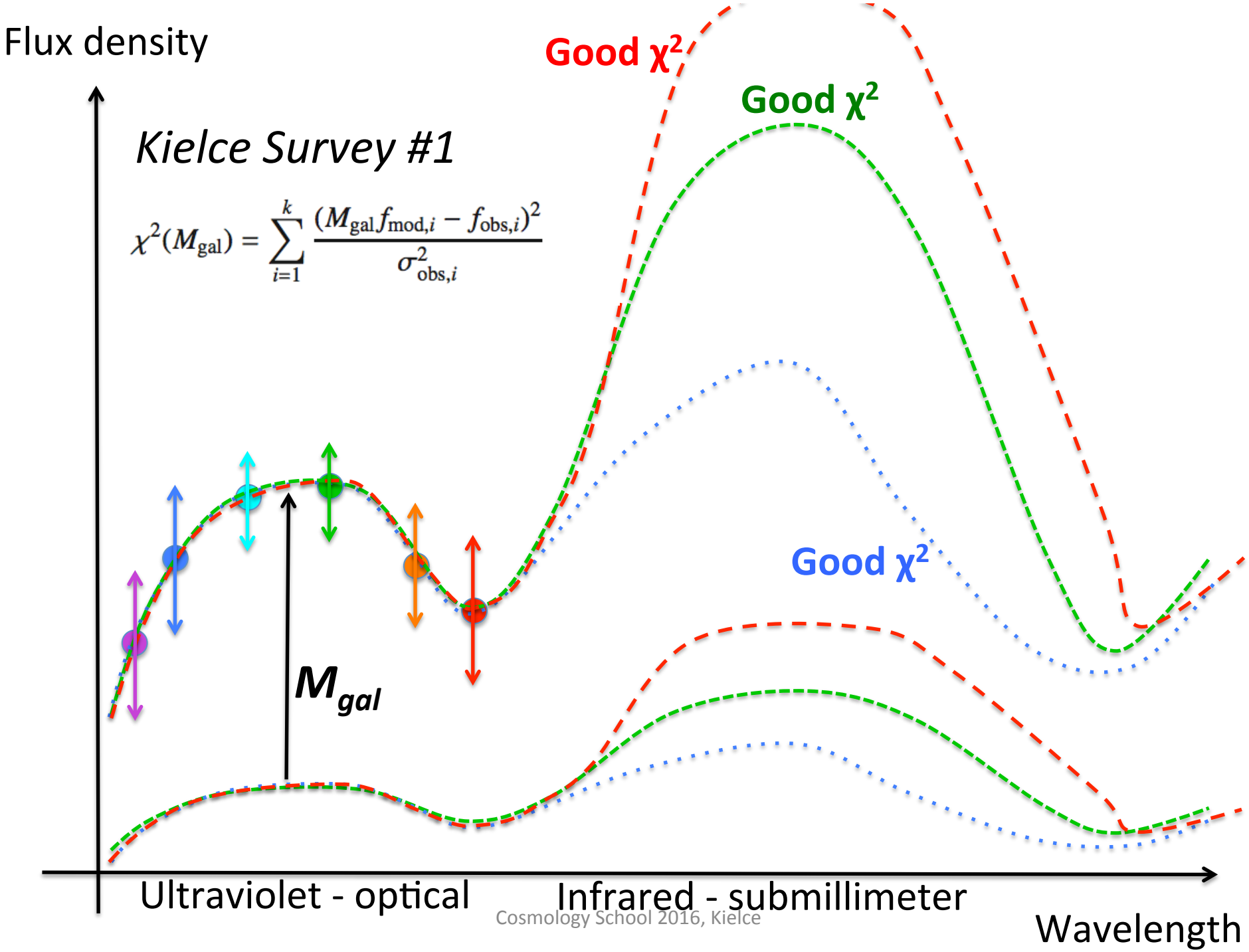
Flux density
Kielce Survey #1
$\chi^2(M_{\rm gal}) = \sum_{i=1}^{k} \frac{(M_{\rm gal} f_{{\rm mod},i} - f_{{\rm obs},i})^2}{\sigma^2_{{\rm obs},i}}$
Good χ^2
Good χ^2
Good χ^2
M_{gal}
Ultraviolet - optical
Infrared - submillimeter
Wavelength

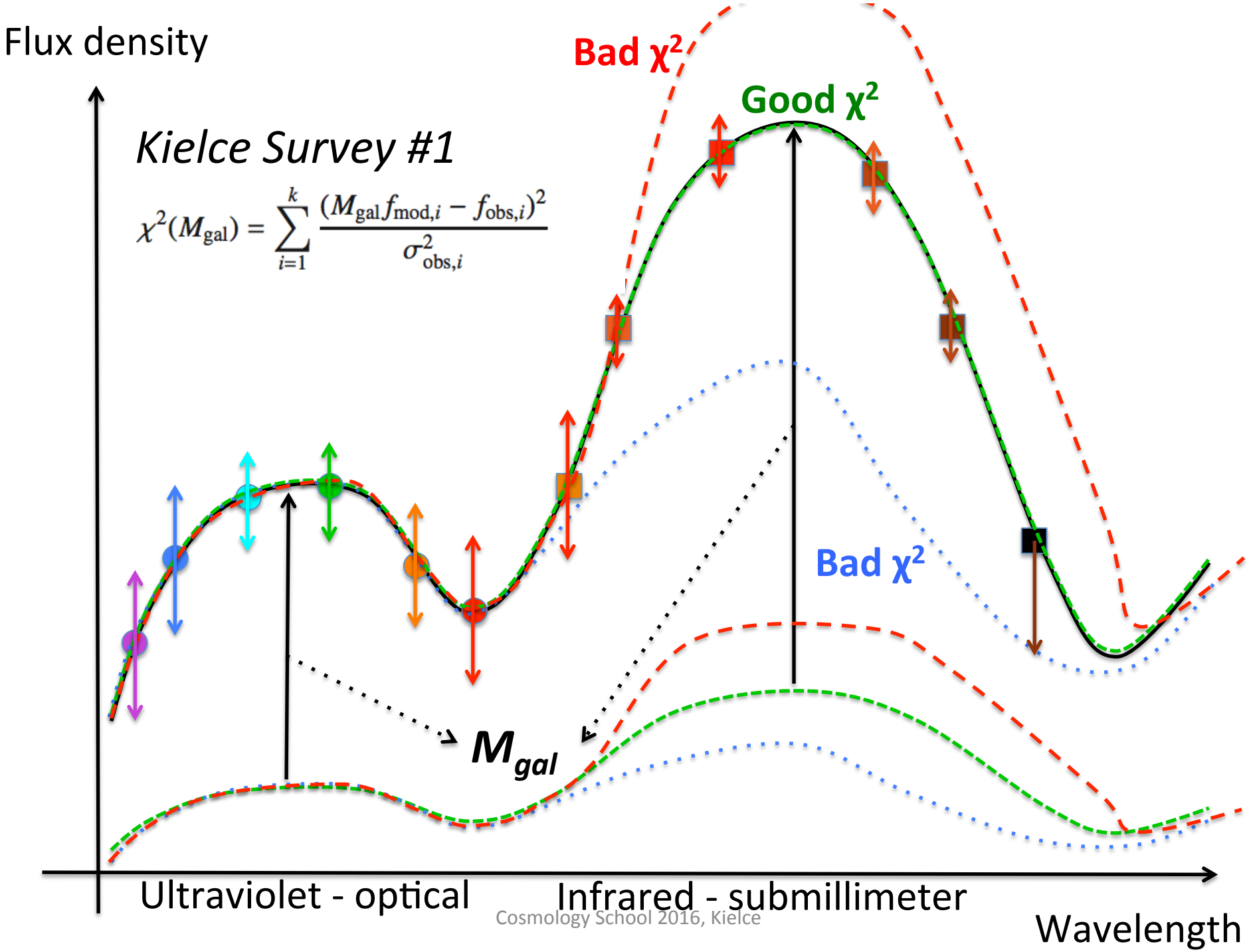
Flux density
Kielce Survey #1
$\chi^2(M_{\rm gal}) = \sum_{i=1}^{k} \frac{(M_{\rm gal} f_{{\rm mod},i} - f_{{\rm obs},i})^2}{\sigma^2_{{\rm obs},i}}$
Bad χ²
Good χ²
Bad χ²
M_{gal}
Ultraviolet - optical
Infrared - submillimeter
Wavelength

A few fits from the Herschel HerMES programme by Buat et al. (2011)

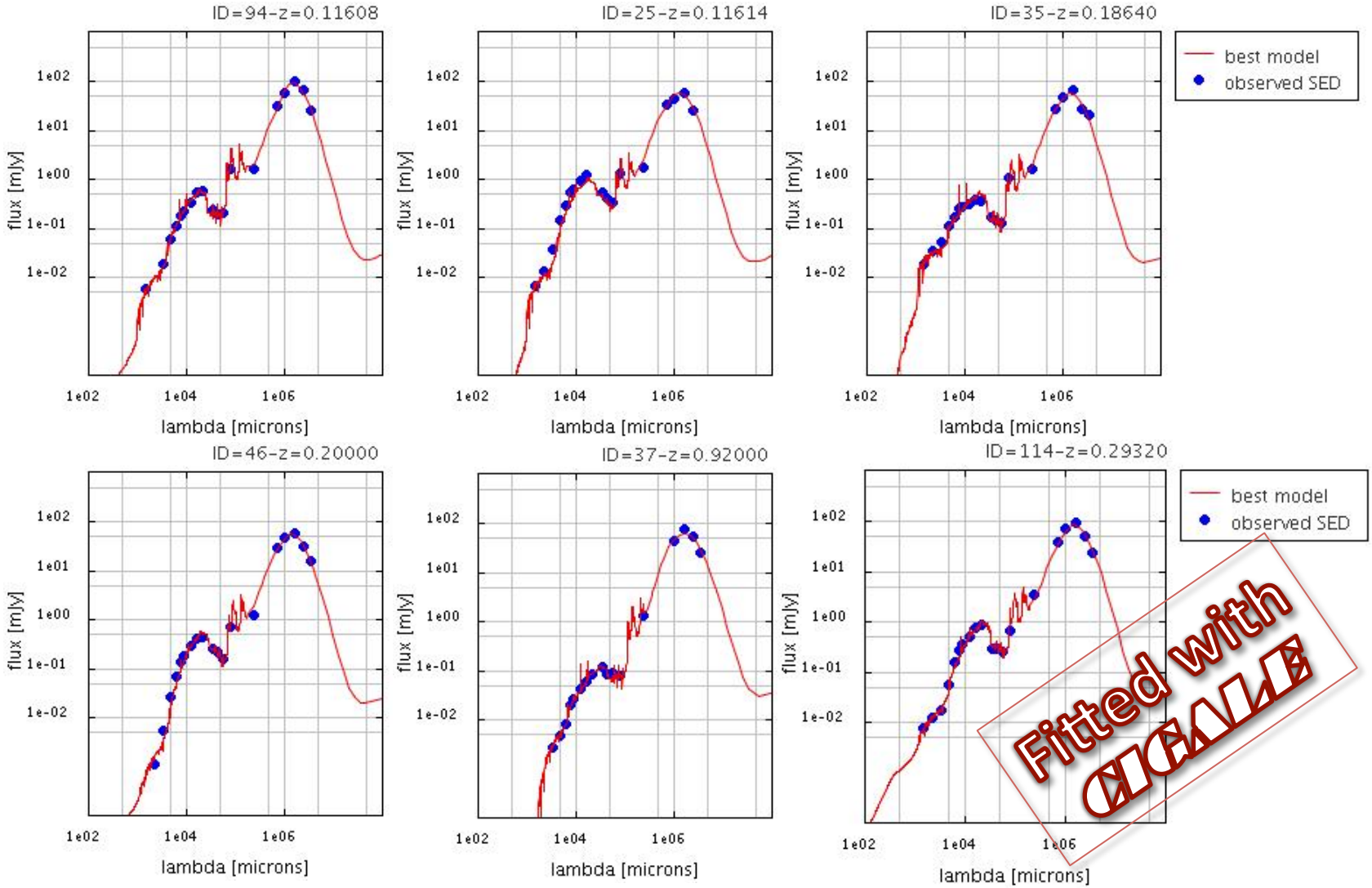

The infrared is crucial to get a good fit

Table 5. Change of the SINGS sample mean for different properties by running *CIGALE* without IR data.

Par.	Run A	Run B
$\log M_{\rm star}$	−0.19	−0.20
$\log SFR$	+0.83	+0.67
$\log L_{\rm bol}$	+0.37	+0.31
$\log L_{\rm dust}$	+0.75	+0.15
$\log f_{\rm burst}$	+1.05	+0.72
$\log t_{\rm D4000}$	−0.78	−0.71
$A_{\rm FUV}$	+2.16	+1.59
A_V	+0.65	+0.57
α	−0.40	−0.44

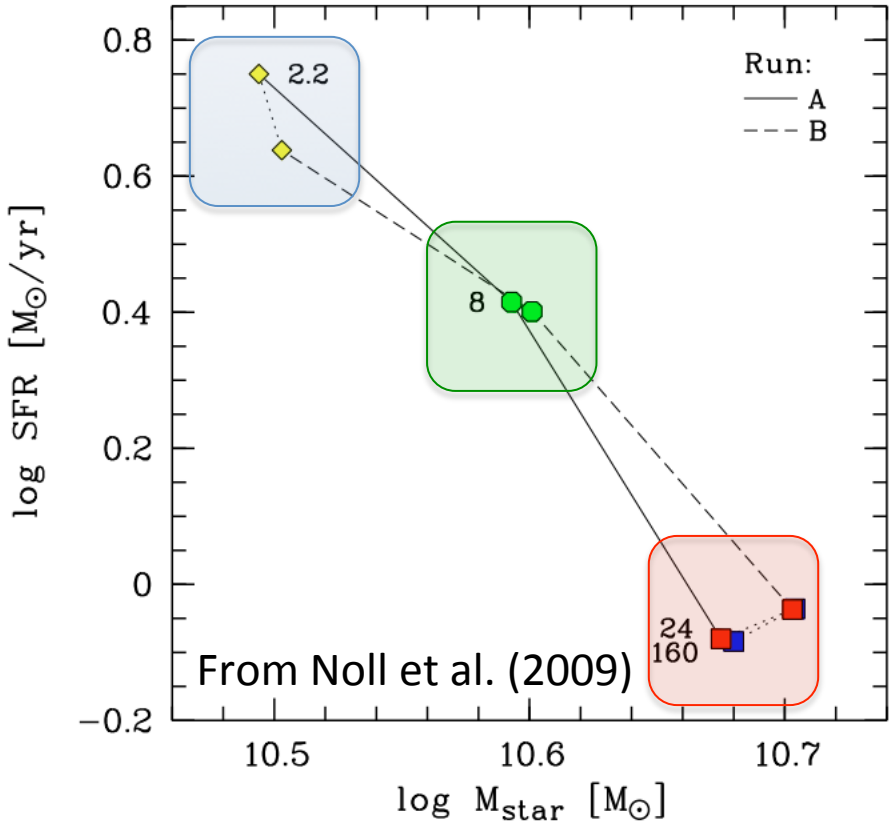

Fig. 16. Effect of the reduction of IR filters on the basic galaxy properties total stellar mass and SFR. The diagram provides the sample means and mean errors of these quantities for run A (solid lines) and run B (dashed lines) and different filter combinations. The labels near the symbols indicate the mean wavelength of the last filter in the filter set in μm. 160 means that all filters from *GALEX* FUV to MIPS 160 μm are used for the analysis. 2.2 refers to the K_s band as the reddest filter.

Last band used at 2.2µm (K-band)

Last band used at 24µm (MIPS)

Last band used at 16µm (MIPS)

Modeling the SEDs (borrowed to V. Buat):

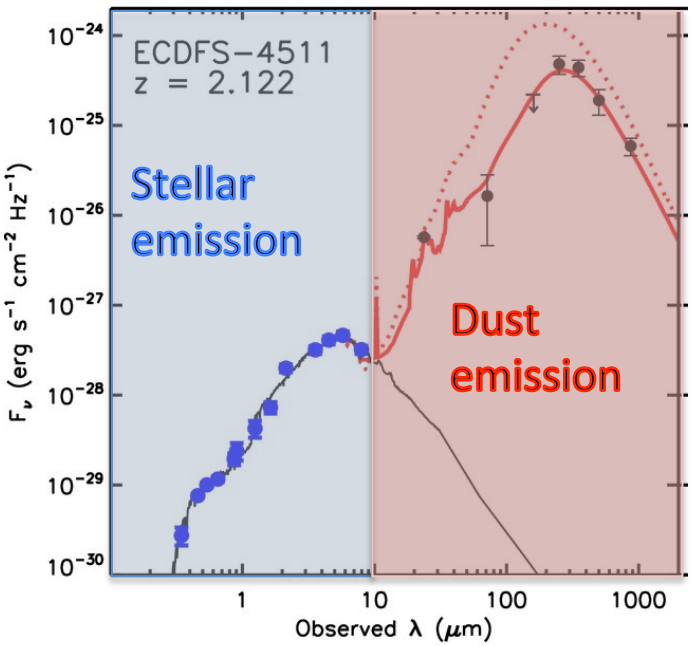

e.g. Muzzin+10

- Stellar and dust emission fitted separately
- It seems better to use all the data in a consistent way

Radiation transfer on multi-components is one option:

→ valid for handful of galaxies with a lot of observed data

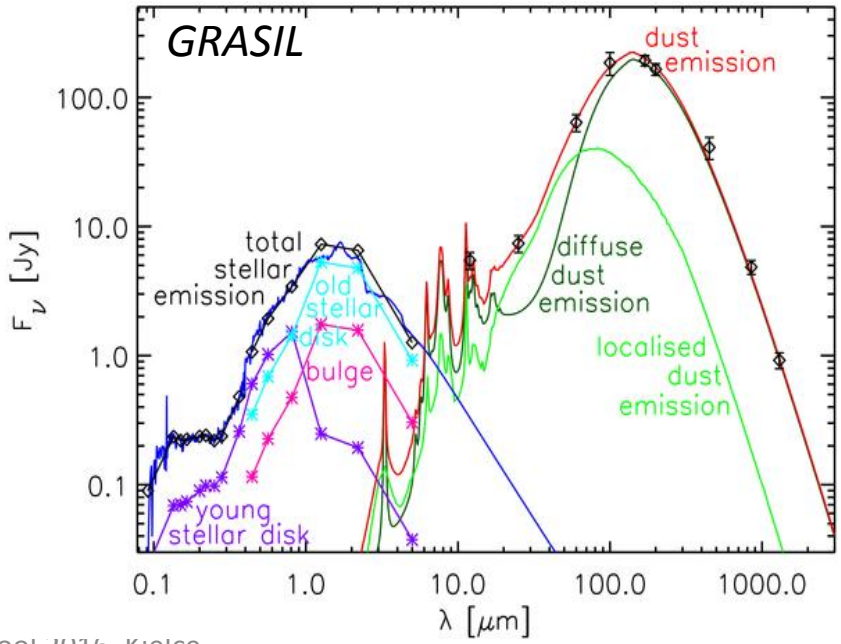

Modelling Spectral Energy Distributions (SEDs): Radiative Transfer Modelling

Radiative Transfer (RT) models computes the transport of radiation in the dusty circumstellar environments of galaxies.

RT models solve the radiation transport equation coupled self-consistently with the equation of motion for the outflow of gas and dust grains. The radiation from the star is scattered, absorbed and re-emitted by dust, and the emerging processed spectrum often provides the only available information about the embedded star.

They include the properties for the most common types of astronomical dust and supports various analytical forms for the density distribution in galaxies.

Modelling Spectral Energy Distributions (SEDs) : RT Models

- There are several essential steps included in any self-consistent model for the transfer of radiation and dust reprocessing.

- One of the essential steps is the specification of geometry, which means the specification of the distributions of stellar emissivity and dust, both on kpc scales and on pc scales.

- Having specified the geometry of the problem the next step in any SED model is to run radiative transfer calculations (see Kylafis & Xilouris (2005) for a comprehensive review on radiative transfer techniques) to derive the radiation fields in galaxies.

Modelling Spectral Energy Distributions (SEDs) : RT Models

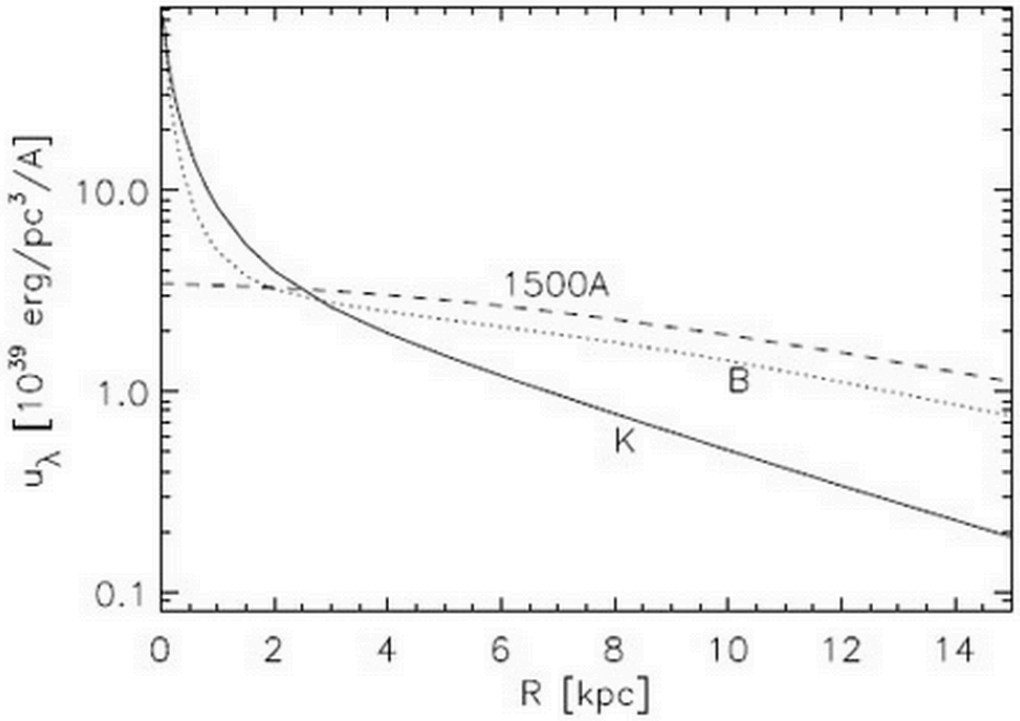

Example of radial profiles of radiation fields (calculated using the model of Popescu et al. (2000) in the plane of a typical spiral galaxy having a bulge-to-disk ratio B / D = 0.33.

Modelling Spectral Energy Distributions (SEDs): RT Models

- Once radiation fields in galaxies are calculated one can derive the temperature distribution of grains of different sizes and composition as a function of position in the galaxy.
- The spatially integrated dust and PAH SEDs can then be obtained by integrating over all positions in a galaxy.

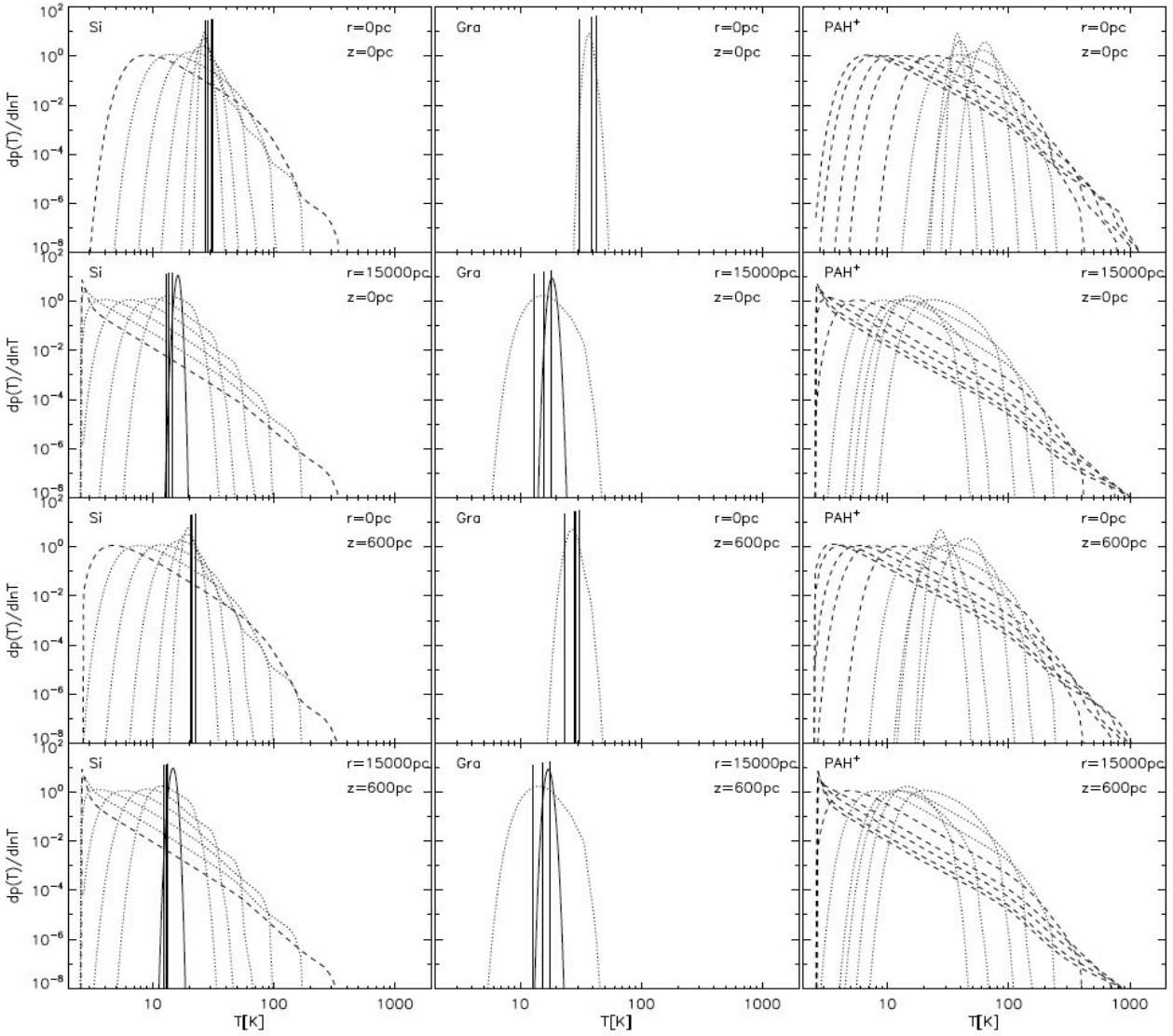

Physically-motivated models

CIGALE (CODE INVESTIGATING THE GALAXIES EMISSION) THROUGH AN ENERGY BUDGET

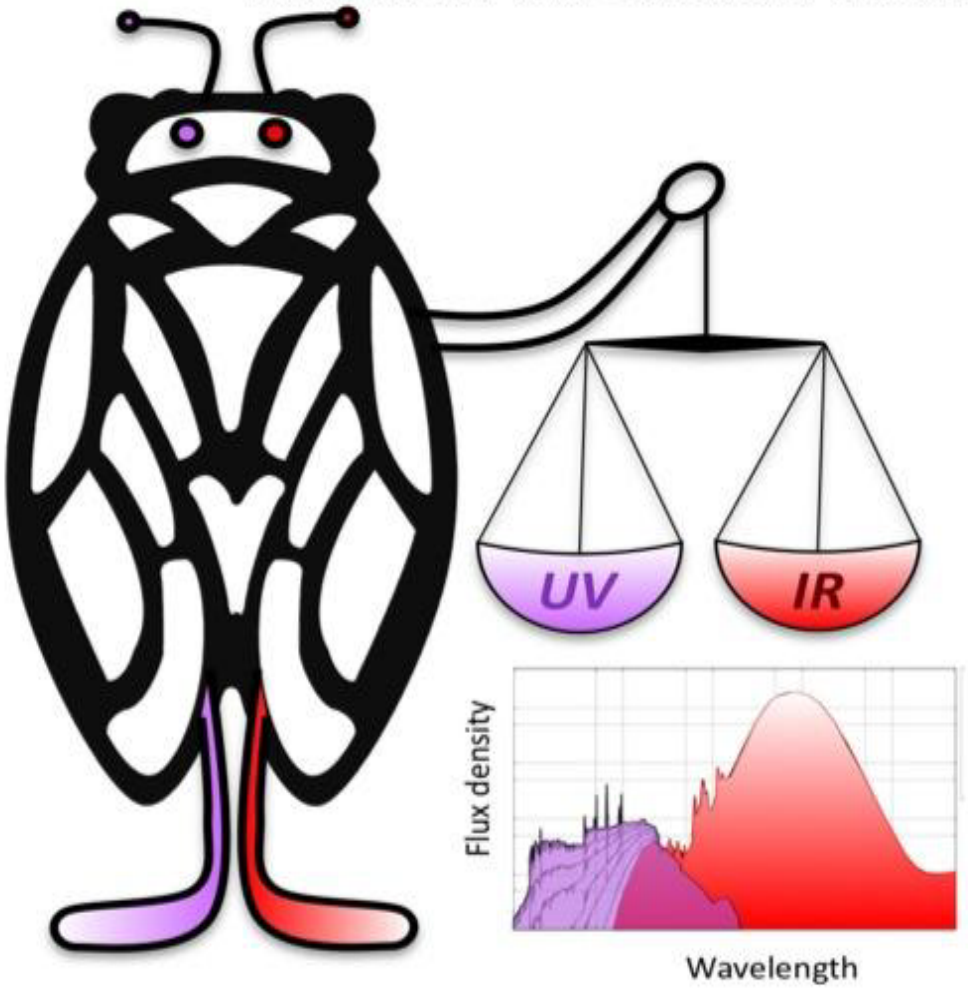

tion
ubmm

CIGALE
CICADAS
SUMMER CRICKET
CICALE
蝉
蟬
CIGARRAS
ZIKADEN
الزيز
ARBUSTA CICADAE
Τζιτζίκια
में पाए जाने वाले
cicaden

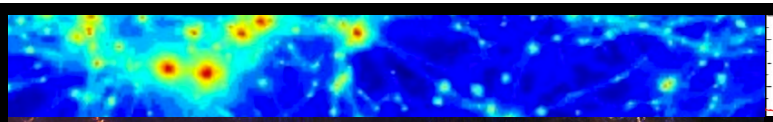

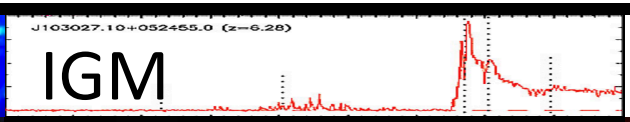

IGM

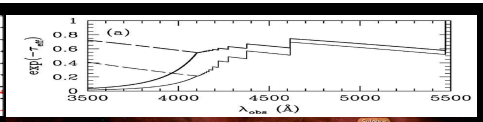

Credit: ESA/Herschel/PACS, SPIRE

gas

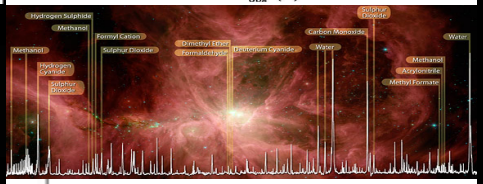

Credit: ESO / VISTA

stars

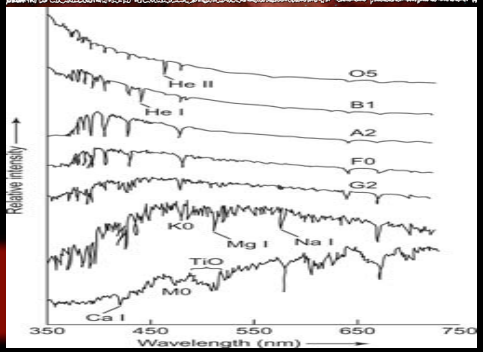

Credit: L. Tomley

Credit: V. Beckman

AGN

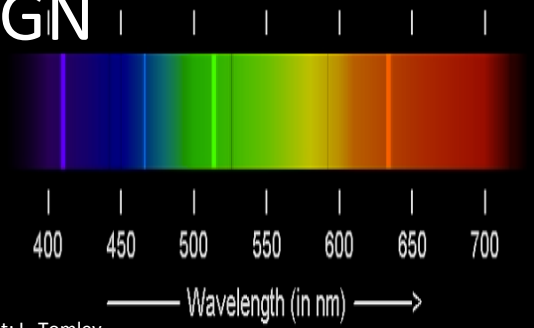

Credit: L. Tomley

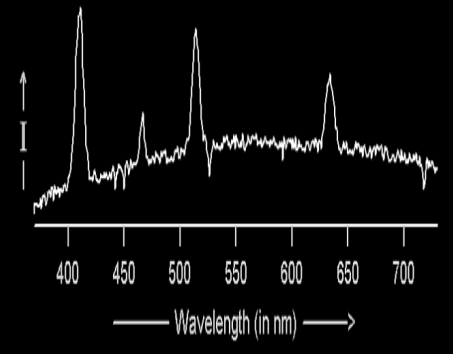

Credit: The Hubble Heritage Team, STScI/AURA, ESA, NASA

dust

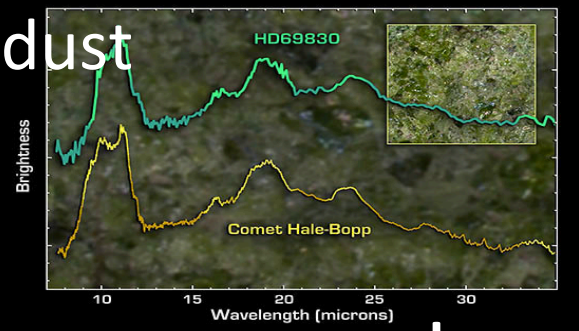

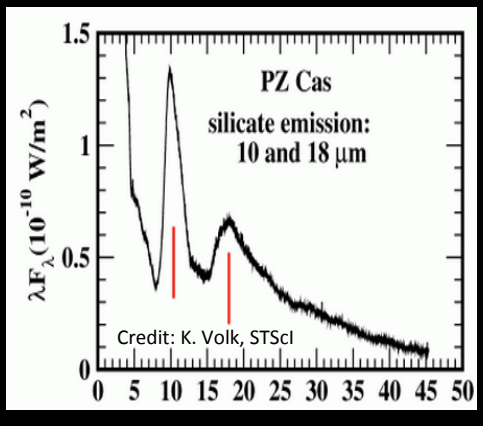

Credit: K. Volk, STScI

The components

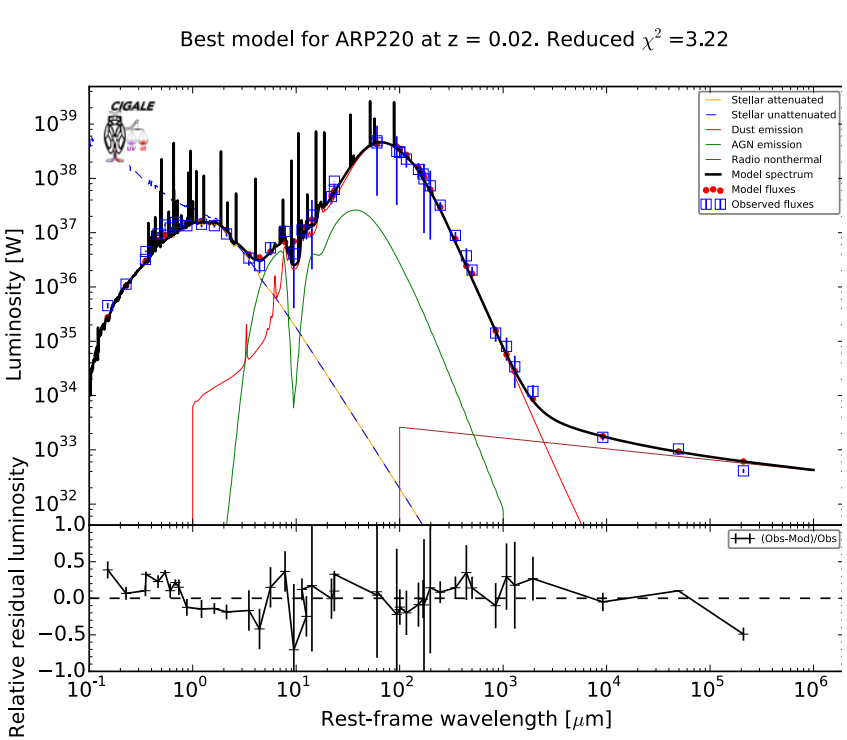
Best model for ARP220 at z = 0.02. Reduced χ^2 =3.22
CIGALE
Stellar attenuated
Stellar unattenuated
Dust emission
AGN emission
Radio nonthermal
Model spectrum
Model fluxes
Observed fluxes
Luminosity [W]
Relative residual luminosity
(Obs-Mod)/Obs
Rest-frame wavelength [μm]

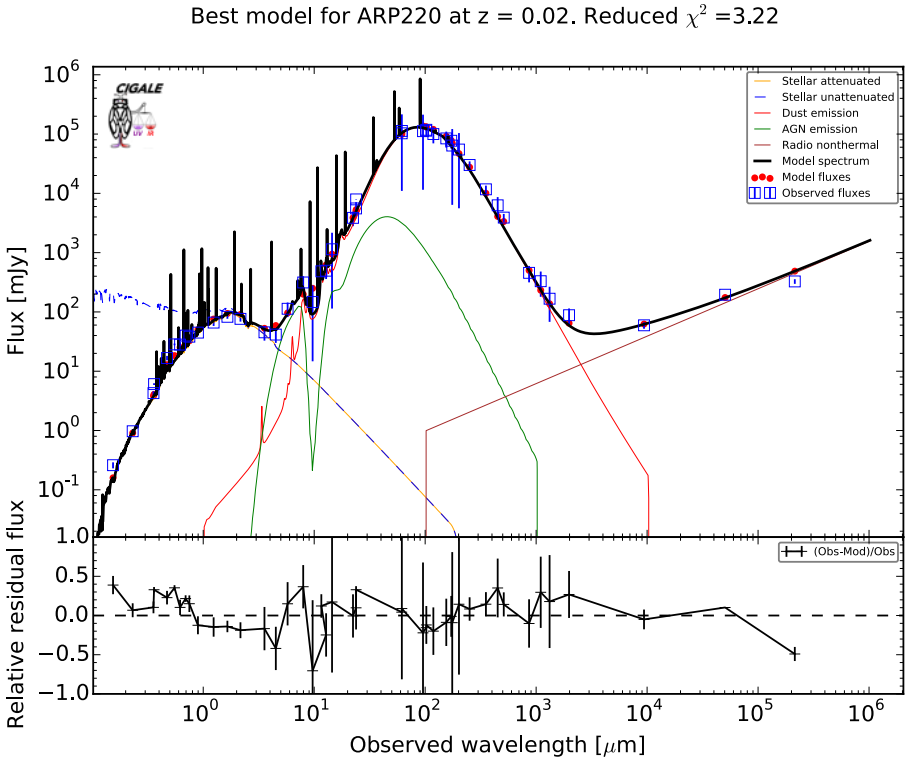
Best model for ARP220 at z = 0.02. Reduced χ^2 =3.22
CIGALE
Stellar attenuated
Stellar unattenuated
Dust emission
AGN emission
Radio nonthermal
Model spectrum
Model fluxes
Observed fluxes
Flux [mJy]
Relative residual flux
(Obs-Mod)/Obs
Observed wavelength [μm]

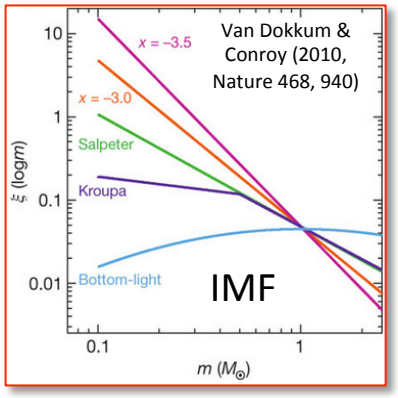

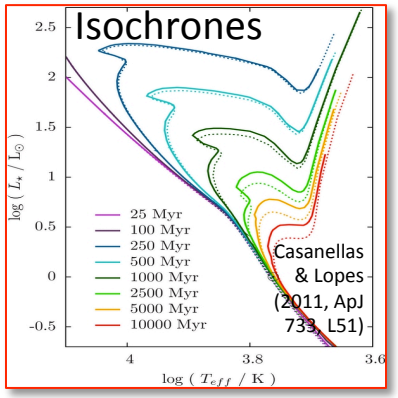

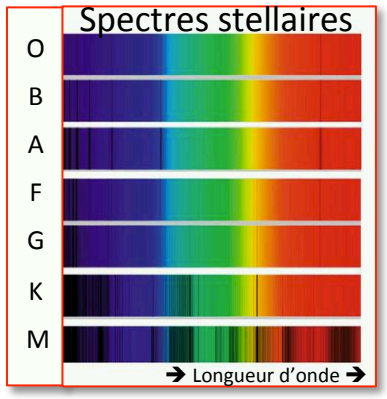

O

B

A

F

G

K

M

Spectres stellaires

➔ Longueur d'onde ➔

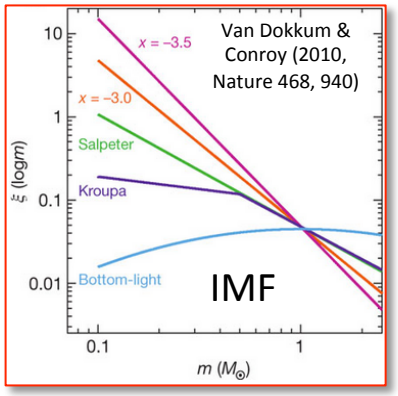
Van Dokkum & Conroy (2010, Nature 468, 940)
x = −3.5
x = −3.0
Salpeter
Kroupa
Bottom-light
IMF
ξ (logm)
m (M⊙)

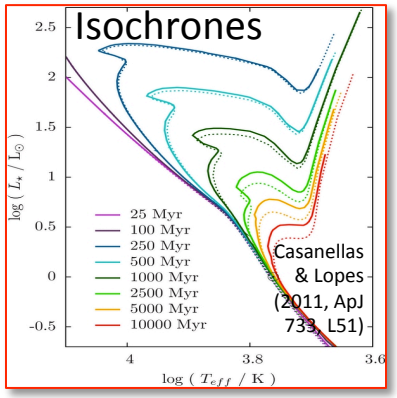
Isochrones
25 Myr
100 Myr
250 Myr
500 Myr
1000 Myr
2500 Myr
5000 Myr
10000 Myr
Casanellas & Lopes (2011, ApJ 733, L51)
log (L* / L⊙)
log (Teff / K)

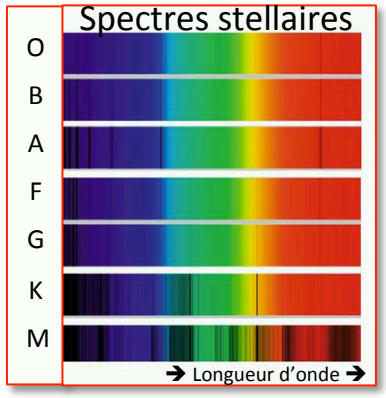
Spectres stellaires
O
B
A
F
G
K
M
➔ Longueur d'onde ➔

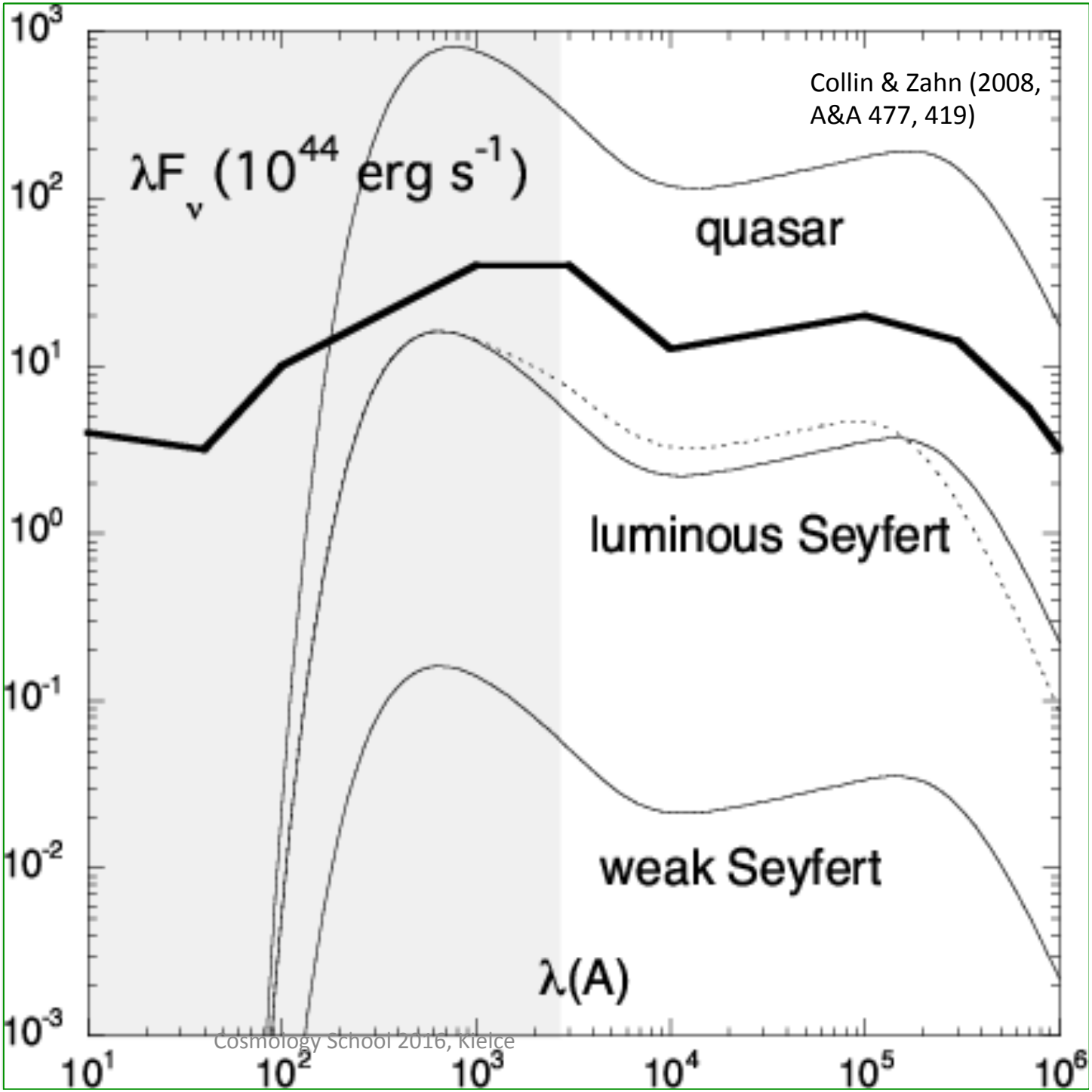
Collin & Zahn (2008, A&A 477, 419)
λF_ν (10^44 erg s^-1)
quasar
luminous Seyfert
weak Seyfert
λ(A)

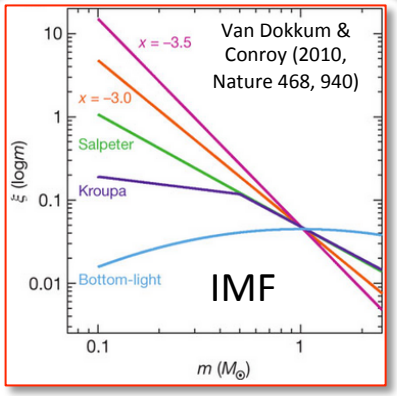
Van Dokkum & Conroy (2010, Nature 468, 940)
x = −3.5
x = −3.0
Salpeter
Kroupa
Bottom-light
IMF
ξ (logm)
m (M⊙)

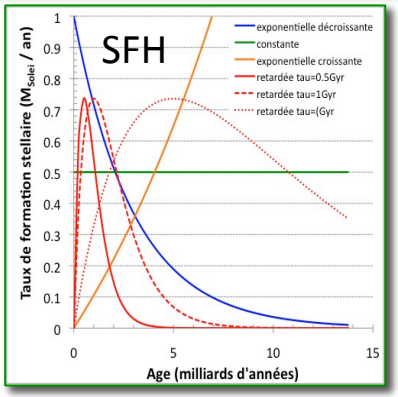
SFH
exponentielle décroissante
constante
exponentielle croissante
retardée tau=0.5Gyr
retardée tau=1Gyr
retardée tau=(Gyr
Taux de formation stellaire (M_Soleil / an)
Age (milliards d'années)

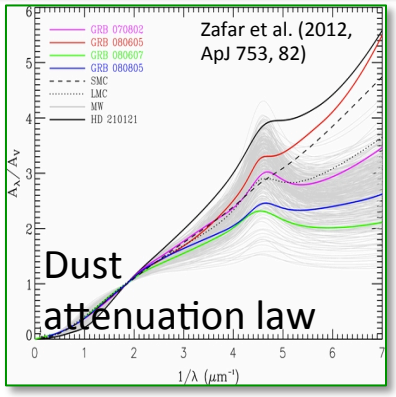
Zafar et al. (2012, ApJ 753, 82)
GRB 070802
GRB 080605
GRB 080607
GRB 080805
SMC
LMC
MW
HD 210121
Dust attenuation law
A_λ / A_V
1/λ (μm⁻¹)

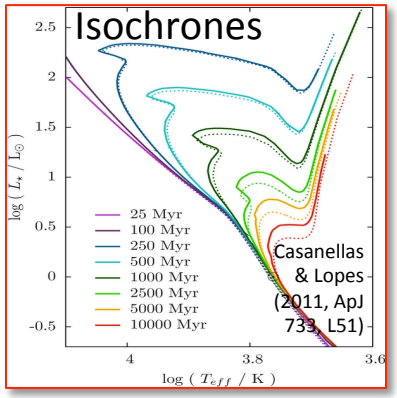
Isochrones
25 Myr
100 Myr
250 Myr
500 Myr
1000 Myr
2500 Myr
5000 Myr
10000 Myr
Casanellas & Lopes (2011, ApJ 733, L51)
log (L* / L⊙)
log (T_eff / K)

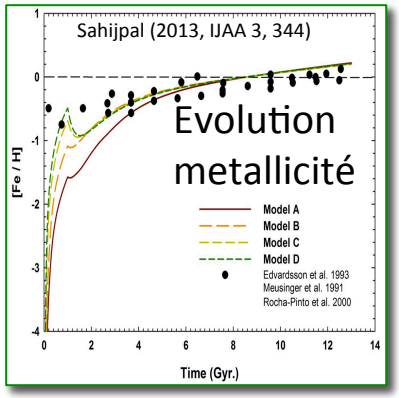
Sahijpal (2013, IJAA 3, 344)
Evolution metallicité
Model A
Model B
Model C
Model D
Edvardsson et al. 1993
Meusinger et al. 1991
Rocha-Pinto et al. 2000
[Fe / H]
Time (Gyr.)

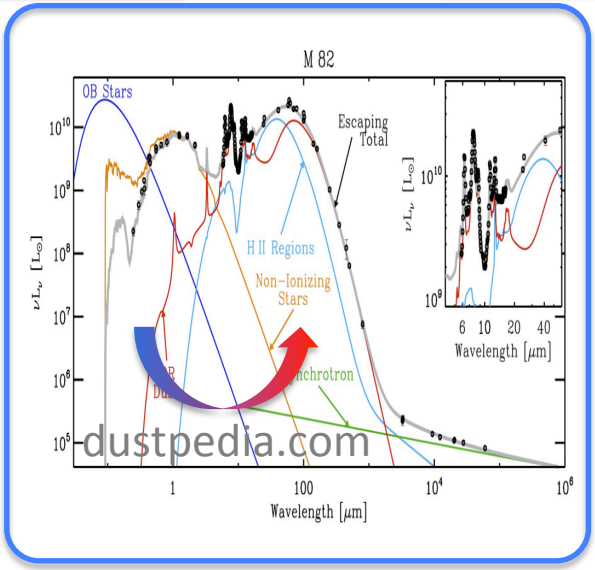
M 82
OB Stars
Escaping Total
H II Regions
Non-Ionizing Stars
Wavelength [μm]
dustpedia.com

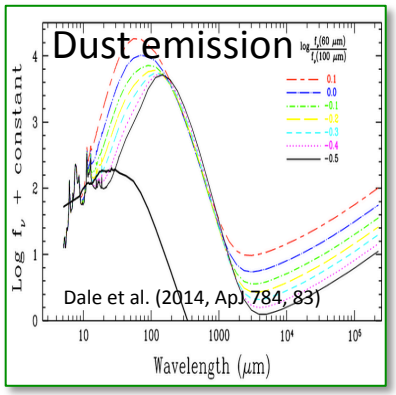
Dust emission
Dale et al. (2014, ApJ 784, 83)
Log f_ν + constant
Wavelength (μm)

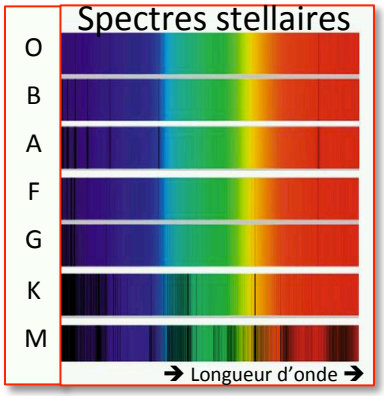
Spectres stellaires
O
B
A
F
G
K
M
➔ Longueur d'onde ➔

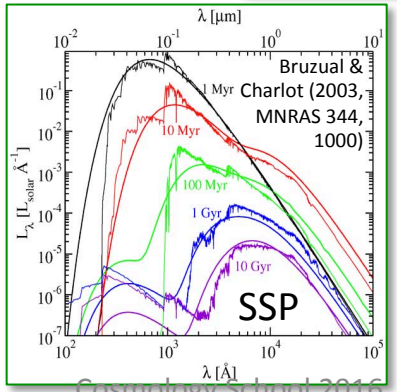
Bruzual & Charlot (2003, MNRAS 344, 1000)
1 Myr
10 Myr
100 Myr
1 Gyr
10 Gyr
SSP
λ [μm]
λ [Å]

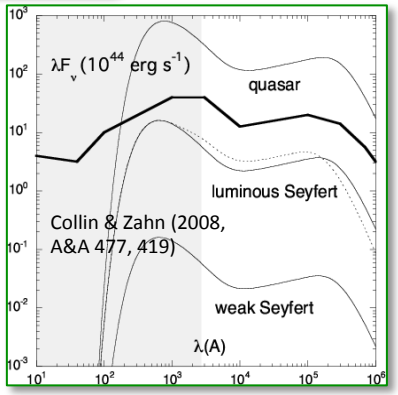
λF_ν (10^44 erg s^-1)
quasar
luminous Seyfert
Collin & Zahn (2008, A&A 477, 419)
weak Seyfert
λ(A)

What types of Star Formation Histories ?

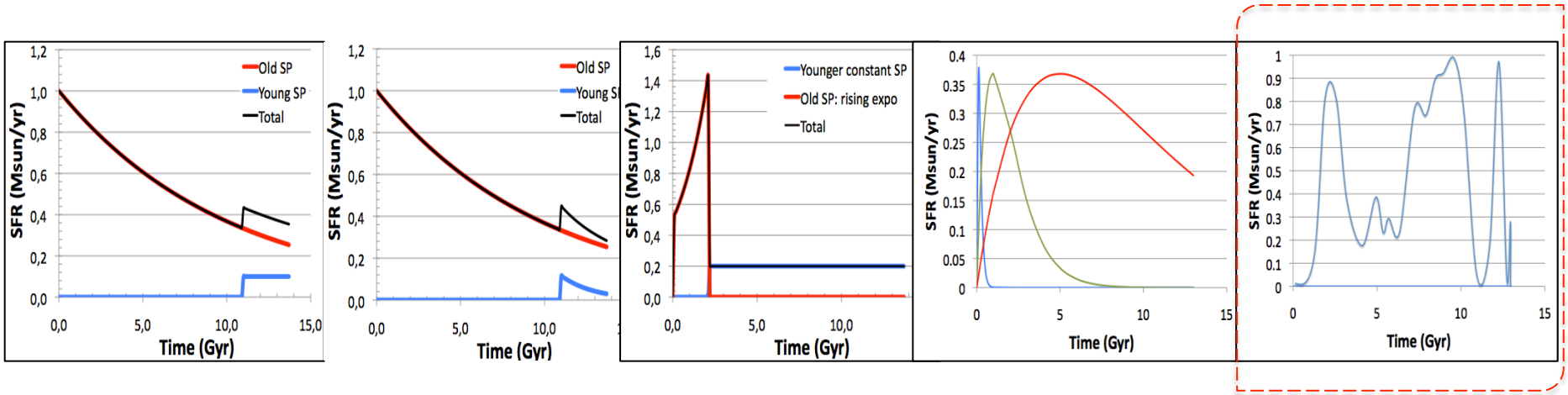

DUST ATTENUATION: *AGE-DEPENDENT* AMOUNTS FOR THE YOUNG AND OLD STELLAR POPULATION (BUT THE SAME ATTENUATION CURVE)

Calzetti et al. (2000) + UV bump × power law

$$k(\lambda) = \left[A(\lambda) / E(B-V) + \frac{E_{bump}\,\lambda^2\,\gamma^2}{(\lambda^2 - \lambda_0^2)^2 + \lambda^2\,\gamma^2} \right] \times (\lambda / \lambda_V)^{\delta}$$

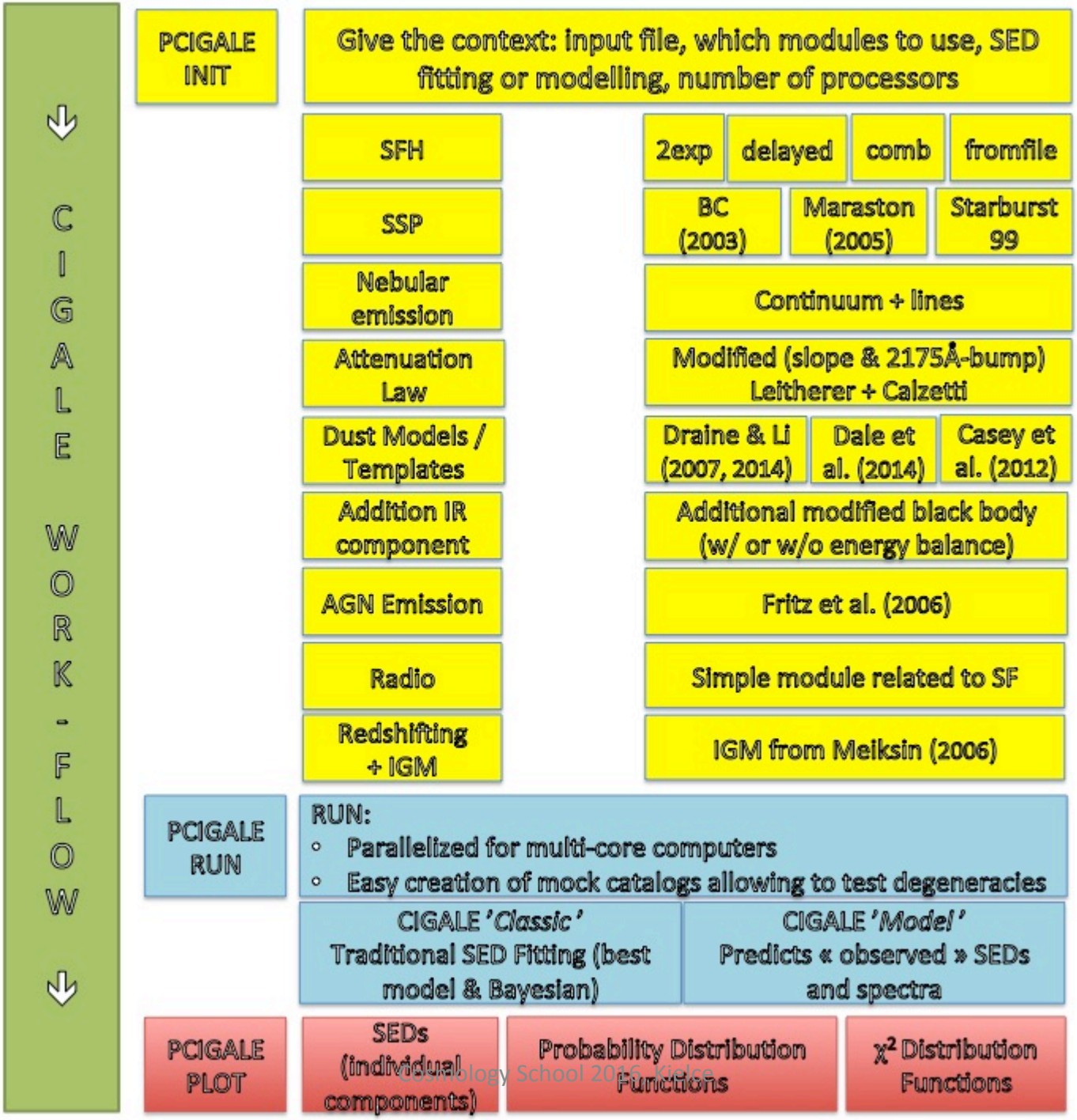
CIGALE WORK-FLOW
PCIGALE INIT
Give the context: input file, which modules to use, SED fitting or modelling, number of processors
SFH
2exp
delayed
comb
fromfile
SSP
BC (2003)
Maraston (2005)
Starburst 99
Nebular emission
Continuum + lines
Attenuation Law
Modified (slope & 2175Å-bump) Leitherer + Calzetti
Dust Models / Templates
Draine & Li (2007, 2014)
Dale et al. (2014)
Casey et al. (2012)
Addition IR component
Additional modified black body (w/ or w/o energy balance)
AGN Emission
Fritz et al. (2006)
Radio
Simple module related to SF
Redshifting + IGM
IGM from Meiksin (2006)
PCIGALE RUN
RUN:
Parallelized for multi-core computers
Easy creation of mock catalogs allowing to test degeneracies
CIGALE 'Classic'
Traditional SED Fitting (best model & Bayesian)
CIGALE 'Model'
Predicts « observed » SEDs and spectra
PCIGALE PLOT
SEDs (individual components)
Probability Distribution Functions
χ² Distribution Functions

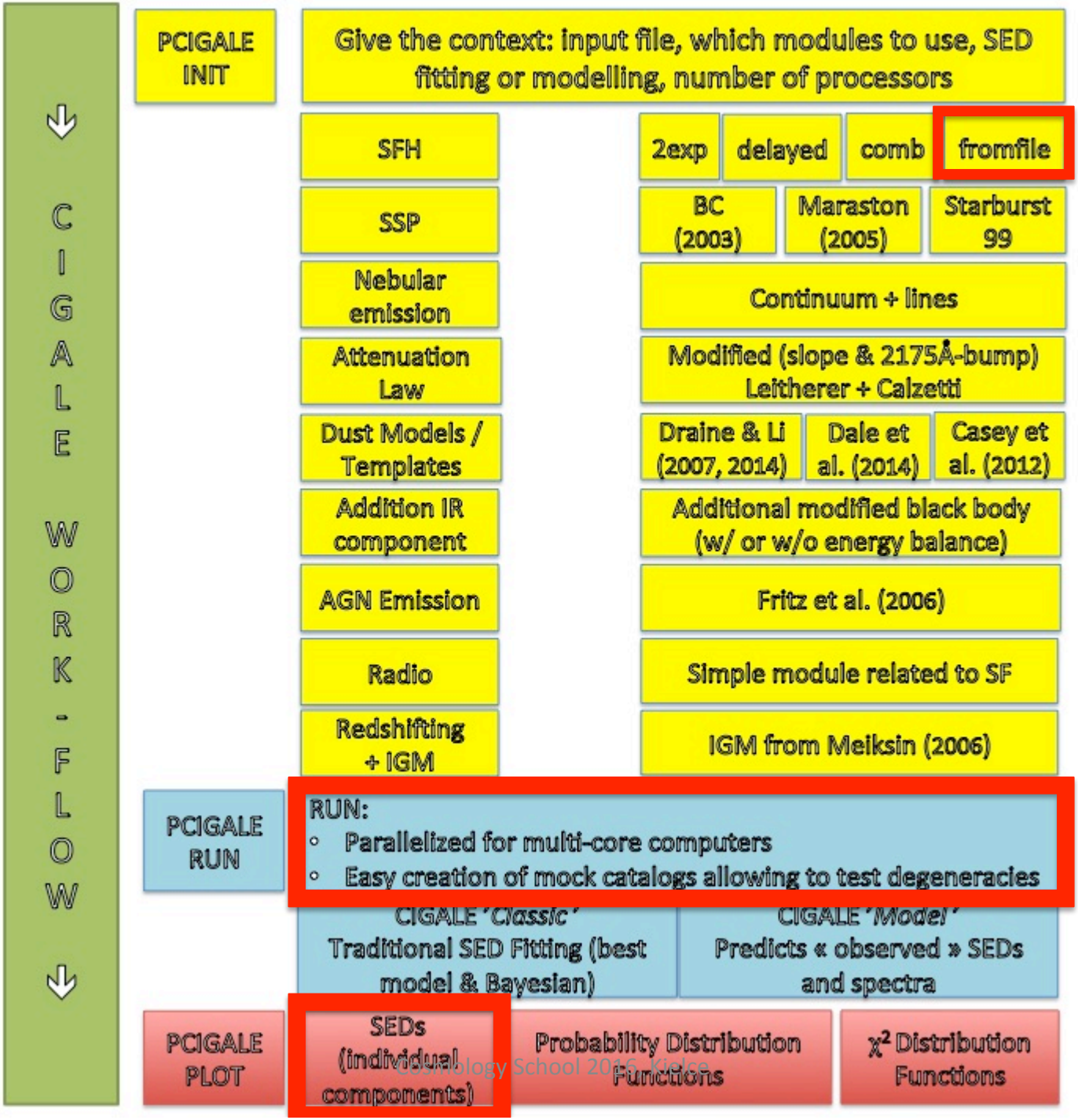
CIGALE WORK-FLOW
PCIGALE INIT
Give the context: input file, which modules to use, SED fitting or modelling, number of processors
SFH
2exp
delayed
comb
fromfile
SSP
BC (2003)
Maraston (2005)
Starburst 99
Nebular emission
Continuum + lines
Attenuation Law
Modified (slope & 2175Å-bump) Leitherer + Calzetti
Dust Models / Templates
Draine & Li (2007, 2014)
Dale et al. (2014)
Casey et al. (2012)
Addition IR component
Additional modified black body (w/ or w/o energy balance)
AGN Emission
Fritz et al. (2006)
Radio
Simple module related to SF
Redshifting + IGM
IGM from Meiksin (2006)
PCIGALE RUN
RUN:
Parallelized for multi-core computers
Easy creation of mock catalogs allowing to test degeneracies
CIGALE 'Classic'
Traditional SED Fitting (best model & Bayesian)
CIGALE 'Model'
Predicts « observed » SEDs and spectra
PCIGALE PLOT
SEDs (individual components)
Probability Distribution Functions
χ^2 Distribution Functions

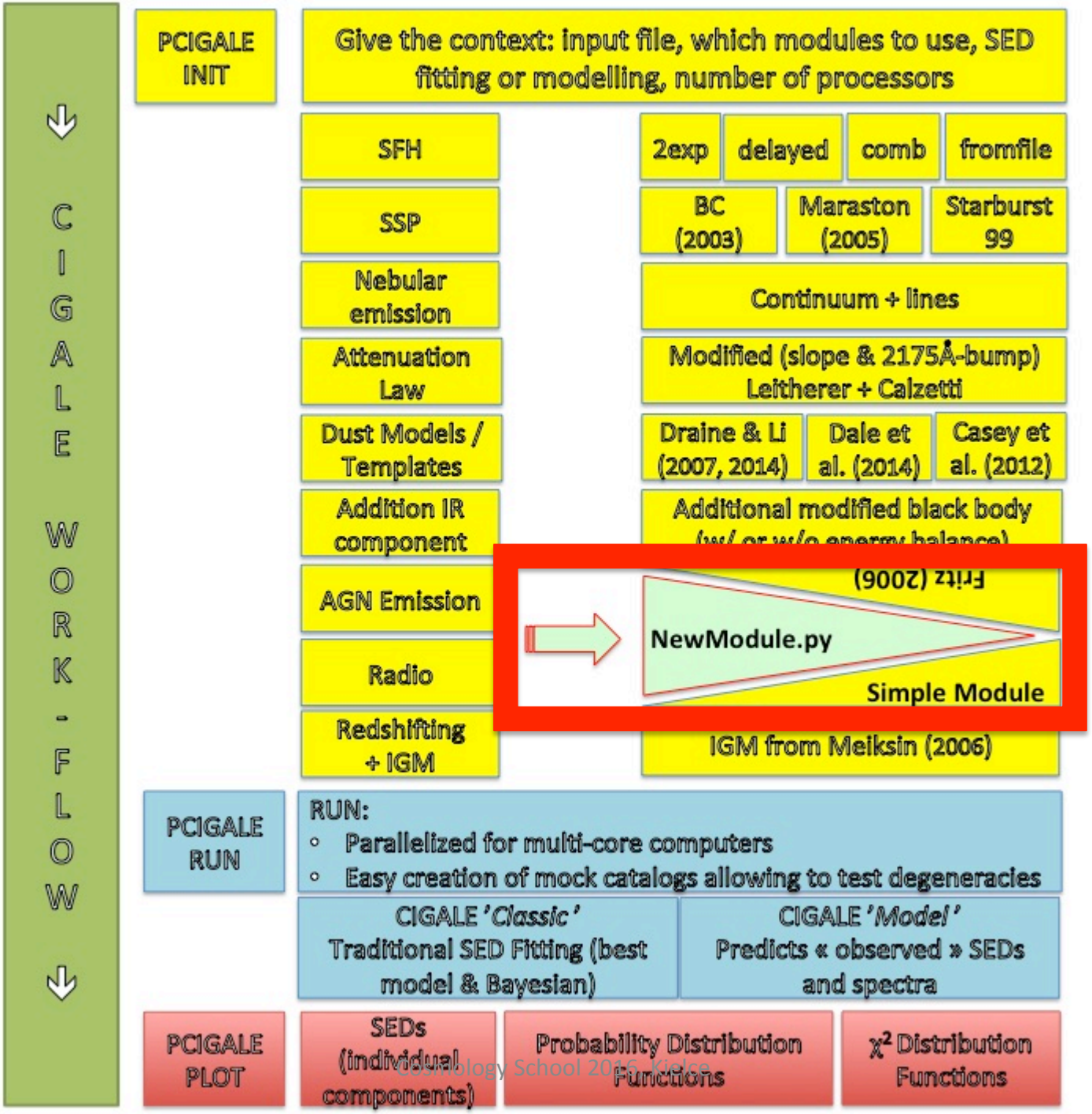
CIGALE WORK-FLOW
PCIGALE INIT
Give the context: input file, which modules to use, SED fitting or modelling, number of processors
SFH
2exp
delayed
comb
fromfile
SSP
BC (2003)
Maraston (2005)
Starburst 99
Nebular emission
Continuum + lines
Attenuation Law
Modified (slope & 2175Å-bump) Leitherer + Calzetti
Dust Models / Templates
Draine & Li (2007, 2014)
Dale et al. (2014)
Casey et al. (2012)
Addition IR component
Additional modified black body
AGN Emission
Fritz (2006)
NewModule.py
Simple Module
Radio
Redshifting + IGM
IGM from Meiksin (2006)
PCIGALE RUN
RUN:
Parallelized for multi-core computers
Easy creation of mock catalogs allowing to test degeneracies
CIGALE 'Classic'
Traditional SED Fitting (best model & Bayesian)
CIGALE 'Model'
Predicts « observed » SEDs and spectra
PCIGALE PLOT
SEDs (individual components)
Probability Distribution Functions
χ² Distribution Functions

Examples of Probability Distribution Functions used by *CIGALE* to estimate the parameters for two objects

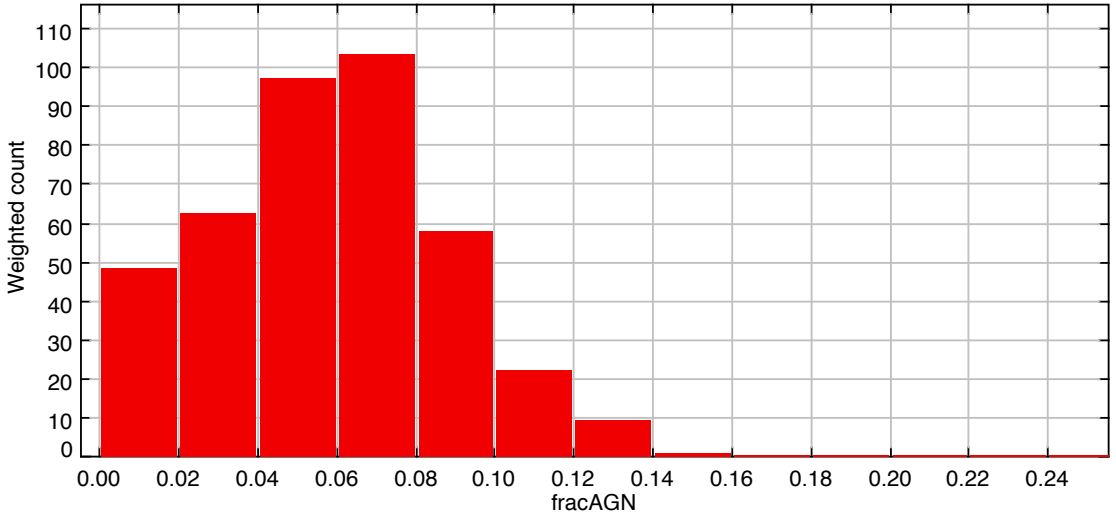

FracAGN

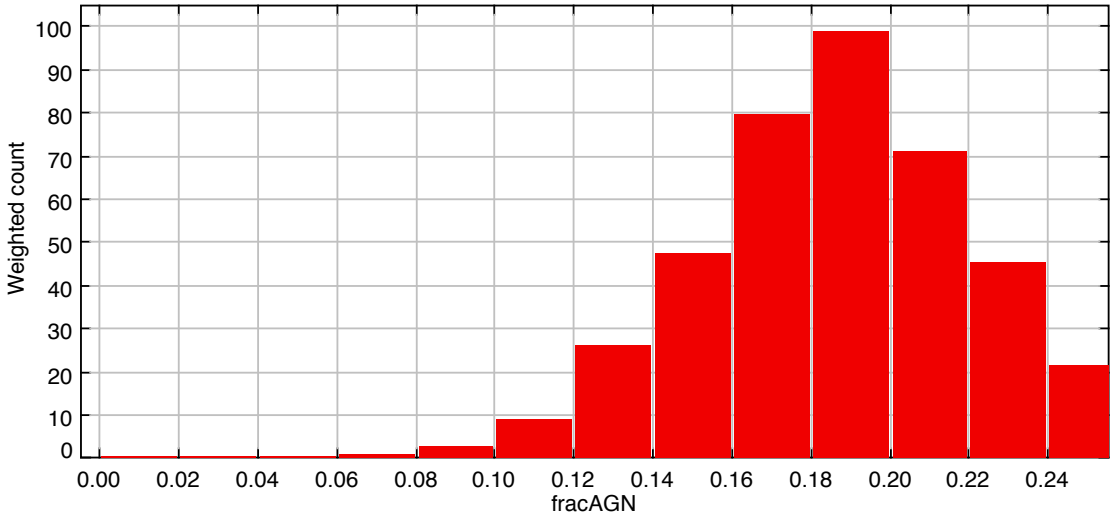

FracAGN

CREATE REALISTIC SEDS OF GALAXIES HOSTING AN AGN

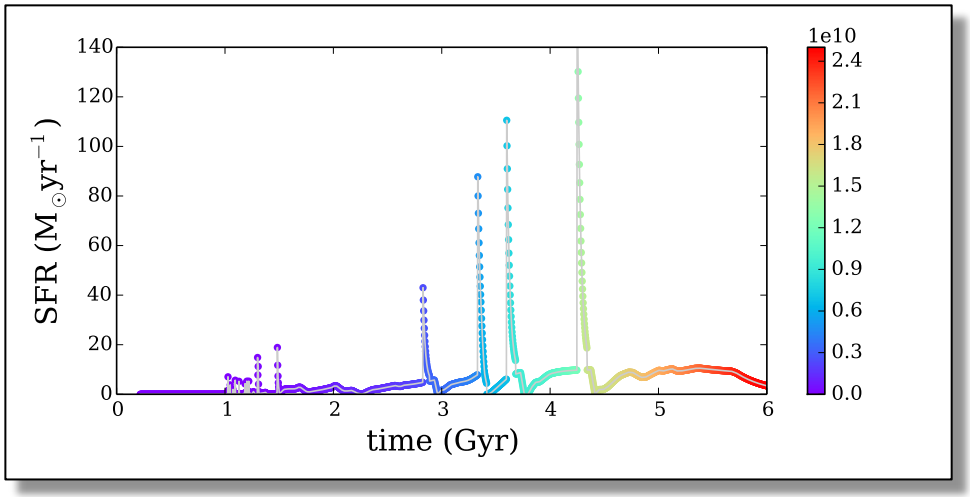

① Model SED of galaxies from realistic SFH of the SAM code GALFORM (Durham)

② Add the IR of Type 1 and Type 2 AGNs

$$L_{AGN} = frac_{AGN} * L_{IR}$$
$$L_{AGN} = frac_{AGN} * (L_{SB} + L_{AGN})$$

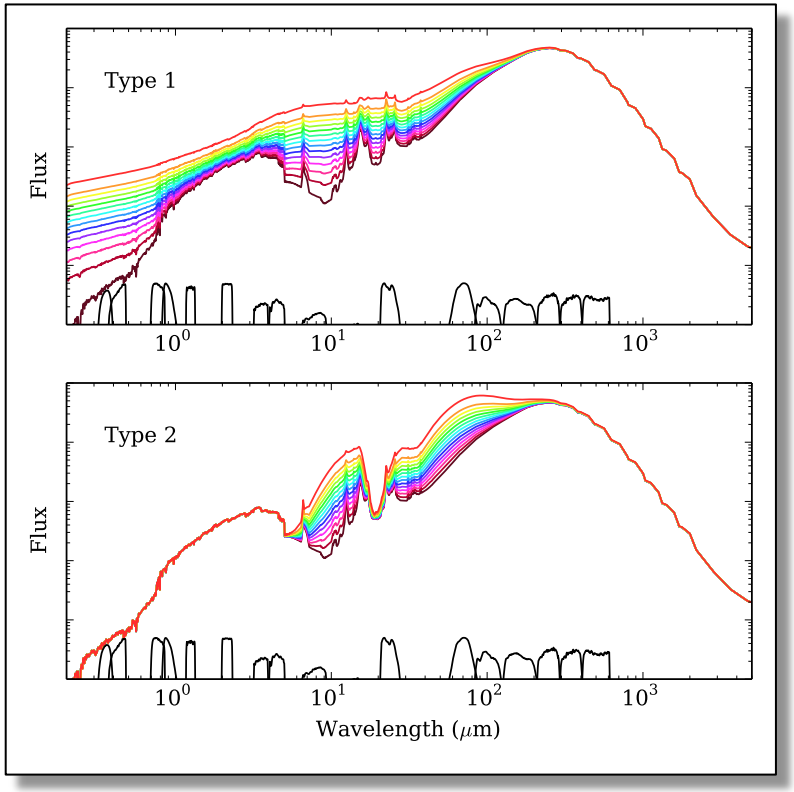

THE IR AGN EMISSION

Note: All the necessary information is available is the *.xml files (one per fitted object)

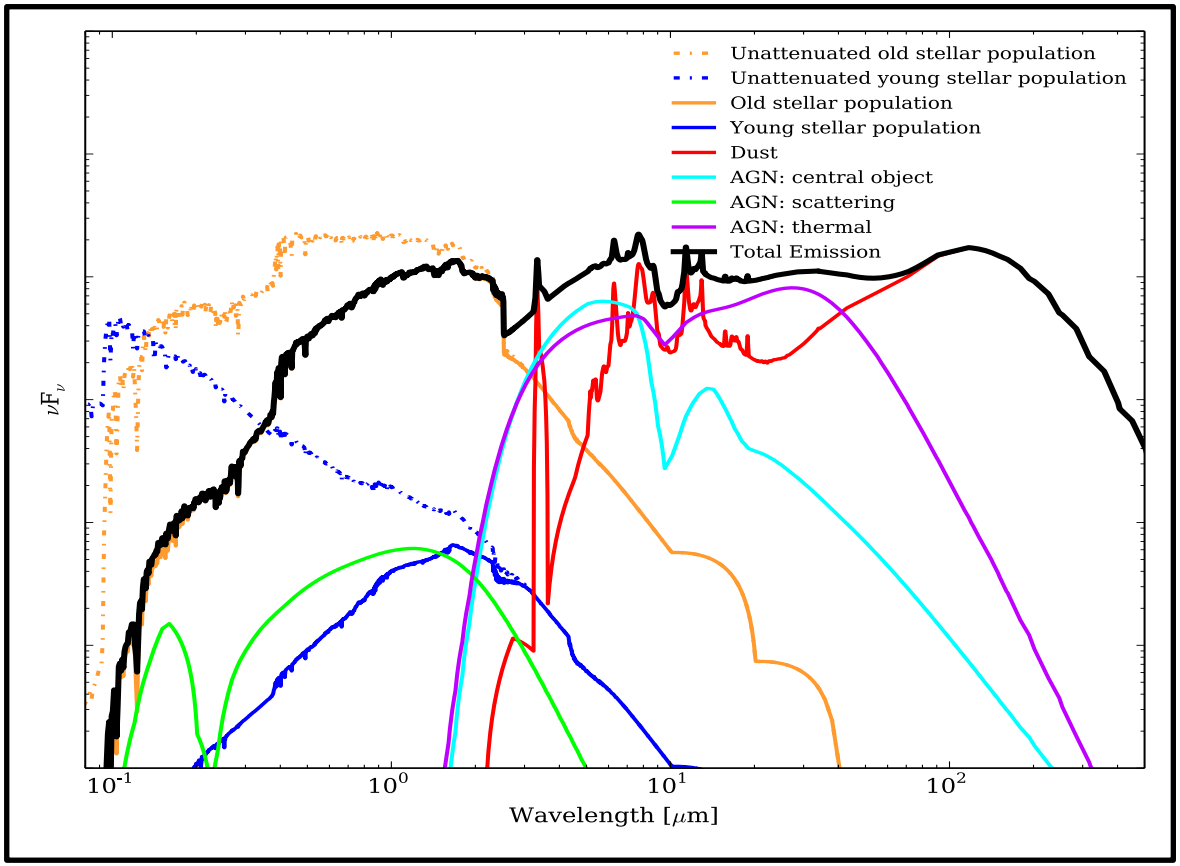

Ciesla et al. (2014)

AGN models of Fritz+06:
- central object
- dust torus emission
- photon scattering

PDF analysis on all of the parameters
(geometrical, silicate absorption, contribution to the L_{IR})

Building mock catalogues

Input photometric catalogue

Run CIGALE

Best Fit Model

Mock photometric catalogue

Run CIGALE

Model from PDF analysis

Compare input and output parameters

Model from PDF analysis

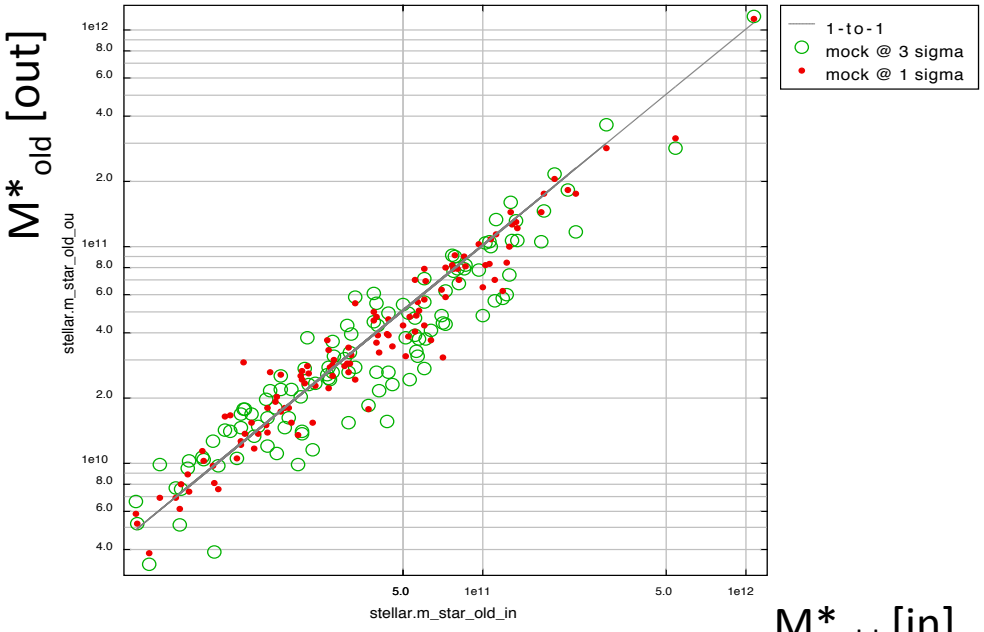

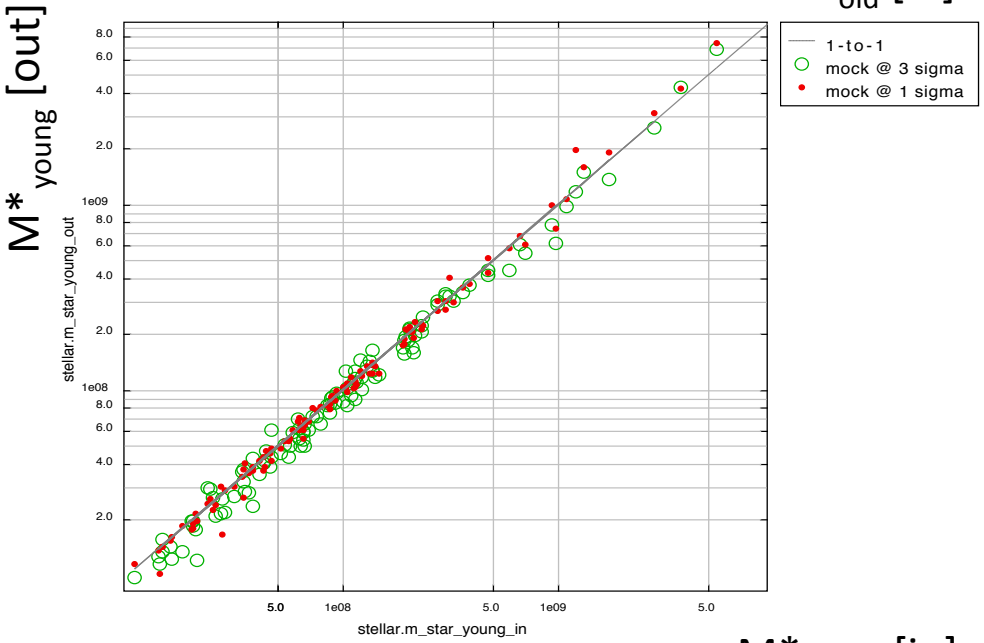

Building mock catalogues

- Some of the parameters are well estimated (e.g., SFR, A_{FUV}, M*) others are not (e.g., age).
- Mock catalogues allows to have a better idea of what is good and what is not.

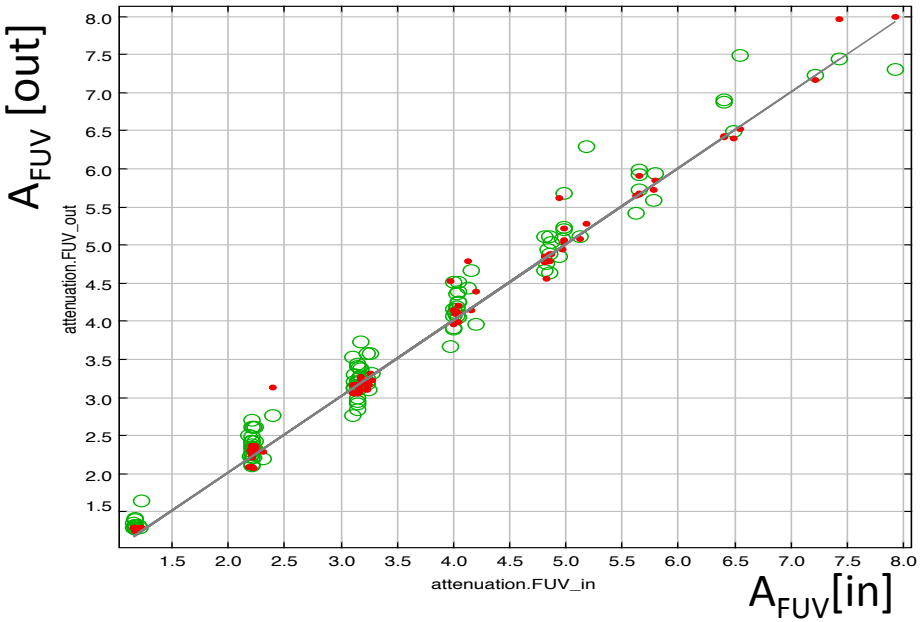

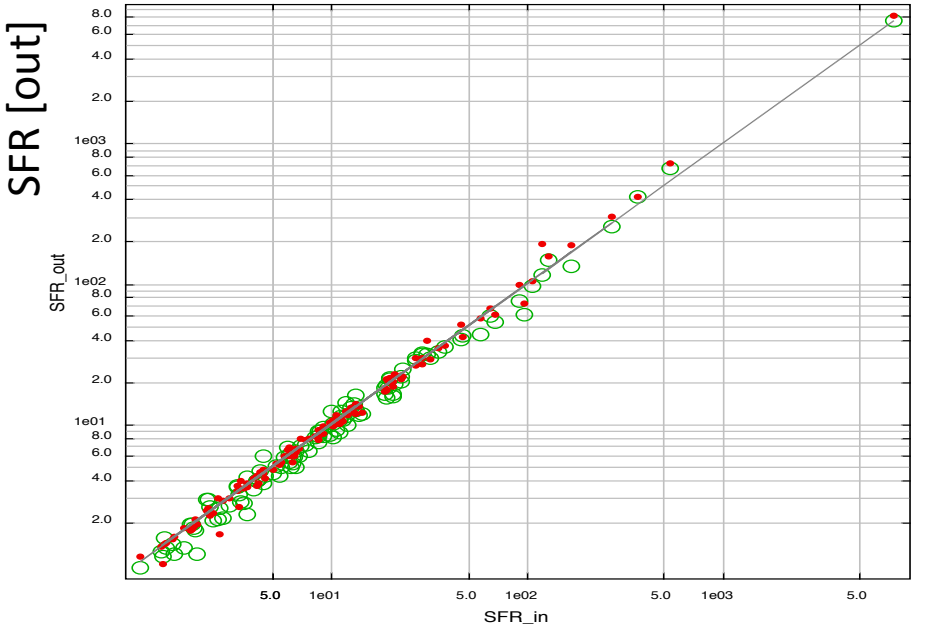

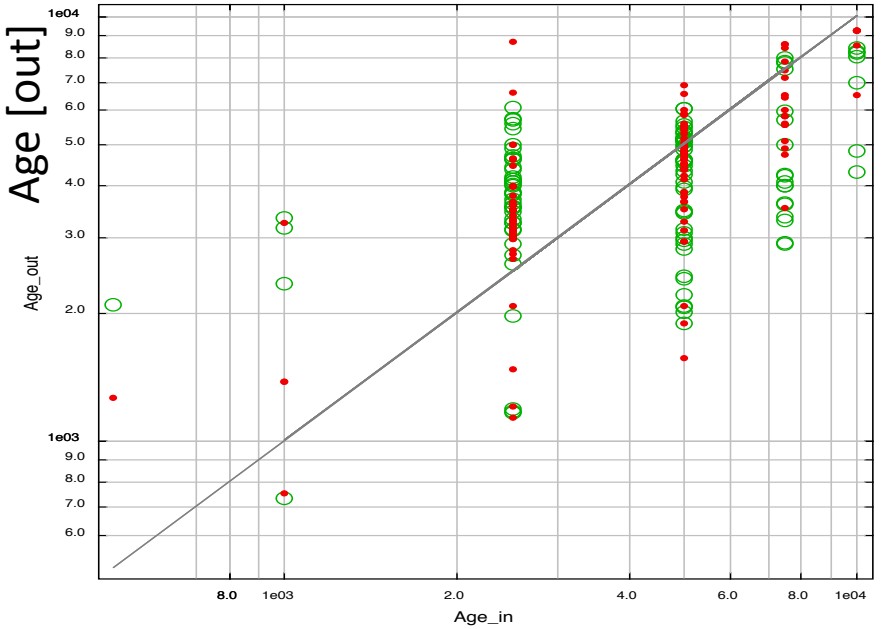

New fits with the New Python CIGALE: M82

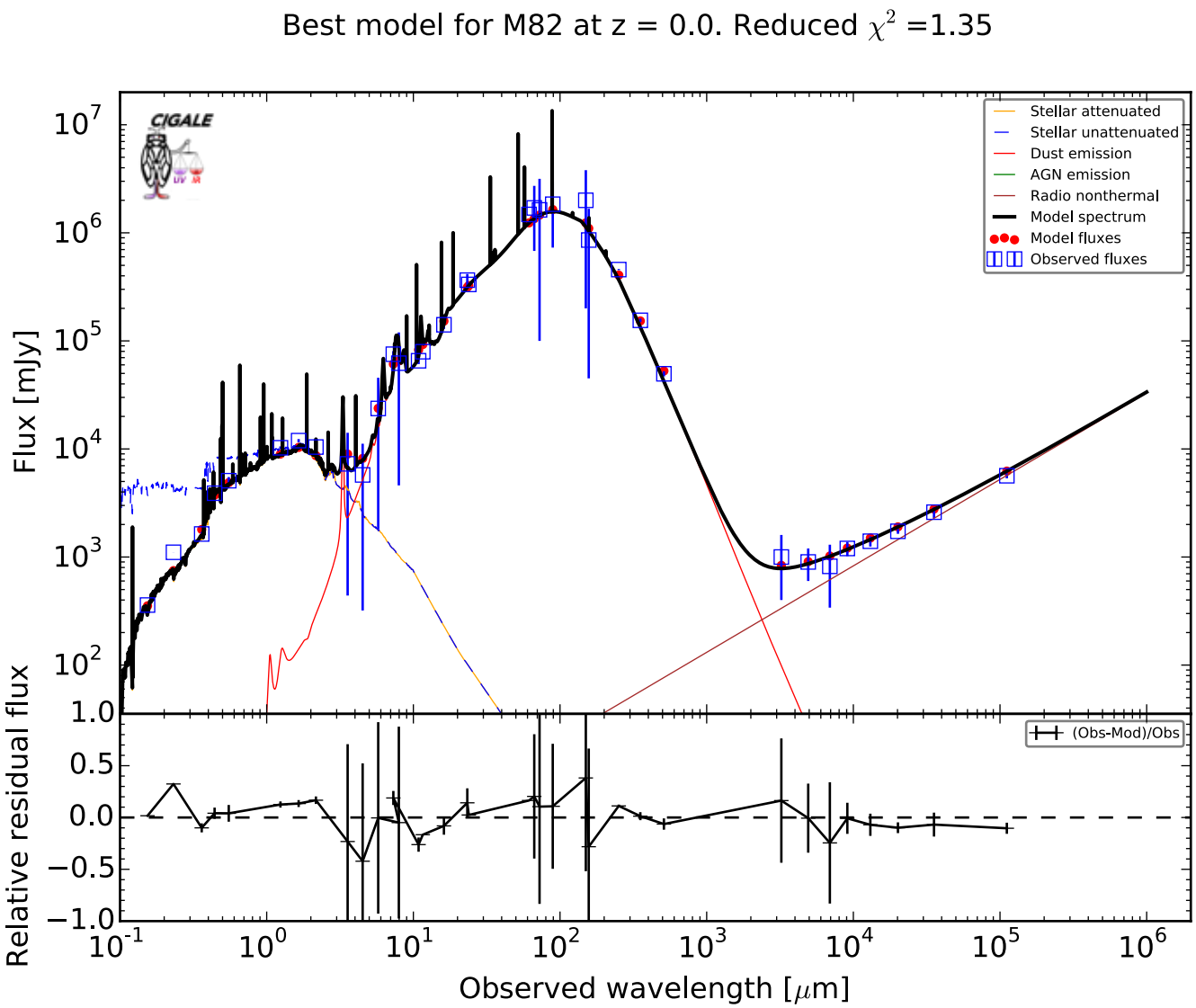

New fits with the New Python CIGALE: M82

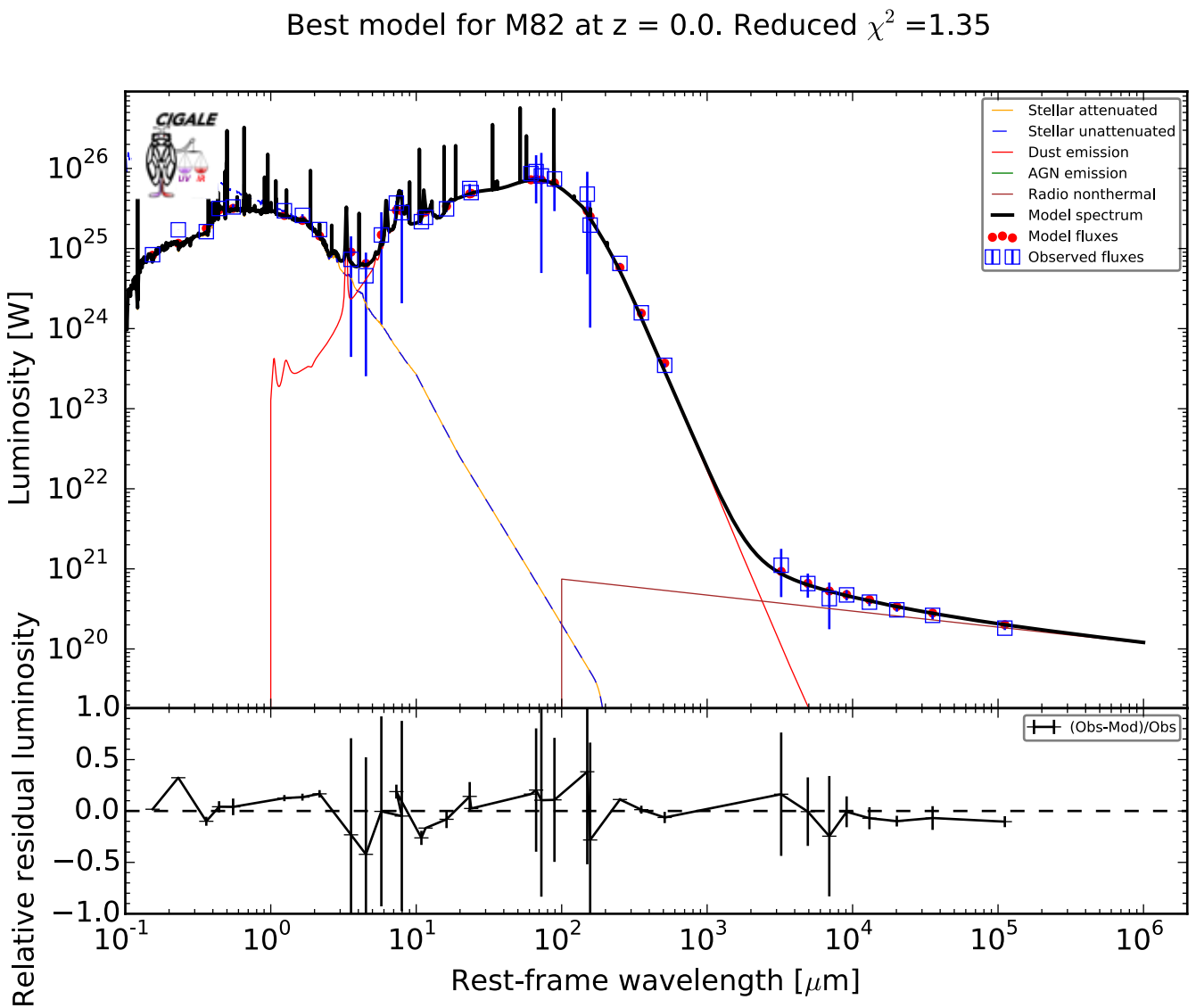

New fits with the *New* Python CIGALE: ARP 220

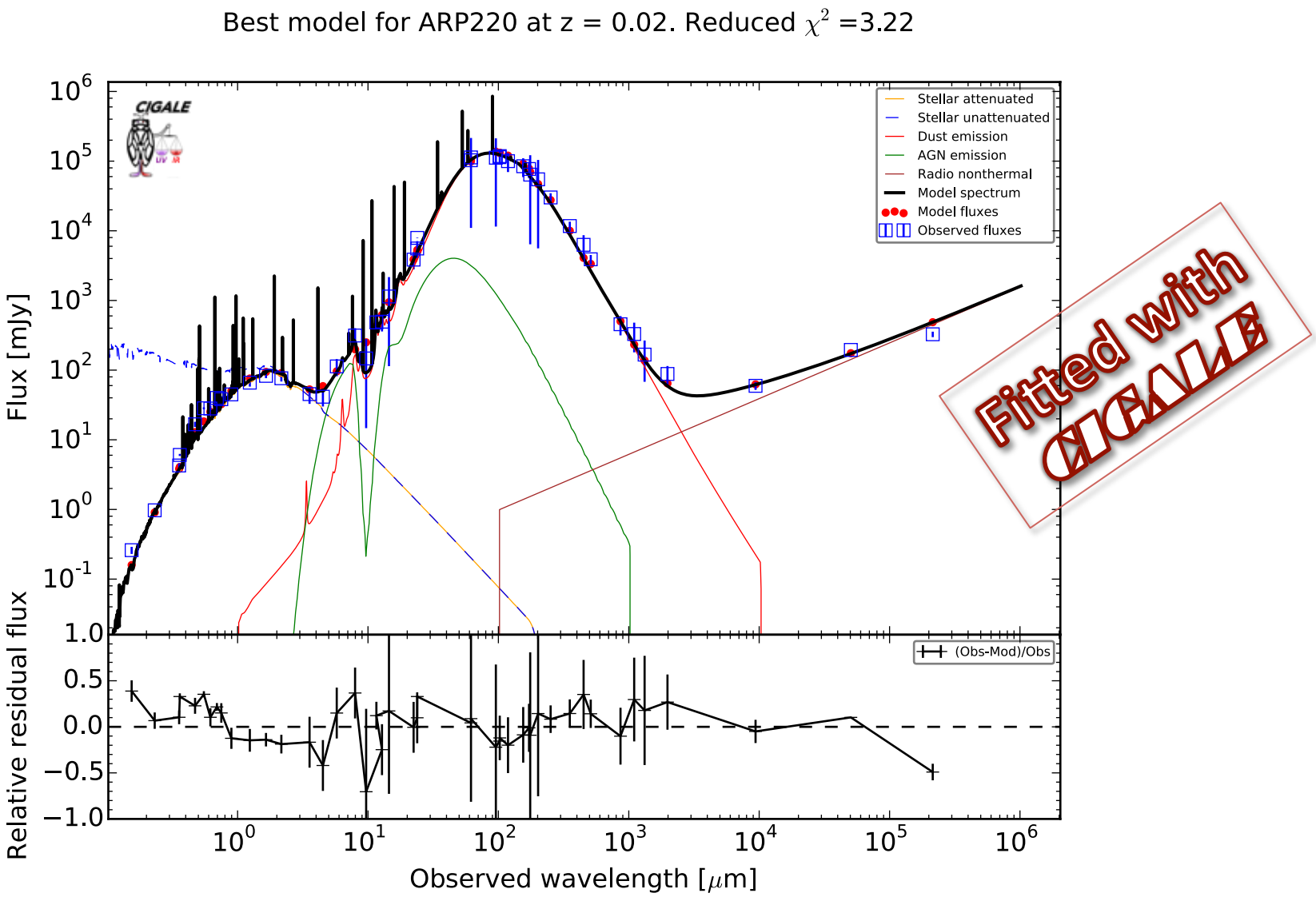

New fits with the *New* Python CIGALE: ARP 220

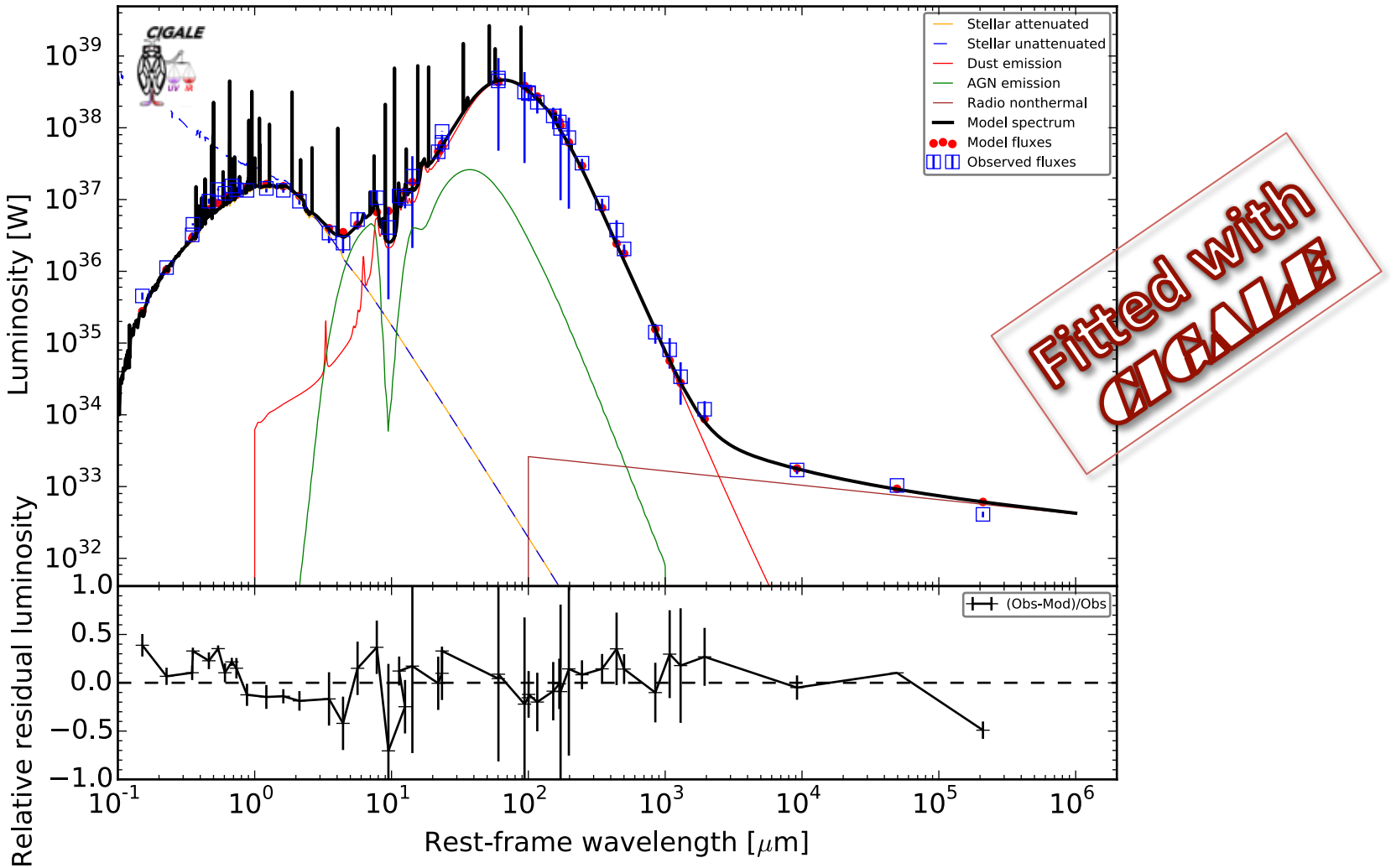

Fitting the SEDs of elliptical galaxies

Best model for M86 at z = 0.0. Reduced χ^2 =1.55

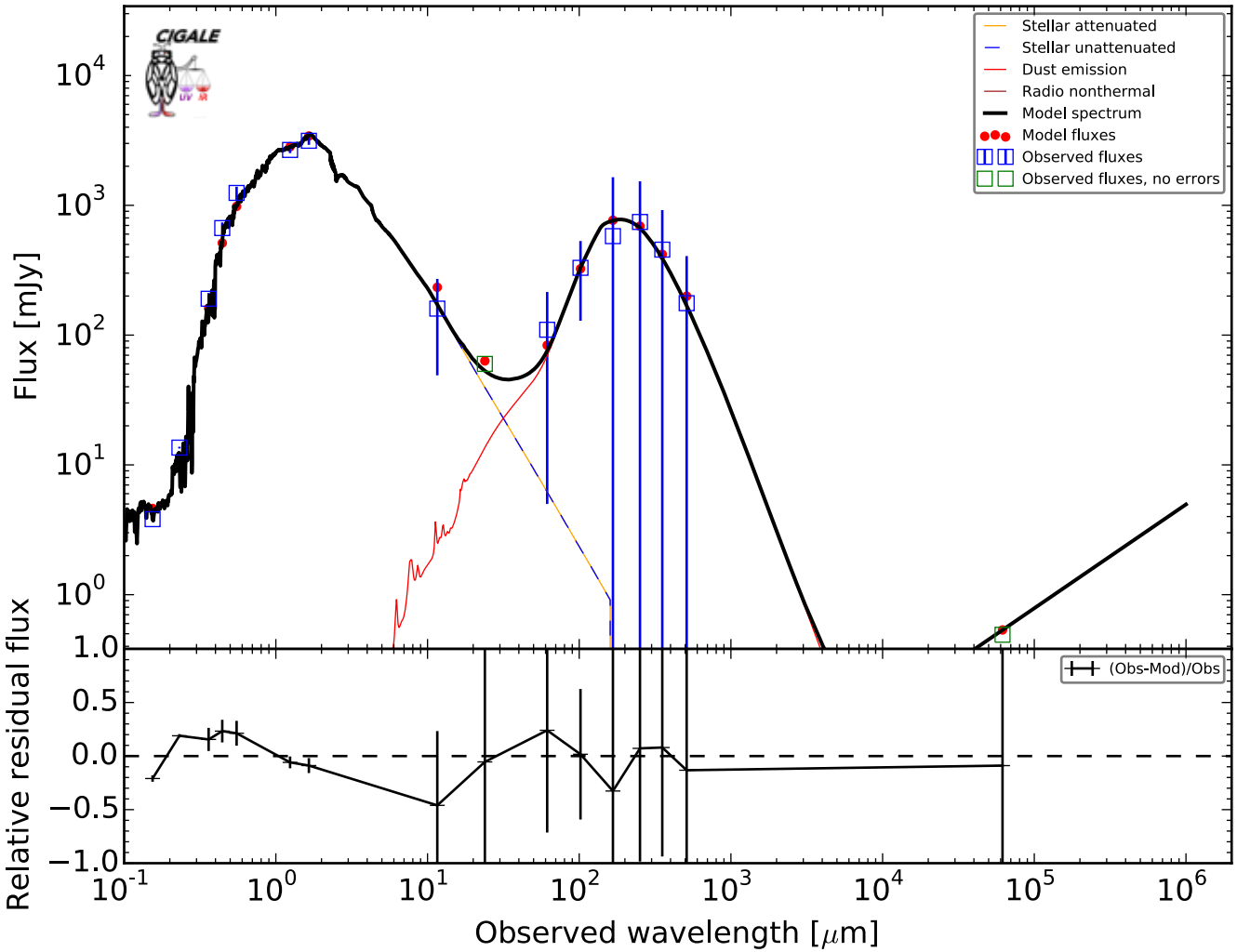

STAR F BREAK

Square)DL, UK

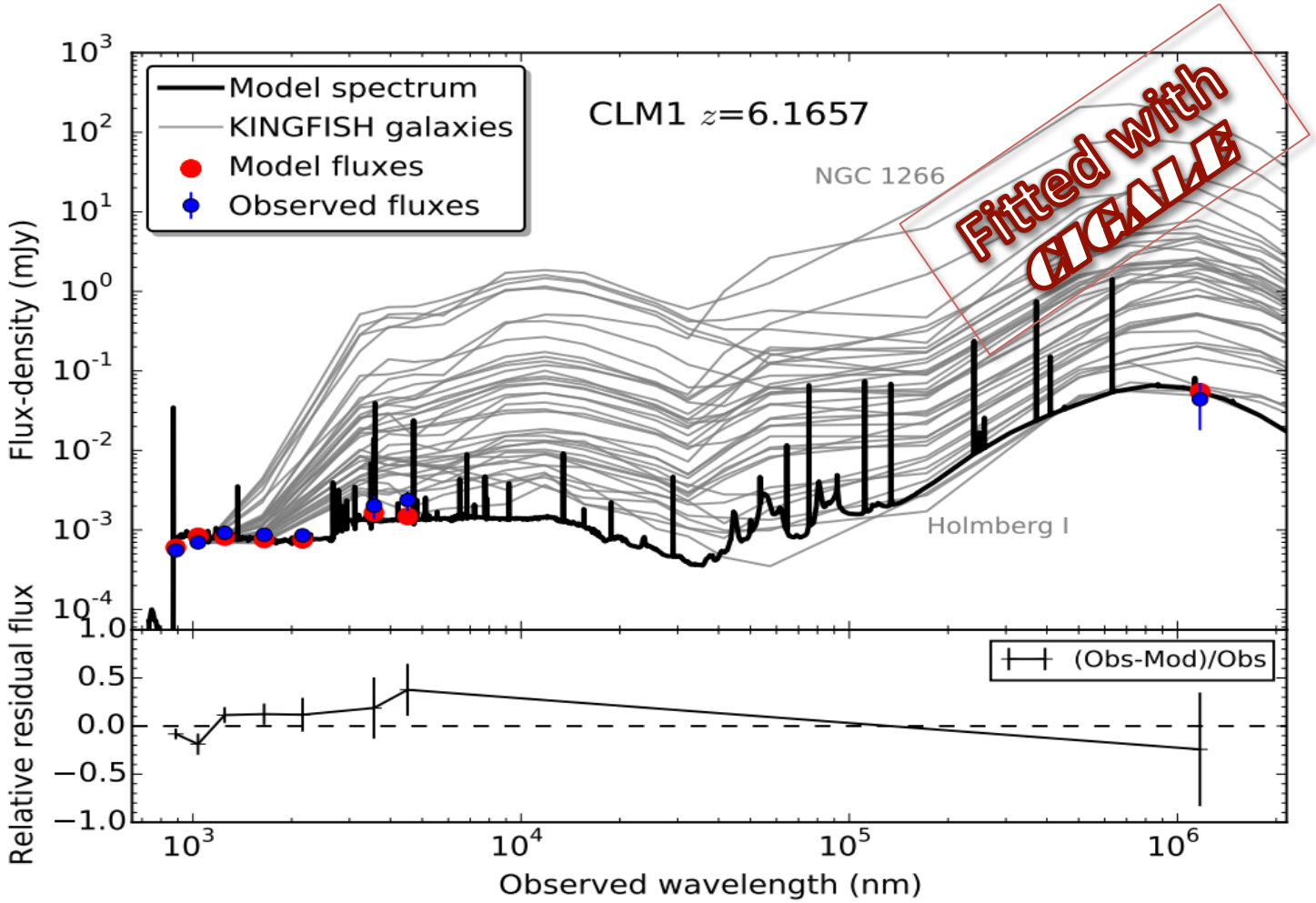

FIG. 3.— Observed-frame optical to far-IR SED of CLM 1 (blue circles). The best-fit model from CIGALE is shown as a black curve and the model fluxes through the observed filters as red circles. The grey curves are 39 nearby galaxy SEDs with UV to far-IR photometry from the KINGFISH survey (Dale et al. 2012) ranging from dusty infra-red galaxies to dwarf irregulars with very low thermal dust emission. The lower panel shows the residuals from the best-fit model. CLM 1 has a SED most similar to the least dusty nearby dwarf irregulars.

One interesting possibility provided by CIGALE

CIGALE can now be run
in a « model mode ».

This means that, assuming a star formation history (SFH), you can build the spectrum of a galaxy for whatever physical parameters you wish.

Variation of the SFH on short time scales from modelled merging galaxies from a MIRAGE simulation Perret et al. 2014

- The Lyman continuum the SFR even for high frequency variations. SFR estimators at longer wavelengths cannot capture these variations and lead to discrepancies on the estimates of SFR_{inst}.
- There is also a systematic offset that is visible in FUV and NUV but which is especially prominent in the U band.

Boquien et al. (2014)

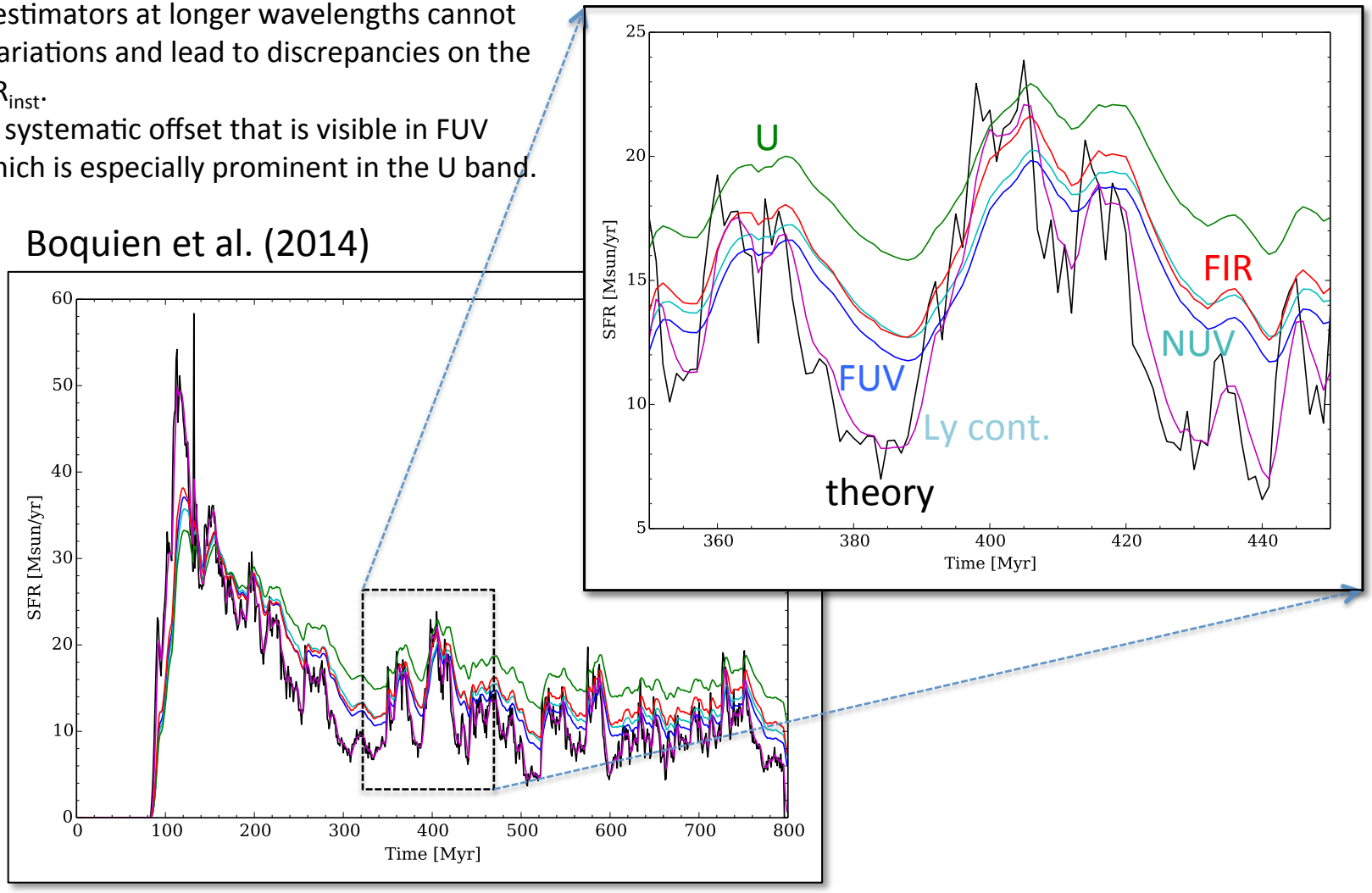

Photometric redshifts

Photometric redshifts

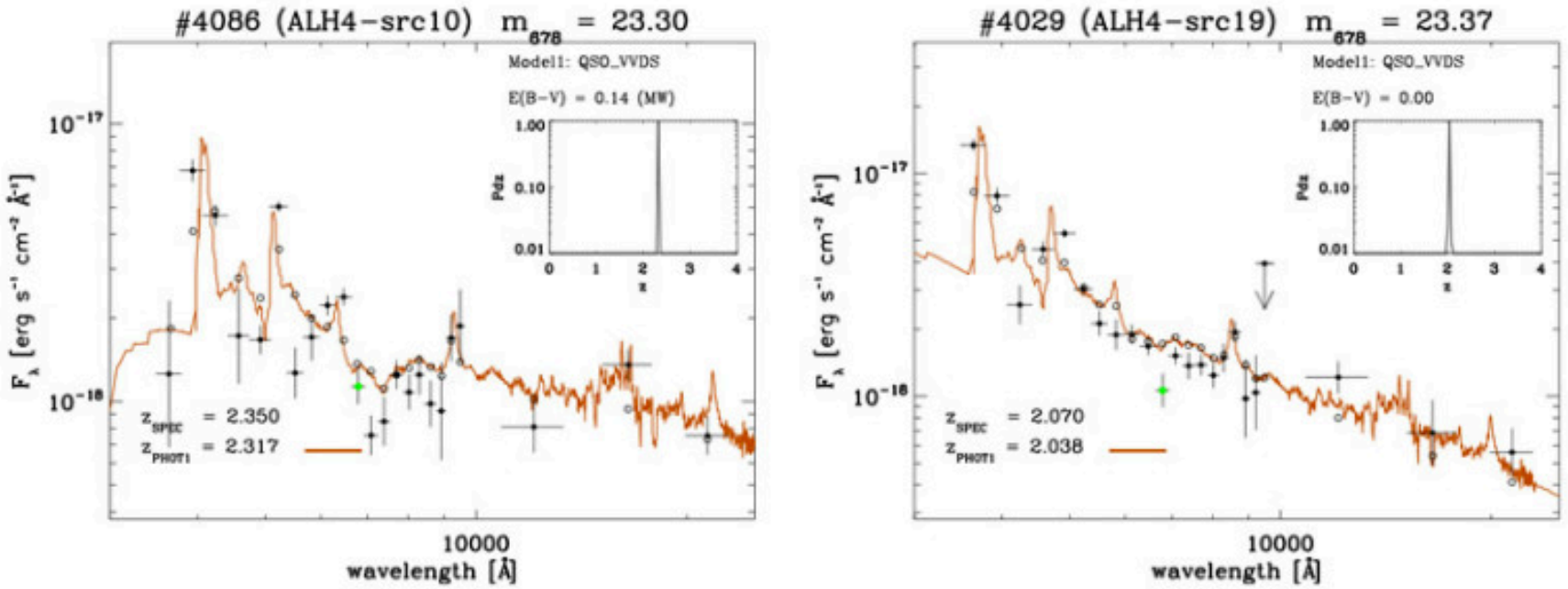

Fig. 4. Examples of best–fit solutions assuming a SMC extinction law for 6 sources covering a wide range of magnitudes ($\sim 20 \leq m_{678} \leq \sim 23.5$) and spectroscopic redshifts ($0.7 \leq z \leq 2.3$). Each panel includes the observed photometry, associated errors, and FWHM for each of the 23 ALHAMBRA filter set (black dots, vertical and horizontal error bar respectively). Photometric upper limits are indicated by arrows. The continuous line shows the best-fit solution, while the open circles give the expected magnitude from the model corrected from systematic offsets. Additional info for each source includes: model name, reduced χ^2, amount of extinction, the normalized probability distribution as a function of z (Pdz), the spectro–z (and its source catalog), and the best–fit photo–z solution. The title of each panel is labeled with the source ID in the ALHAMBRA catalog and the measured magnitude in the m_{678} filter (green dot).

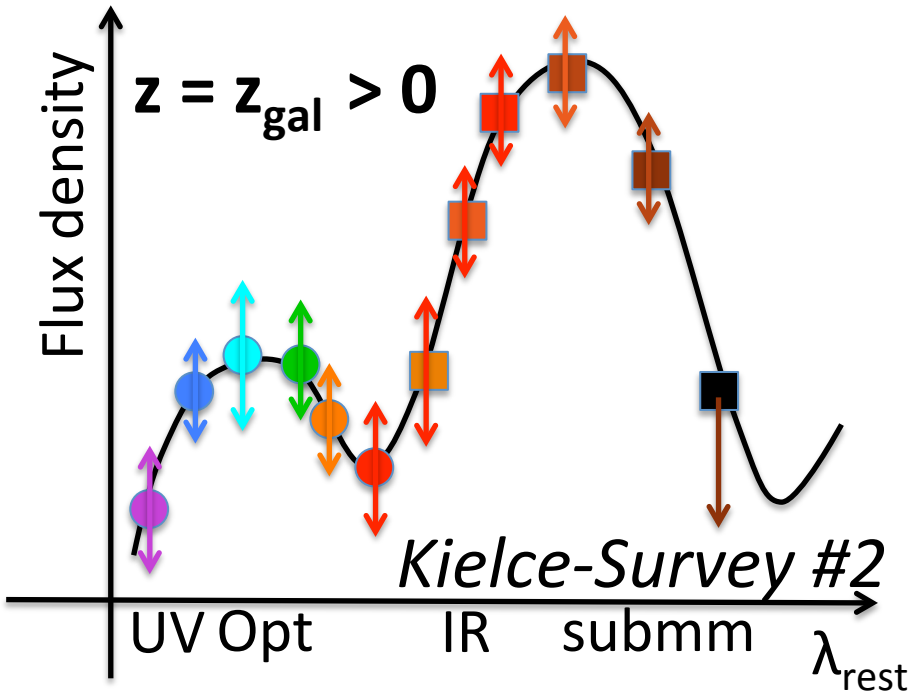

- Computing photometric redshifts also is SED fitting. The main output is the redshift but other physical parameters can be estimated, e.g., stellar mass (M_{star}).
- However, most photometric redshifts are estimated using UV+opt+NIR and dust-related parameters like the dust attenuation and therefore the star formation rate should be taken with care.

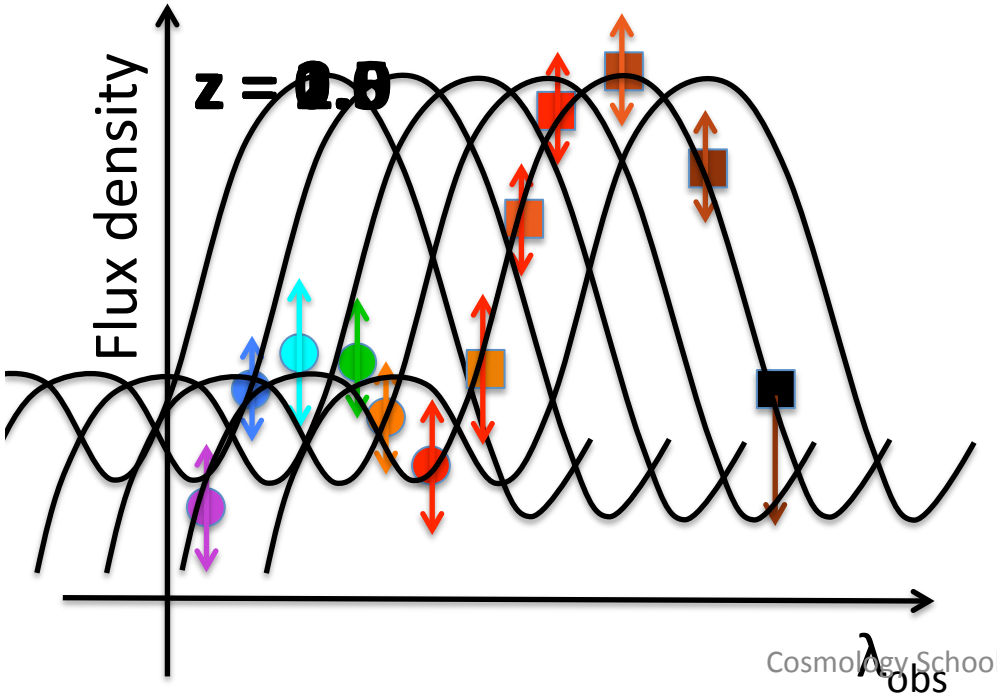

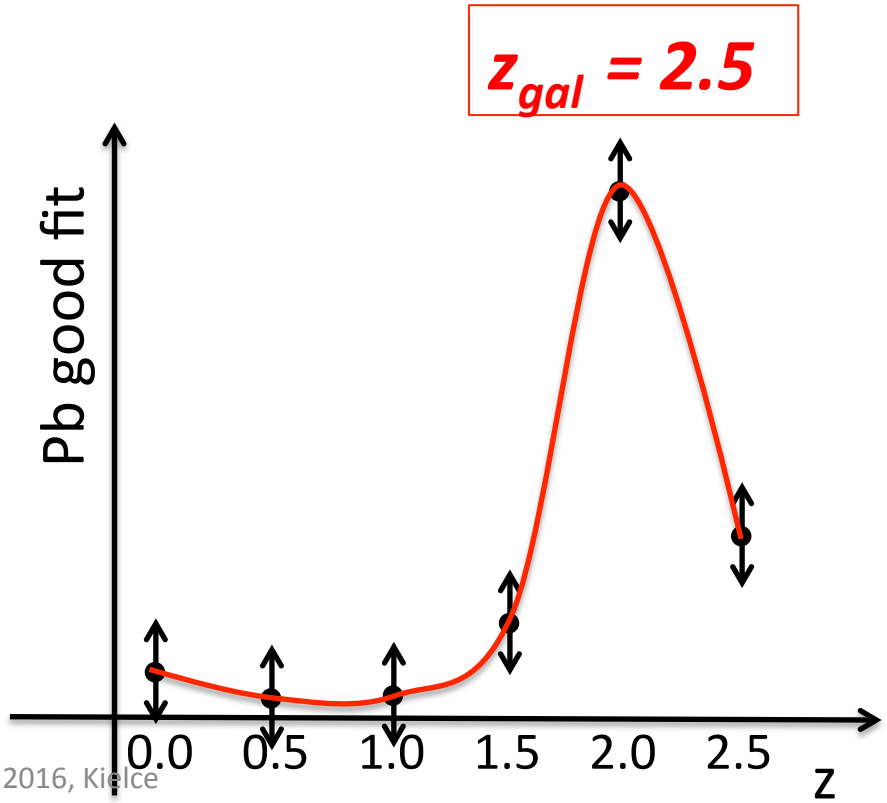

Spectroscopic redshifts are needed to calibrate the photometric redshifts

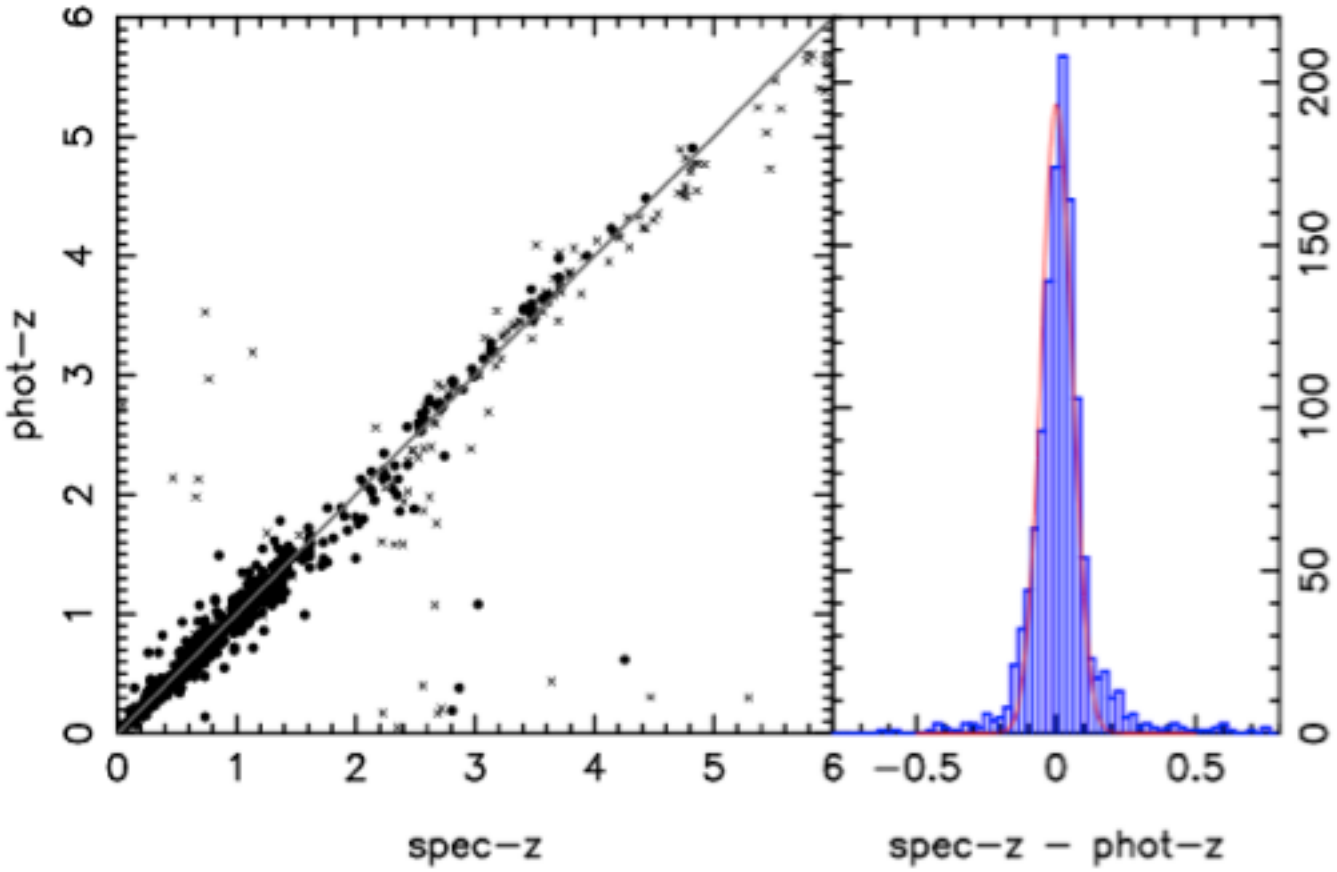

What are the next steps for SED fitting?

- Extending the models to X-rays on the one hand and to radio on the other hand.

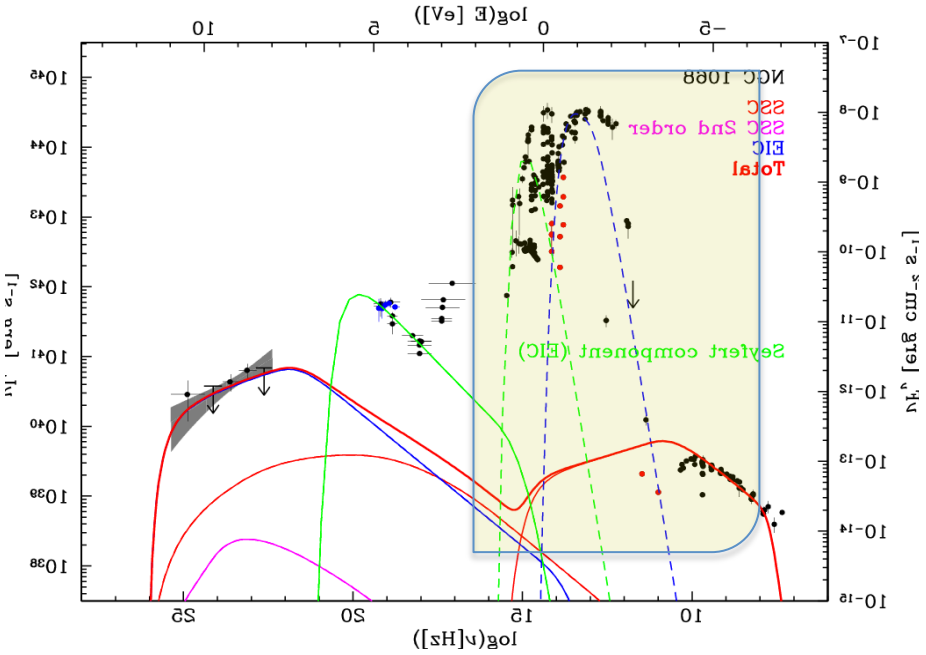

$3x10^{-11}$ $3x10^{-6}$ $3x10^{-1}$ $3x10^{4}$ μm

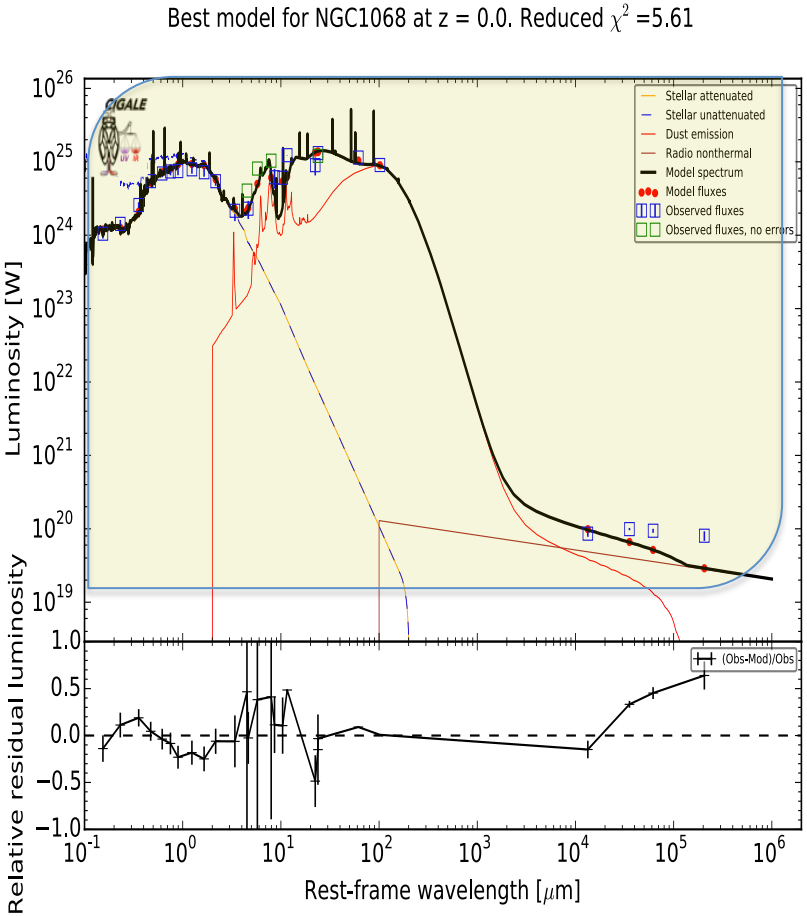

SED of NGC 1068 from Lenain et al. (2010)

Spectral energy distribution of NGC 1068, including the Fermi/LAT spectrum. The black and red points are archival data from the NED, the red ones denote data taken from the central region of NGC 1068. For clarity, we only show the INTEGRAL IBIS/ISGRI data in blue in the hard X-rays. The EIC model for the outflow is shown in blue, and the corresponding SSC emission is shown in thin red and magenta lines for first and second order components, respectively. The thick red line shows the sum of the different emission components from the large outflow. The EIC component from the accretion disc is shown in green.

Turner et al. (2001): « XMM-Newton first-light observations of the Hickson galaxy group 16 »

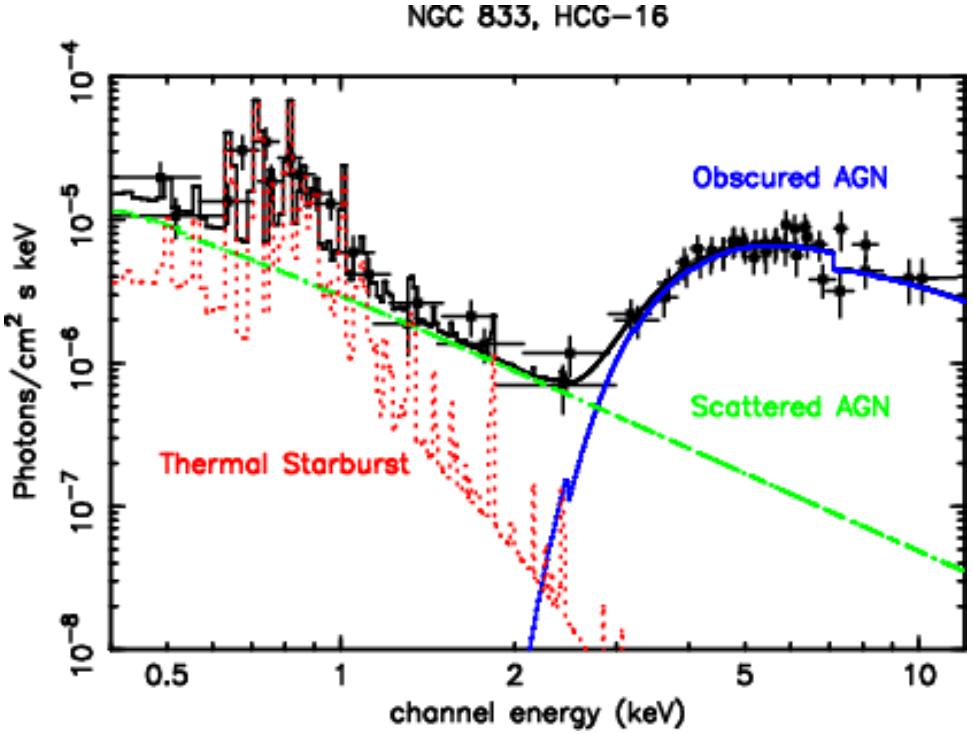

The X-ray spectrum of the galaxy NGC 833:

- high-energy, absorbed power-law (at > 3 keV) is the direct emission from the active black hole at the centre of the galaxy
- un-absorbed power-law, resulting from radiation scattered into our line of sight, by material directly illuminated by the AGN.

These two spectral components together show the presence of an AGN of luminosity 1.4x10^{42} erg s-1.

- weak soft X-ray emission from an optically thin plasma, perhaps originating from starburst activity

Distant Radio Galaxies and their Environments by Miley et al. (2008)

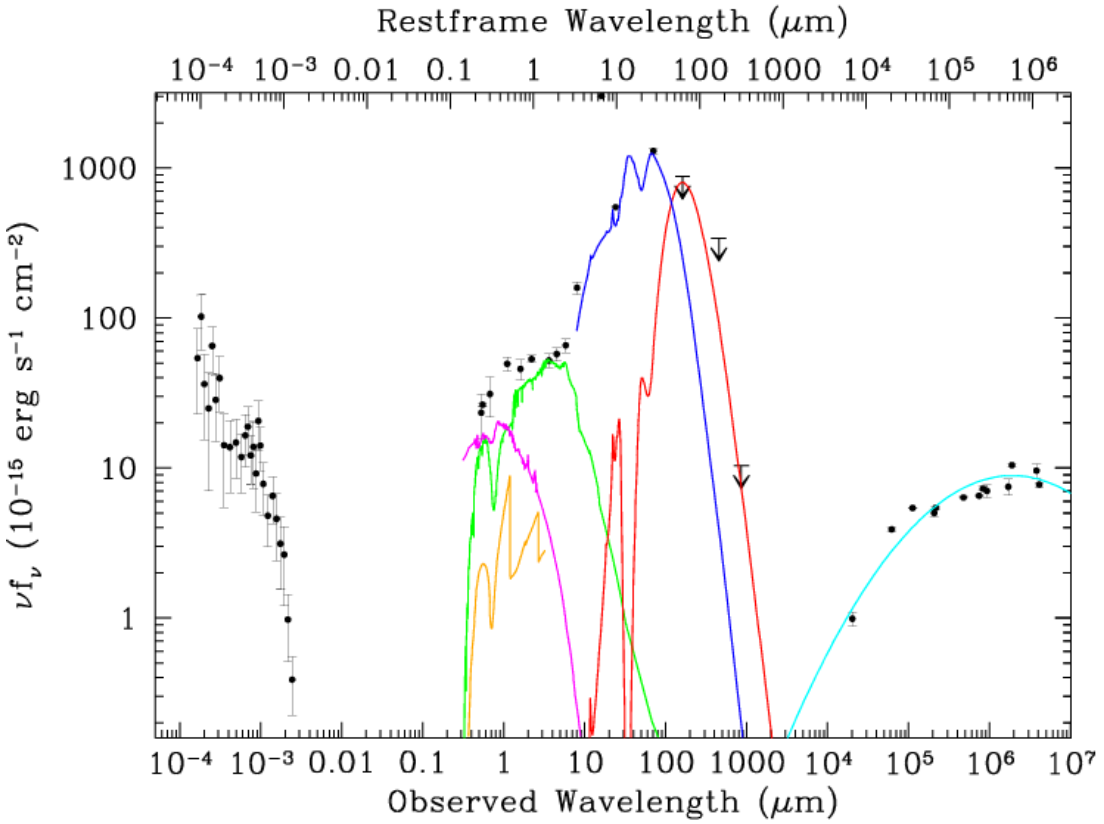

SED of the continuum emission from HzRG 4C23.56 at z = 2.5, illustrating the contributions from the various constituents. Coloured lines show the decomposition of the SED into individual components, under many assumptions. Cyan = radio synchrotron. Black = Absorbed nonthermal X-ray AGN. Yellow = nebular continuum. Blue = AGN-heated thermal dust emission. Red = Starburst-heated dust emission. Green = Stars. Magenta = scattered quasar. The addition of the overlapping modeled components fits the SED well.

CIGALE Python (v9.5)
became a French National Service
(like, e.g., CDS in Strasbourg)
and full support is available
24/7 (well, almost… 😉)

cigale.lam.fr

Dziękuję / Thank you / Merci